MOLECULAR MECHANISMS OF β-III-SPECTRIN IN DENDRITIC ARBORIZATION AND SPINOCEREBELLAR ATAXIA TYPE 5

by

SARAH DENHA

A dissertation submitted in partial fulfillment of the
requirements for the degree of

DOCTOR OF PHILOSOPHY IN BIOMEDICAL SCIENCES: HEALTH AND ENVIRONMENTAL CHEMISTRY

2024

Oakland University
Rochester, Michigan

Doctoral Advisory Committee:

Adam W. Avery, Ph.D., Chair
Colin G. Wu, Ph.D.
Randal J. Westrick, Ph.D.

To my parents, mentor, brothers, and friends

ACKNOWLEDGMENTS

I would like to express my deepest gratitude to everyone who has supported, encouraged, and helped me throughout the journey of completing this dissertation.

To my advisor and mentor, Dr. Adam W. Avery: your guidance, support, and tailored advice have been instrumental in every stage of my PhD. Your unwavering belief in my abilities, coupled with the opportunities you have opened for me, has been pivotal to my growth as a scientist. I am deeply fortunate to have been your student and to follow in your footsteps in academia. Your mentorship has not only shaped my academic journey but has left an unforgettable mark on my life.

I extend my sincere thanks to my committee members, Dr. Colin Wu and Dr. Randal Westrick, for their invaluable advice and support. Learning from your journeys and perspectives has profoundly enriched my experience.

To my beloved family—my parents and my brothers: your unwavering support and belief in me have been the foundation of my strength. I could not have come this far without your encouragement and love.

To my lab mates and friends, especially Lexie, Amanda, Cristal, and Naomi: you shared this journey with me, navigating the highs and lows. I am endlessly grateful for the laughter and friendship we shared.

To my cherished friends Maryam, Rand, Mena, Farah, and Summer: your belief in me and your constant support have been a source of motivation and inspiration. Thank you for standing by me and cheering me on every step of the way.

Finally, to everyone I may not have mentioned by name: please accept my heartfelt apologies. Your support, belief, and contributions—no matter how big or small—have played a crucial role in my journey. I am profoundly grateful to you all.

Sarah Denha

ABSTRACT

MOLECULAR MECHANISMS OF β-III-SPECTRIN IN DENDRITIC ARBORIZATION AND SPINOCEREBELLAR ATAXIA TYPE 5

by

SARAH DENHA

Adviser: Adam W. Avery, Ph.D.

β-III-spectrin is a membrane-associated cytoskeletal protein predominantly expressed in the cerebellum, and is essential for the maintenance and development of the complex dendritic arbors extended by Purkinje neurons. Mutations in various functional domains of β-III-spectrin cause the neurodegenerative disease spinocerebellar ataxia type 5 (SCA5). My dissertation has focused on understanding the molecular mechanisms by which β-III-spectrin supports neuronal structure and function and how SCA5 mutations disrupt this function. Specifically, my work has shown that the β-III-spectrin N-terminal domain, preceding the actin-binding domain, is required for SCA5-induced high-affinity actin binding and arborization defects *in vivo*. Furthermore, through characterizing the molecular consequences of SCA5 mutations in the spectrin-repeat domains (SRDs) of β-III-spectrin, I have shown that SRD2- and SRD3-localized mutations disrupt the physical interaction of β-III-spectrin with actin and α-II-spectrin. My dissertation work has provided significant insights into the role of β-III-spectrin in the actin cytoskeleton and the mechanisms underlying SCA5, laying the groundwork for developing a drug compound to treat this currently untreatable disease.

TABLE OF CONTENTS

TABLE OF CONTENTS - CONTINUED

TABLE OF CONTENTS - CONTINUED

TABLE OF CONTENTS - CONTINUED

LIST OF TABLES

LIST OF FIGURES

LIST OF FIGURES – CONTINUED

CHAPTER ONE

INTRODUCTION

1.0 Spectrin

Spectrins are plasma membrane-associated cytoskeletal proteins expressed in metazoans and found in all tissue types. Spectrins were first identified as components of the erythrocyte plasma membrane (1). The name spectrin is derived from the Latin and French words for ghost "spectra" because spectrin was the major isolated protein component of the denatured erythrocyte membrane "ghosts", which are the plasma membrane remains. On SDS-PAGE gels, spectrin runs as two protein bands of high molecular weight ~240 kDa and 220 kDa, which were named later as α-spectrin and β-spectrin, respectively (2). Later, other spectrin proteins were identified in other cells including neurons, cardiomyocytes, and skeletal muscles, and were referred to as non-erythroid spectrin proteins (3-8). In mammals, seven genes in multiple chromosomal loci have been identified to encode two α-spectrin proteins and five β-spectrin proteins. Although there are only seven genes, multiple spectrin splice-forms are generated through alternative RNA splicing (9, 10). The *SPTA1 and SPTAN1* genes encode erythroid α-I-spectrin and non-erythroid α-II-spectrin, respectively (11, 12). The *SPTB* gene encodes both erythroid-specific β-I-spectrin splice-form and a non-erythroid splice-form that is abundantly expressed in the nervous system (13-15). The *SPTBN1, SPTBN2, SPTBN4,* and *SPTBN5* genes encode non-erythroid β-II-spectrin, β-III-spectrin, β-IV-spectrin, and β-V-spectrin, respectively (15-18). In invertebrates, like *Drosophila melanogaster* and *Caenorhabditis elegans*, only a single α-spectrin protein is present,

which is homologous of the mammalian α-II-spectrin (19, 20). Invertebrates also express two β-spectrin proteins. In *Drosophila*, these are known as β-spectrin and β-H-spectrin. Invertebrate β-spectrin is most similar to vertebrate β-I, β-II and β-III-spectrin. *Drosophila* β-H-spectrin is homologous to vertebrate β-V-spectrin (15, 21, 22).

Although spectrins are ubiquitously expressed, several types of spectrins have distinct tissue or subcellular localization patterns. Alpha-I-spectrin is strictly expressed in erythrocytes while α-II-spectrin is found in all other cell types including neurons (10, 23). Beta-I-spectrin is expressed abundantly in erythrocytes, and a different splice-form of β-I-spectrin was also identified in neurons. Although moderate levels of β-V-spectrin were traceable in the cerebellum, β-V-spectrin expression was found to be enriched in the photoreceptor and auditory hair cells (18, 24, 25). Within the neurons, various types of spectrin are localized to specialized subcellular domains (26). Beta-I-spectrin is found in the cell body (soma) of cerebellar Purkinje neurons and granule cells (27). While β-II-spectrin is enriched in the axons and synapses of most neurons, β-III-spectrin is abundant in the dendrites and cell bodies of cerebellar Purkinje neurons (16, 28-30). The axon initial segment (AIS) and nodes of Ranvier are enriched with β-IV-spectrin (31).

Spectrins contain multiple functional domains. The N-terminus of most β-spectrins is comprised of an actin-binding domain (ABD), **Figure 1.1**. The ABD is followed by seventeen spectrin-repeat domains (SRDs) in all β-spectrin proteins except for β-V-spectrin and the invertebrate homolog β-H-spectrin, which contain thirty SRDs instead (18). The C-terminus is not conserved among β-spectrin proteins. Neuronal β-II-spectrin and β-III-spectrin contain a pleckstrin homology (PH) domain at the C-terminus that targets the protein to the cell membrane through interaction with membrane

phospholipids (32, 33). However, different a splice-form of β-II-spectrin is expressed in the liver and lacks the PH domain (34). On the other hand, α-spectrin is comprised of twenty-one SRDs followed by a C-terminal EF-hand domain. In addition, α-spectrin contains a Src homology (SH3) domain within SRD10.

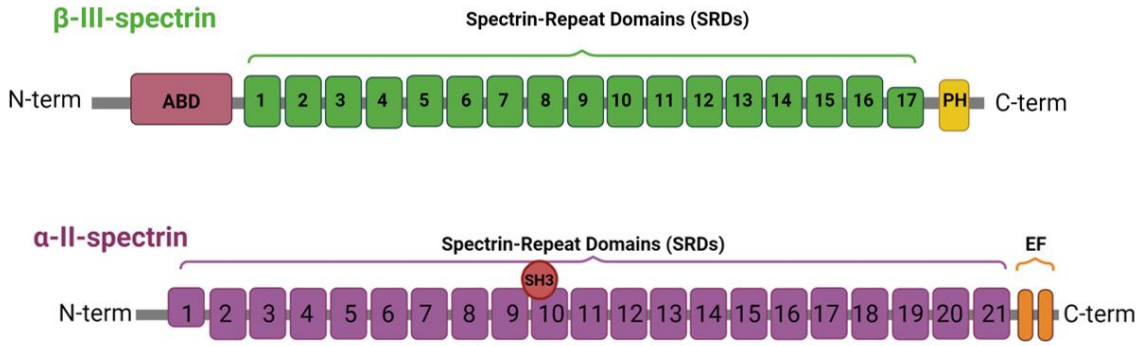

Figure 1.1. Domian diagrams of β-III-spectrin and α-II-spectrin. Diagrams generated using BioRender.com

The functional unit of spectrin is a tetramer of two α/β-spectrin heterodimers. The heterodimer is formed by anti-parallel side-to-side non-covalent interaction of α-spectrin and β-spectrin. The two heterodimers associate by non-covalent head-to-head interactions to form the spectrin heterotetramer. The spectrin heterotetramer has an overall filament structure with contractible, flexible conformation measuring up to 190-200 nm at the extended form (35, 36). The N-terminal ABDs of the two β-spectrin subunits are located at the opposite ends of the spectrin tetramer. This arrangement allows the spectrin tetramer to cross-link actin filaments, **Figure 1.2A**. In this way, spectrin and actin interact to form a spectrin-actin cytoskeleton that lines the cytoplasmic side of the plasma membrane. In erythrocytes, the spectrin-actin cytoskeleton has a 2-D hexagonal arrangement (37). On the other hand, the spectrin-actin cytoskeleton has a distinct

arrangement in neurons, **Figure 1.2B**. In the axons and dendrites, actin filaments form a ring structure (35, 38). Each actin ring lines the plasma membrane and is centered on the longitudinal axis of the neurite. Multiple actin rings are present along the axons or dendrites with a highly periodic spacing of ~190 nm. Spectrin tetramers, with an extended length of 190 nm, cross-link consecutive actin rings. This arrangement of the spectrin-actin cytoskeleton is called the membrane periodic skeleton (MPS). Beta-spectrin links the spectrin-actin cytoskeleton to the inner leaf of the plasma membrane through multiple mechanisms. Beta-spectrin either directly interacts with membrane phospholipids through the PH domain or interacts with adaptor protein ankyrin, which in turn interacts with transmembrane proteins (39, 40).

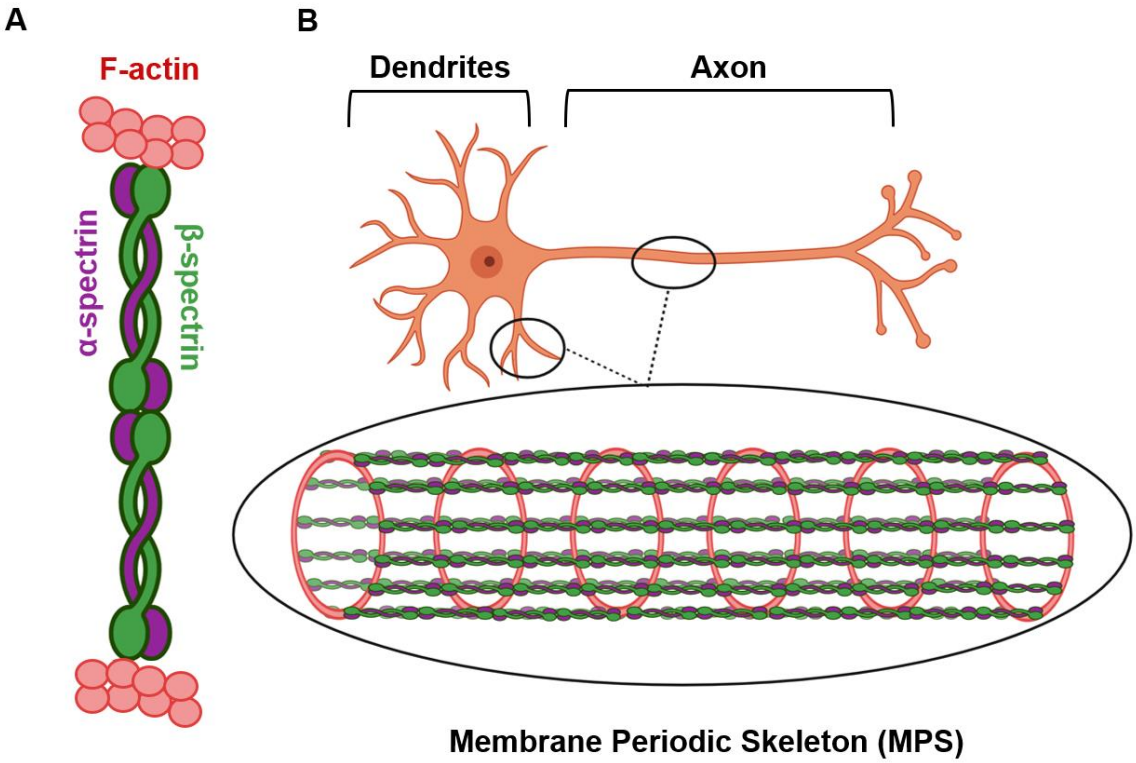

Figure 1.2. Spectrin-actin cytoskeletal arrangement in neurites. (A) Two α/β-spectrin heterodimers form a heterotetramer that cross-links actin filament (F-actin) through β-spectrin. (B) Periodic spectrin-actin cytoskeleton arrangement in neurons. Generated using BioRender.com.

Spectrins contribute to a variety of cellular processes and functions in different tissues. In general, spectrins function to maintain the structure and integrity of the plasma membrane. Numerous studies have shown that spectrins are required for the unique cell morphologies adopted by neurons. Loss of β-spectrin in *C. elegans* leads to axonal breakages (41). Knocking down β-spectrin in *Drosophila* causes presynaptic retraction, synapse elimination, and a reduction of the complex dendritic tree extended by class IV da neurons (42, 43). Knockout or knockdown of β-III-spectrin in Purkinje and hippocampal neurons decreases dendrite length and reduces density of dendritic spines, highlighting a requirement of β-III-spectrin in dendrites (44-46). In addition, β-spectrin is

required to stabilize transmembrane proteins and cell-adhesion molecules at discrete membrane domains. Loss of β-IV-spectrin causes abnormal AIS, nodal membrane disruption, and abnormal clustering of sodium and potassium channels (47-49). Furthermore, the stabilization of EAAT4 glutamate transporters at the plasma membrane of Purkinje cells is reduced in β-III-spectrin knockout mice, supporting an important role in glutamate neurotransmission (50). Spectrins also contribute to cellular signaling and intracellular transport by maintaining the structure of the AIS and associating with different motor proteins, including myosin, dynein, and kinesin (26, 51).

Mutations in spectrins cause a wide spectrum of diseases. Mutations in erythroid α-I-spectrin and β-I-spectrin cause hemolytic anemia, characterized by fragile red blood cell membranes (52-54). On the other hand, mutations in neuronal β-I-spectrin are linked to autism and spinal cord diseases (55-57). Alpha-II-spectrin mutations cause early infantile epileptic encephalopathies type 5 (EIEE5; A.K.A West syndrome) and juvenile-onset hereditary motor neuropathy (58). EIEE5 is characterized by severe infantile spasms, developmental and cognitive delay (59-64). Mutations in β-II-spectrin result in neurodevelopmental syndrome, characterized by global developmental delay, language and motor deficits, and behavioral abnormalities (65). Dominant mutations in β-III-spectrin cause infantile or late onset spinocerebellar ataxia type 5 (SCA5), while recessive mutations lead to spinocerebellar ataxia autosomal recessive type 14 (SCAR14) (also known as spectrin-associated autosomal recessive cerebellar ataxia type 1 (SPARCA1)) (66-83). Both SCA5 and SCAR14/SPARCA1 are characterized by ataxia of upper and lower limbs and cerebellar cortex degeneration (84-86). In addition, developmental or intellectual delays are seen in infantile onset SCA5 and

SCAR14/SPARCA1. Mutations in β-IV-spectrin cause congenital hypotonia, motor axonal neuropathy, and deafness (87, 88). The focus of my dissertation research is to uncover the molecular mechanisms by which mutations in different functional domains of β-III-spectrin lead to adult onset and infantile onset SCA5.

1.1 Spinocerebellar Ataxia Type 5

Spinocerebellar ataxia (SCA) is a group of rare genetic neurodegenerative disorders. There are more than forty genetically distinct SCA subtypes known so far. These disorders are monogenic and stem from mutations in distinct genes, such as those encoding transcription factors or ion channel proteins (89). As the name suggests, SCA disorders affect both the spinal cord and the cerebellum. However, some SCAs, like SCA5, are restricted to the cerebellum, while others, like SCA1, affect additional regions of the nervous system, including the peripheral nerves, brainstem, and basal ganglion (90, 91). Inherited autosomal dominant mutations are the primary cause of SCAs; however, sporadic autosomal dominant, autosomal recessive, and X-linked mutations are also associated with some SCAs (92, 93). Clinical phenotype includes progressive loss of motor coordination of the proximity, wide gait, slurred speech, abnormal eye movements, and degeneration of the cerebellum observed in MRI images (94). Most cases present late onset motor incoordination symptoms; however, some severe cases are early onset, and are additionally characterized by developmental and intellectual disabilities (95). Many SCAs result from GAC repeat expansion, causing long uninterrupted stretches of glutamines in the disease proteins (A.K.A poly-Q ataxias) including SCA1, SCA2, and SCA3 (96). Other SCAs, including SCA5, SCA11 and SCA13, stem from traditional mutations including missense, frame shift, and nonsense mutations (97). At the tissue

level, degeneration of the cerebellum, the spinal cord, and loss of the Purkinje neurons has been reported for SCAs (66, 98-100). Among the various SCAs, our lab focuses on the understudied pathogenesis of spinocerebellar ataxia type 5 (SCA5).

Unlike other SCAs targeting nuclear and ion channel proteins, SCA5 is typically caused by inherited autosomal mutations in *SPTBN2* gene in chromosome 11 encoding the cytoskeletal protein β-III-spectrin (66). SCA5, like other SCAs, is characterized by limb and gait ataxia, slurred speech and abnormal eye movements (nystagmus). The typical age for symptoms onset is in the third or fourth decade of life, averaging around the early 30s. MRI images and autopsy tissues taken from SCA5 patients show progressive degeneration of the cerebellar cortex with loss of Purkinje neurons and thinning of the molecular layer of the cerebellum (66, 85). However, recently reported SCA5 cases, caused by sporadic dominant mutations in β-III-spectrin, show more severe clinical features including infantile onset of nonprogressive cerebellum degeneration, global developmental, and intellectual defects (80). These symptoms mimic the more severe and early onset SCAR14 recessive mutations in β-III-spectrin (79). Thus, a new category of SCA5 has emerged and is referred to as infantile/early onset SCA5 or *SPTBN2*-associated nonprogressive cerebellar ataxia (NPCA) (82, 101). SCA5 missense and in-frame deletion mutations localize to multiple functional domains of β-III-spectrin, including the N-terminal ABD and the proximal SRDs (SRDs 1-6), **Figure 1.3**. However, the molecular consequences of these SCA5 mutations are poorly understood.

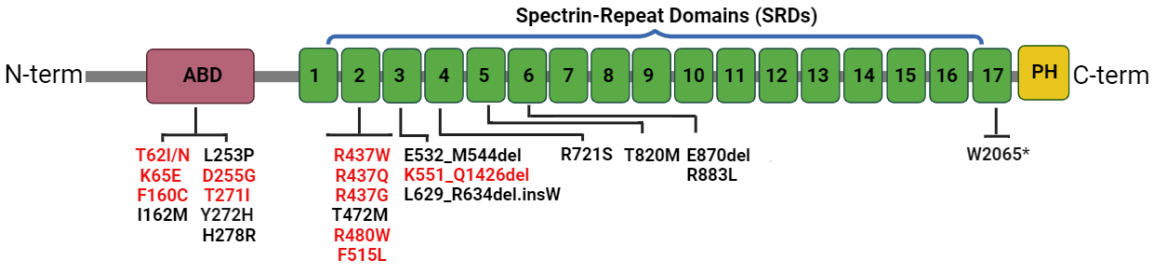

Figure 1.3. Dominant mutations in β-III-spectrin lead to SCA5. Mutations in red are associated with early onset SCA5 and in black are associated with late onset SCA5. However, Y272H in the ABD and W2065* in SRD17 were found to be a compound mutation in a reported early onset case with non-symptomatic parents carrying only a single mutation (79).

In general, SCAs remain incurable without any FDA-approved treatments used currently. However, there are some pharmacological drug treatments and other non-pharmacologic treatments that have reached clinical trials. The non-pharmacologic treatments include physical therapy, non-invasive neurostimulation, and branched-chain amino acids (BCAAs) treatments have shown to be affective to alleviate the severity of common SCAs diseases, like SCA1 and SCA3 (102). Other promising treatments that repair SCA at DNA or RNA level, including gene therapy, CRISPR editing, antisense oligonucleotides (ASOs), adeno-associated virus (AAV)-mediated gene therapy, and DNA mismatch repair, are still in their early stages (102). Most of these treatments are focused on poly-Q based ataxias. For SCA5, there are no known clinical trials. However, the Avery lab has initiated the development of pharmacological treatments for SCA5. Using a novel high-throughput FRET screening assay combined with biochemical co-sedimentation binding assays, Avery lab with collaborators at University of Minnesota screened a library of ~3,000 FDA-approved small molecule compounds (103, 104). This screening revealed that ginsenoside Rb1 and micafungin can alleviate the high-affinity

actin binding caused by a specific ABD-localized SCA5 mutation (104). Increased actin binding is a shared molecular consequence of other cytoskeletal proteins targeted by disease mutations including α-actinin, utrophin and dystrophin. Thus, developing an effective pharmacological drug capable of restoring the dynamic interaction between spectrin and the actin may prove effective as a SCA5 therapeutic.

1.2 The N-Terminus

Actin monomers assemble into various types of filament structures. These different actin filament structures are further organized into distinct cytoskeletal networks or lattices with different shapes. The structure of different actin-cytoskeleton lattices is formed and maintained by a group of actin-binding proteins (105). Two tandem calponin homology (CH1-CH2) domains are typically located at the N-terminus of various actin-binding proteins including spectrin, α-actinin, filamin, utrophin and dystrophin (106). These tandem CH1-CH2 domains form the actin-binding domain (ABD) in these proteins. Each CH domain consists of six or seven α-helices, and are assembled into a compact α-helical globular structure (107, 108), **Figure 1.4A**. Cryo-EM and AlphaFold structures of β-III-spectrin ABD bound to actin show that only the CH1 domain interacts directly with actin filaments (109, 110), **Figure 1.4B**. On the other hand, the CH2 domain has never been resolved experimentally in the actin bound state, and is predicted to position away from actin. Recently, novel N-terminal helices preceding the CH1 domain were also found to directly bind to actin in β-III-spectrin and utrophin (110, 111).

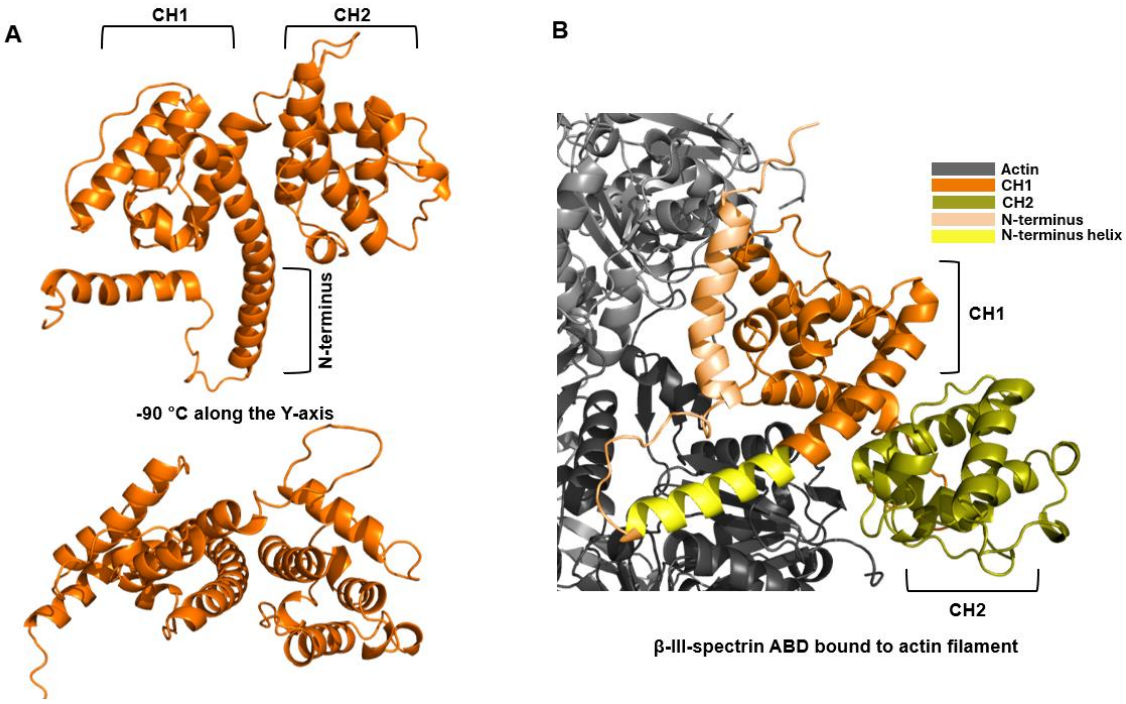

Figure 1.4. AlphaFold predicted structure of β-III-spectrin ABD bound to actin. (A) Structure of β-III-spectrin ABD showing that the ABD is comprised of tandem CH1 and CH2 subdomains. (B) Predicted structure of the ABD bound to actin showing that both CH1 (orange) and the experimentally resolved N-terminal helix (yellow) are directly bound to actin. The CH2 (olive) is predicted to be positioned away from actin. Notability, there are thirty-six amino acids preceding the N-terminal helix (wheat) never resolved experimentally; however, this structure is predicted to form another helix and is linked to the yellow N-terminal helix through a loop.

The affinity of the CH1-CH2 ABD for actin filaments is regulated by multiple mechanisms. Overlaying the cryo-EM structures of known ABDs, in their actin-bound states, with the corresponding crystal structures, in their unbound states, reveals the CH1-CH2 interface must shift to an open conformation (112, 113). This conformation change removes the steric hindrance exerted by CH2, thereby exposing the actin-binding surface on CH1. The ABD-localized SCA5 mutations disrupt this dynamic equilibrium between the open and the closed states of the CH1-CH2 interface. In particular, the CH2-localized L253P mutation, found at the interface of CH1-CH2 domains, was experimentally shown

to shift the equilibrium toward a more open conformation, enhancing actin-binding affinity by 1000-fold (110, 114). Furthermore, the affinity of ABD for actin can be modulated by the linker sequence that connects CH1 and CH2 (111, 115). Swapping the linker sequence of utrophin with that of dystrophin reduced the aberrant affinity of utrophin for actin, and vice versa. Additionally, replacing the linker sequence with that of filamin A resulted in a two-fold increase of utrophin binding affinity for actin. The actin-binding affinity of the CH1-CH2 ABD is further regulated by an N-terminal sequence preceding the CH1 domain. These N-terminal sequences are highly variable in length and amino acids among different actin-binding proteins, suggesting unique biological function. Truncation of the N-terminus reduces utrophin ABD affinity for actin (116). Additionally, the N-termini of both dystrophin and utrophin have been shown to impact the targeting of ABDs to various actin isoforms and structures in cultured cells (111, 117). Furthermore, multiple phosphorylation sites have been identified in the N-terminus of α-actinin, and were shown to modulate the binding of the ABD to actin (118). Similarly, the cryo-EM structure of the SCA5 mutant β-III-spectrin ABD bound to actin revealed a short α-helical sequence of sixteen amino acids within the N-terminus that directly interacts with actin filaments in addition to the CH1 domain (110). Truncating the N-terminus abolishes the affinity of the wild-type β-III-spectrin ABD for actin *in vitro*, indicating that the N-terminus is essential for binding. However, the functional significance of the N-terminus *in vivo* and its functional interaction with ABD-localized SCA5 mutations has yet to be explored.

1.3 Spectrin-Repeat Domains

A common feature of the spectrin family of proteins, including α-spectrin, β-spectrin, α-actinin, utrophin and dystrophin, is the presence of multiple spectrin-repeat domains (SRDs) arranged in tandem (119). Each SRD consists of 106-114 amino acids that form a coiled-coil structure comprised of three anti-parallel α-helices (termed helices A, B, and C), **Figure 1.5A**. Within each SRDs, the three α-helices are connected by flexible, unstructured loops. However, two consecutive SRDs are connected by an extended α-helix linking helix C of the first SRD with helix A of the next SRD, **Figure 1.5B**. These elongated coiled-coil helices confer an overall rod-shape structure to the protein. The amino acid sequence is not highly conserved among different SRDs, but the overall secondary and tertiary structures are similar. Furthermore, the number of SRDs varies among different proteins, ranging from 4 to 72. This range in SRD numbers is likely due to the duplication events that led to the addition of multiple SRDs to the four SRDs of the ancestral α-actinin protein (120). In particular, α-actinin shares similarity with both α-spectrin and β-spectrin. Alpha-actinin is comprised of an N-terminal tandem CH1-CH2 ABD, central four SRDs, and C-terminal EF-hand domain. Evolution progression added multiple SRDs to α-actinin. These duplication events resulted in an elongated protein that separated into α-spectrin and β-spectrin. Alpha-spectrin contains twenty-one SRDs fused to a C-terminal EF-hand domain, similar to the α-actinin C-terminus. On the other hand, β-spectrin consists of an N-terminal ABD followed by seventeen SRDs, which is similar to the α-actinin N-terminus. SRDs 20-21 of α-spectrin and SRDs 1-2 of β-spectrin are homologous to α-actinin SRDs 3-4 and SRDs 1-2, respectively.

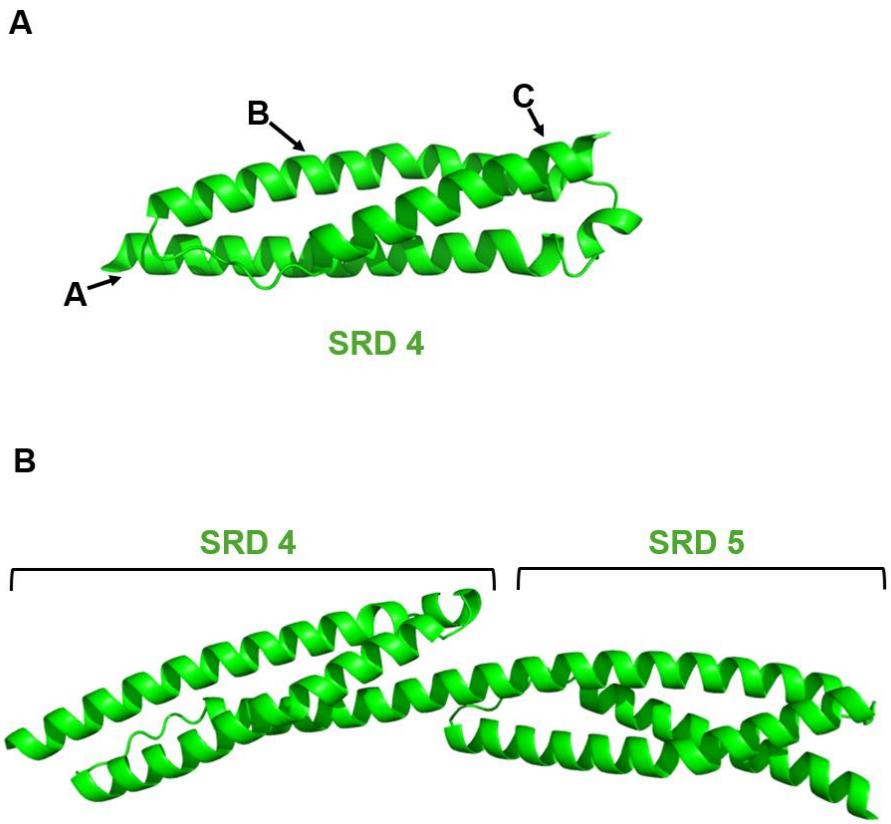

Figure 1.5. Structure of the β-III-spectrin SRDs. (A) AlphaFold structure of β-III-spectrin SRD4 showing the typical three α-helices comprising the overall structure of SRDs. (B) Predicted structure of β-III-spectrin SRD4 and SRD5 showing the helical linker connecting both SRDs.

Our understanding about the function of the SRDs has greatly expanded over time. Traditionally, SRDs were considered to be a molecular spacer shaping the architecture of the spectrin-actin cytoskeleton (121). Due to their flexible conformation, the SRDs were also thought to confer mechanical resilience to the plasma membrane, allowing erythrocyte deformation as they pass through small capillaries (122, 123). Furthermore, SRDs have been proposed to be a docking platform for multiple membrane-associated proteins including transmembrane, adaptor, and signal transduction proteins (119). β-spectrin SRDs 15-16 are well established to bind the adaptor protein, ankyrin.

Ankyrin directly binds diverse transmembrane proteins. Thus, β-spectrin binding to ankyrin provides a link between the spectrin-actin cytoskeleton and the plasma membrane (40). In addition, SRDs 1-2 of β-spectrin binds to α-spectrin SRDs 21-20, to nucleate α/β-spectrin heterodimer formation (124, 125), **Figure 1.6**. This nucleation of the dimer is thought to force the remaining complementary SRDs along the length of the proteins to weakly interact further enhancing the overall stability of the α/β-spectrin dimer. Similarly, SRDs 1-2 of one α-actinin interact with SRDs 3-4 of another α-actinin forming an antiparallel homodimer (126). Moreover, SRD17 of β-spectrin interacts with SRD1 of α-spectrin to form α-β-spectrin tetramer (127, 128). The SRDs were also found to interact with actin or regulate the ABD affinity for actin. Specifically, SRD1 was shown to enhance the affinity of β-spectrin ABD for actin (129). In dystrophin, SRDs 11-17 bind directly to actin filaments and increases the overall affinity of dystrophin for actin (130). SCA5 mutations target multiple SRD domains emphasizing the significance of the SRDs to the function of β-III-spectrin in neurons. However, the protein-protein interactions of various SRDs in β-III-spectrin are poorly understood and thus hinder our understanding of SCA5 disease mechanisms.

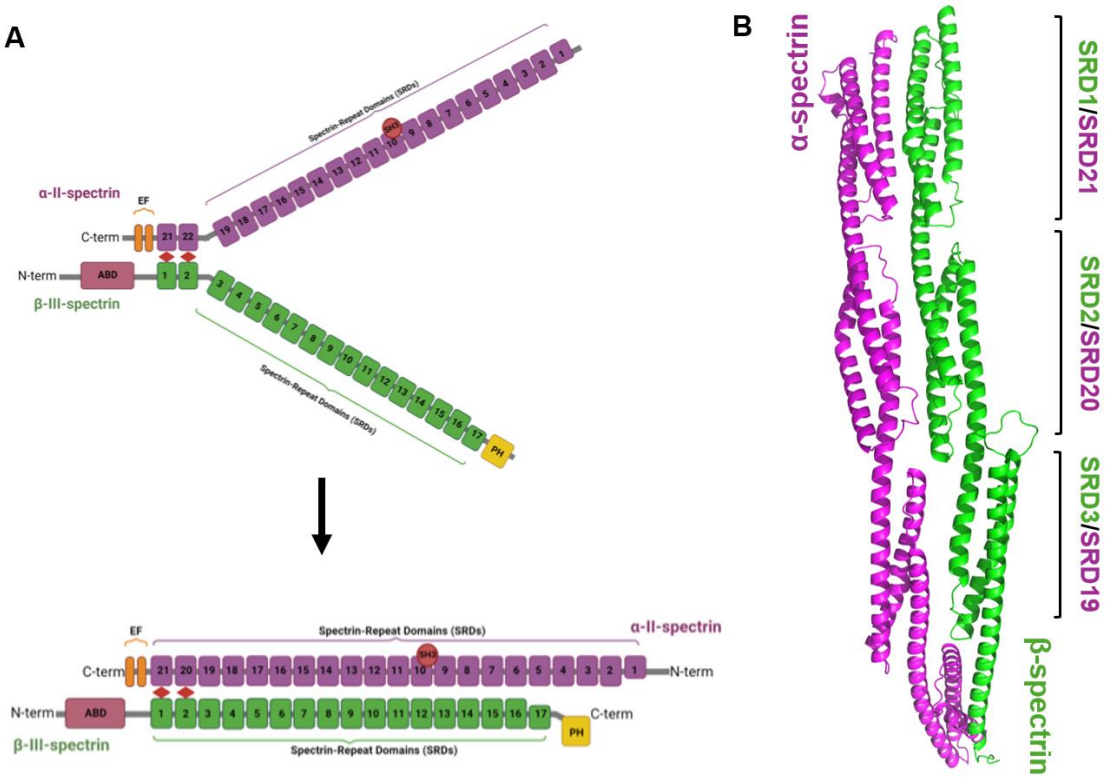

Figure 1.6. α/β-spectrin heterodimer. (A) Diagram showing the α/β-spectrin dimer is nucleated first by the interaction of SRDs 1-2 of β-spectrin with SRDs 21-20 of α-spectrin. The remaining repeats come together via weak interaction along the length of the protein. (B) AlphaFold prediction showing the N-terminal SRDs 1-4 of β-III-spectrin bound to the C-terminal SRDs 18-21 of α-II-spectrin.

1.4 Dissertation Aims

This dissertation aims to understand the molecular function of multiple domains of β-III-spectrin and how β-III-spectrin function is disrupted by SCA5 mutations. One goal is to determine the significance of the N-terminus to high-affinity actin binding caused by an ABD-localized SCA5 missense mutation, L253P. Further, my work seeks to understand the significance of the N-terminus to β-spectrin function and SCA5 neurotoxicity in *vivo* using *Drosophila.* A second research goal is to reveal the molecular consequences of SRD-localized SCA5 mutations to β-III-spectrin function. In particular,

my research seeks to shed light on the molecular impacts of an early onset SCA5 mutation, R480W, in β-III-spectrin SRD2 and a late onset SCA5 mutation, E532_M544del, in SRD3. By characterizing the molecular consequences of SCA5 mutations across multiple functional domains of β-III-spectrin, targeted therapies for SCA5 may be developed to address specific molecular mechanisms underlying the disease.

References

1. Marchesi, V. T., andSteers, E., Jr. (1968) Selective solubilization of a protein component of the red cell membrane Science **159**, 203-204 10.1126/science.159.3811.203
2. Marchesi, V. T. (1979) Spectrin: present status of a putative cyto-skeletal protein of the red cell membrane J Membr Biol **51**, 101-131 10.1007/bf01869164
3. Levine, J., Skene, P., andWillard, M. (1981) GAPs and fodrin: Novel axonally transported proteins Trends in Neurosciences **4**, 273-277 10.1016/0166-2236(81)90086-2
4. Goodman, S. R., Zagon, I. S., andKulikowski, R. R. (1981) Identification of a spectrin-like protein in nonerythroid cells Proceedings of the National Academy of Sciences **78**, 7570-7574,
5. Burridge, K., Kelly, T., andMangeat, P. (1982) Nonerythrocyte spectrins: actin-membrane attachment proteins occurring in many cell types The Journal of cell biology **95**, 478-486,

6. Bennett, V., Davis, J., andFowler, W. E. (1982) Brain spectrin, a membrane-associated protein related in structure and function to erythrocyte spectrin Nature **299**, 126-131,

7. Glenney Jr, J. R., andGlenney, P. (1983) Fodrin is the general spectrin-like protein found in most cells whereas spectrin and the TW protein have a restricted distribution Cell **34**, 503-512,

8. Goodman, S. R., andZagon, I. S. (1984) Brain spectrin: a review Brain research bulletin **13**, 813-832,

9. Cianci, C. D., Zhang, Z., Pradhan, D., andMorrow, J. S. (1999) Brain and muscle express a unique alternative transcript of αII spectrin Biochemistry **38**, 15721-15730,

10. Zhang, Y., Chen, K., Sloan, S. A., Bennett, M. L., Scholze, A. R., O'Keeffe, S. *et al.* (2014) An RNA-sequencing transcriptome and splicing database of glia, neurons, and vascular cells of the cerebral cortex Journal of neuroscience **34**, 11929-11947,

11. Sahr, K., Laurila, P., Kotula, L., Scarpa, A., Coupal, E., Leto, T. *et al.* (1990) The complete cDNA and polypeptide sequences of human erythroid alpha-spectrin Journal of Biological Chemistry **265**, 4434-4443,

12. Moon, R. T., andMcMahon, A. (1990) Generation of diversity in nonerythroid spectrins. Multiple polypeptides are predicted by sequence analysis of cDNAs encompassing the coding region of human nonerythroid alpha-spectrin Journal of Biological Chemistry **265**, 4427-4433,

13. Winkelmann, J. C., Chang, J. G., Tse, W., Scarpa, A. L., Marchesi, V. T., andForget, B. G. (1990) Full-length sequence of the cDNA for human erythroid beta-spectrin Journal of Biological Chemistry **265**, 11827-11832,

14. Winkelmann, J. C., andForget, B. G. (1993) Erythroid and nonerythroid spectrins,

15. Machnicka, B., Grochowalska, R., Bogusławska, D. M., Sikorski, A. F., andLecomte, M. C. (2012) Spectrin-based skeleton as an actor in cell signaling Cell Mol Life Sci **69**, 191-201 10.1007/s00018-011-0804-5

16. Ohara, O., Ohara, R., Yamakawa, H., Nakajima, D., andNakayama, M. (1998) Characterization of a new beta-spectrin gene which is predominantly expressed in brain Brain Res Mol Brain Res **57**, 181-192 10.1016/s0169-328x(98)00068-0

17. Hu, R.-J., Watanabe, M., andBennett, V. (1992) Characterization of human brain cDNA encoding the general isoform of beta-spectrin Journal of Biological Chemistry **267**, 18715-18722,

18. Stabach, P. R., andMorrow, J. S. (2000) Identification and Characterization of βV Spectrin, a Mammalian Ortholog of Drosophila βHSpectrin* 210 Journal of Biological Chemistry **275**, 21385-21395,

19. Byers, T. J., Dubreuil, R., Branton, D., Kiehart, D. P., andGoldstein, L. (1987) Drosophila spectrin. II. Conserved features of the alpha-subunit are revealed by analysis of cDNA clones and fusion proteins The Journal of cell biology **105**, 2103-2110,

20. Dubreuil, R. R., Byers, T. J., Sillman, A. L., Bar-Zvi, D., Goldstein, L., andBranton, D. (1989) The complete sequence of Drosophila alpha-spectrin:

conservation of structural domains between alpha-spectrins and alpha-actinin The Journal of cell biology **109**, 2197-2205,

21. Byers, T. J., Brandin, E., Lue, R. A., Winograd, E., andBranton, D. (1992) The complete sequence of Drosophila beta-spectrin reveals supra-motifs comprising eight 106-residue segments Proceedings of the National Academy of Sciences **89**, 6187-6191,

22. McKeown, C., Praitis, V., andAustin, J. (1998) sma-1 encodes a βH-spectrin homolog required for Caenorhabditis elegans morphogenesis Development **125**, 2087-2098,

23. Huang, C. Y.-M., Zhang, C., Ho, T. S.-Y., Oses-Prieto, J., Burlingame, A. L., Lalonde, J. *et al.* (2017) αII spectrin forms a periodic cytoskeleton at the axon initial segment and is required for nervous system function Journal of Neuroscience **37**, 11311-11322,

24. Papal, S., Cortese, M., Legendre, K., Sorusch, N., Dragavon, J., Sahly, I. *et al.* (2013) The giant spectrin βV couples the molecular motors to phototransduction and Usher syndrome type I proteins along their trafficking route Human Molecular Genetics **22**, 3773-3788 10.1093/hmg/ddt228

25. Legendre, K., Safieddine, S., Küssel-Andermann, P., Petit, C., andEl-Amraoui, A. (2008) αII-βV spectrin bridges the plasma membrane and cortical lattice in the lateral wall of the auditory outer hair cells Journal of Cell Science **121**, 3347-3356 10.1242/jcs.028134

26. Morrow, J. S., andStankewich, M. C. (2021) The Spread of Spectrin in Ataxia and Neurodegenerative Disease J Exp Neurol **2**, 131-139,

27. Stankewich, M. C., Peters, L. L., andMorrow, J. S. (2024) The loss of βI spectrin alters synaptic size and composition in the ja/ja mouse Frontiers in Neuroscience **18**, 10.3389/fnins.2024.1415115

28. Galiano, M. R., Jha, S., Ho, T. S.-Y., Zhang, C., Ogawa, Y., Chang, K.-J. *et al.* (2012) A distal axonal cytoskeleton forms an intra-axonal boundary that controls axon initial segment assembly Cell **149**, 1125-1139,

29. Zhang, R., Zhang, C., Zhao, Q., andLi, D. (2013) Spectrin: structure, function and disease Sci China Life Sci **56**, 1076-1085 10.1007/s11427-013-4575-0

30. Stankewich, M. C., Gwynn, B., Ardito, T., Ji, L., Kim, J., Robledo, R. F. *et al.* (2010) Targeted deletion of βIII spectrin impairs synaptogenesis and generates ataxic and seizure phenotypes Proceedings of the National Academy of Sciences **107**, 6022-6027,

31. Berghs, S., Aggujaro, D., Dirkx Jr, R., Maksimova, E., Stabach, P., Hermel, J.-M. *et al.* (2000) βIV spectrin, a new spectrin localized at axon initial segments and nodes of Ranvier in the central and peripheral nervous system The Journal of cell biology **151**, 985-1002,

32. Macias, M. J., Musacchio, A., Ponstingl, H., Nilges, M., Saraste, M., andOschkinat, H. (1994) Structure of the pleckstrin homology domain from β-spectrin Nature **369**, 675-677 10.1038/369675a0

33. Das, A., Base, C., Manna, D., Cho, W., andDubreuil, R. R. (2008) Unexpected complexity in the mechanisms that target assembly of the spectrin cytoskeleton J Biol Chem **283**, 12643-12653 10.1074/jbc.M800094200

34. Mishra, L., Cai, T., Yu, P., Monga, S. P., andMishra, B. (1999) Elf3 encodes a novel 200-kD beta-spectrin: role in liver development Oncogene **18**, 353-364 10.1038/sj.onc.1202313

35. Xu, K., Zhong, G., andZhuang, X. (2013) Actin, spectrin, and associated proteins form a periodic cytoskeletal structure in axons Science **339**, 452-456 10.1126/science.1232251

36. Shotton, D. M., Burke, B. E., andBranton, D. (1979) The molecular structure of human erythrocyte spectrin. Biophysical and electron microscopic studies J Mol Biol **131**, 303-329 10.1016/0022-2836(79)90078-0

37. Liu, S. C., Derick, L. H., andPalek, J. (1987) Visualization of the hexagonal lattice in the erythrocyte membrane skeleton J Cell Biol **104**, 527-536 10.1083/jcb.104.3.527

38. Han, B., Zhou, R., Xia, C., andZhuang, X. (2017) Structural organization of the actin-spectrin-based membrane skeleton in dendrites and soma of neurons Proc Natl Acad Sci U S A **114**, E6678-e6685 10.1073/pnas.1705043114

39. Wang, D.-S., andShaw, G. (1995) The association of the C-terminal region of β1ΣII spectrin to brain membranes is mediated by a pH domain, does not require membrane proteins, and coincides with a inositol-1, 4, 5 trisphosphate binding site Biochemical and biophysical research communications **217**, 608-615,

40. Bennett, V., andBaines, A. J. (2001) Spectrin and ankyrin-based pathways: metazoan inventions for integrating cells into tissues Physiol Rev **81**, 1353-1392 10.1152/physrev.2001.81.3.1353

41. Hammarlund, M., Jorgensen, E. M., andBastiani, M. J. (2007) Axons break in animals lacking beta-spectrin J Cell Biol **176**, 269-275 10.1083/jcb.200611117

42. Pielage, J., Fetter, R. D., andDavis, G. W. (2005) Presynaptic spectrin is essential for synapse stabilization Curr Biol **15**, 918-928 10.1016/j.cub.2005.04.030

43. Avery, A. W., Thomas, D. D., andHays, T. S. (2017) β-III-spectrin spinocerebellar ataxia type 5 mutation reveals a dominant cytoskeletal mechanism that underlies dendritic arborization Proceedings of the National Academy of Sciences **114**, E9376-E9385 10.1073/pnas.1707108114

44. Perkins, E. M., Clarkson, Y. L., Sabatier, N., Longhurst, D. M., Millward, C. P., Jack, J. *et al.* (2010) Loss of beta-III spectrin leads to Purkinje cell dysfunction recapitulating the behavior and neuropathology of spinocerebellar ataxia type 5 in humans J Neurosci **30**, 4857-4867 10.1523/jneurosci.6065-09.2010

45. Gao, Y., Perkins, E. M., Clarkson, Y. L., Tobia, S., Lyndon, A. R., Jackson, M. *et al.* (2011) β-III spectrin is critical for development of purkinje cell dendritic tree and spine morphogenesis J Neurosci **31**, 16581-16590 10.1523/jneurosci.3332-11.2011

46. Efimova, N., Korobova, F., Stankewich, M. C., Moberly, A. H., Stolz, D. B., Wang, J. *et al.* (2017) βIII Spectrin Is Necessary for Formation of the Constricted Neck of Dendritic Spines and Regulation of Synaptic Activity in Neurons The Journal of Neuroscience **37**, 6442-6459 10.1523/jneurosci.3520-16.2017

47. Yang, Y., Lacas-Gervais, S., Morest, D. K., Solimena, M., andRasband, M. N. (2004) βIV spectrins are essential for membrane stability and the molecular organization of nodes of Ranvier Journal of Neuroscience **24**, 7230-7240,

48. Komada, M., andSoriano, P. (2002) βIV-spectrin regulates sodium channel clustering through ankyrin-G at axon initial segments and nodes of Ranvier The Journal of cell biology **156**, 337-348,

49. Liu, C.-H., andRasband, M. N. (2019) Axonal Spectrins: Nanoscale Organization, Functional Domains and Spectrinopathies Frontiers in Cellular Neuroscience **13**, 10.3389/fncel.2019.00234

50. Jackson, M., Song, W., Liu, M.-Y., Jin, L., Dykes-Hoberg, M., Lin, C.-l. G. *et al.* (2001) Modulation of the neuronal glutamate transporter EAAT4 by two interacting proteins Nature **410**, 89-93 10.1038/35065091

51. Lorenzo, D. N., Badea, A., Zhou, R., Mohler, P. J., Zhuang, X., andBennett, V. (2019) βII-spectrin promotes mouse brain connectivity through stabilizing axonal plasma membranes and enabling axonal organelle transport Proc Natl Acad Sci U S A **116**, 15686-15695 10.1073/pnas.1820649116

52. Whitney, T., Yelena, D. M., Bernard, G. F., andPatrick, G. G. (2008) Nonsense mutations of the α-spectrin gene in hereditary pyropoikilocytosis Haematologica **93**, 1752-1754 10.3324/haematol.13639

53. Eber, S., andLux, S. E. (2004) Hereditary spherocytosis--defects in proteins that connect the membrane skeleton to the lipid bilayer Semin Hematol **41**, 118-141 10.1053/j.seminhematol.2004.01.002

54. Narla, J., andMohandas, N. (2017) Red cell membrane disorders Int J Lab Hematol **39 Suppl 1**, 47-52 10.1111/ijlh.12657

55. Griswold, A. J., Ma, D., Sacharow, S. J., Robinson, J. L., Jaworski, J. M., Wright, H. H. *et al.* (2011) A de novo 1.5 Mb microdeletion on chromosome 14q23.2-23.3

in a patient with autism and spherocytosis Autism Research **4**, 221-227 https://doi.org/10.1002/aur.186

56. McCann, S. R., andJacob, H. S. (1976) Spinal Cord Disease in Hereditary Spherocytosis: Report of Two Cases With a Hypothesized Common Mechanism for Neurologic and Red Cell Abnormalities Blood **48**, 259-263 https://doi.org/10.1182/blood.V48.2.259.259

57. Lybaek, H., Øyen, N., Fauske, L., andHouge, G. (2008) A 2.1 Mb deletion adjacent but distal to a 14q21q23 paracentric inversion in a family with spherocytosis and severe learning difficulties Clin Genet **74**, 553-559 10.1111/j.1399-0004.2008.01072.x

58. Beijer, D., Deconinck, T., De Bleecker, J. L., Dotti, M. T., Malandrini, A., Urtizberea, J. A. *et al.* (2019) Nonsense mutations in alpha-II spectrin in three families with juvenile onset hereditary motor neuropathy Brain **142**, 2605-2616 10.1093/brain/awz216

59. Saitsu, H., Tohyama, J., Kumada, T., Egawa, K., Hamada, K., Okada, I. *et al.* (2010) Dominant-negative mutations in alpha-II spectrin cause West syndrome with severe cerebral hypomyelination, spastic quadriplegia, and developmental delay Am J Hum Genet **86**, 881-891 10.1016/j.ajhg.2010.04.013

60. Writzl, K., Primec, Z. R., Stražišar, B. G., Osredkar, D., Pečarič-Meglič, N., Kranjc, B. S. *et al.* (2012) Early onset West syndrome with severe hypomyelination and coloboma-like optic discs in a girl with SPTAN1 mutation Epilepsia **53**, e106-e110 https://doi.org/10.1111/j.1528-1167.2012.03437.x

61. Hamdan, F. F., Gauthier, J., Araki, Y., Lin, D. T., Yoshizawa, Y., Higashi, K. *et al.* (2011) Excess of de novo deleterious mutations in genes associated with glutamatergic systems in nonsyndromic intellectual disability Am J Hum Genet **88**, 306-316 10.1016/j.ajhg.2011.02.001

62. Tohyama, J., Nakashima, M., Nabatame, S., Gaik-Siew, C. n., Miyata, R., Rener-Primec, Z. *et al.* (2015) SPTAN1 encephalopathy: distinct phenotypes and genotypes Journal of Human Genetics **60**, 167-173 10.1038/jhg.2015.5

63. Syrbe, S., Harms, F. L., Parrini, E., Montomoli, M., Mütze, U., Helbig, K. L. *et al.* (2017) Delineating SPTAN1 associated phenotypes: from isolated epilepsy to encephalopathy with progressive brain atrophy Brain **140**, 2322-2336 10.1093/brain/awx195

64. Wang, Y., Ji, T., Nelson, A. D., Glanowska, K., Murphy, G. G., Jenkins, P. M. *et al.* (2018) Critical roles of αII spectrin in brain development and epileptic encephalopathy J Clin Invest **128**, 760-773 10.1172/jci95743

65. Cousin, M. A., Creighton, B. A., Breau, K. A., Spillmann, R. C., Torti, E., Dontu, S. *et al.* (2021) Pathogenic SPTBN1 variants cause an autosomal dominant neurodevelopmental syndrome Nat Genet **53**, 1006-1021 10.1038/s41588-021-00886-z

66. Ikeda, Y., Dick, K. A., Weatherspoon, M. R., Gincel, D., Armbrust, K. R., Dalton, J. C. *et al.* (2006) Spectrin mutations cause spinocerebellar ataxia type 5 Nat Genet **38**, 184-190 10.1038/ng1728

67. Bian, X., Wang, S., Jin, S., Xu, S., Zhang, H., Wang, D. *et al.* (2021) Two novel missense variants in SPTBN2 likely associated with spinocerebellar ataxia type 5 Neurol Sci **42**, 5195-5203 10.1007/s10072-021-05204-3

68. Liu, L. Z., Ren, M., Li, M., Ren, Y. T., Sun, B., Sun, X. S. *et al.* (2016) A Novel Missense Mutation in the Spectrin Beta Nonerythrocytic 2 Gene Likely Associated with Spinocerebellar Ataxia Type 5 Chin Med J (Engl) **129**, 2516-2517 10.4103/0366-6999.191834

69. Cho, E., andFogel, B. L. (2013) A Family with Spinocerebellar Ataxia Type 5 Found to Have a Novel Missense Mutation within a SPTBN2 Spectrin Repeat The Cerebellum **12**, 162-164 10.1007/s12311-012-0408-0

70. Fogel, B. L., Lee, H., Deignan, J. L., Strom, S. P., Kantarci, S., Wang, X. *et al.* (2014) Exome sequencing in the clinical diagnosis of sporadic or familial cerebellar ataxia JAMA Neurol **71**, 1237-1246 10.1001/jamaneurol.2014.1944

71. Wang, Y., Koh, K., Miwa, M., Yamashiro, N., Shindo, K., andTakiyama, Y. (2014) A Japanese SCA5 family with a novel three-nucleotide in-frame deletion mutation in the SPTBN2 gene: a clinical and genetic study J Hum Genet **59**, 569-573 10.1038/jhg.2014.74

72. Lise, S., Clarkson, Y., Perkins, E., Kwasniewska, A., Sadighi Akha, E., Schnekenberg, R. P. *et al.* (2012) Recessive mutations in SPTBN2 implicate β-III spectrin in both cognitive and motor development PLoS Genet **8**, e1003074 10.1371/journal.pgen.1003074

73. Elsayed, S. M., Heller, R., Thoenes, M., Zaki, M. S., Swan, D., Elsobky, E. *et al.* (2014) Autosomal dominant SCA5 and autosomal recessive infantile SCA are

allelic conditions resulting from SPTBN2 mutations European Journal of Human Genetics **22**, 286-288 10.1038/ejhg.2013.150

74. Jacob, F. D., Ho, E. S., Martinez-Ojeda, M., Darras, B. T., andKhwaja, O. S. (2013) Case of infantile onset spinocerebellar ataxia type 5 J Child Neurol **28**, 1292-1295 10.1177/0883073812454331

75. Parolin Schnekenberg, R., Perkins, E. M., Miller, J. W., Davies, W. I., D'Adamo, M. C., Pessia, M. *et al.* (2015) De novo point mutations in patients diagnosed with ataxic cerebral palsy Brain **138**, 1817-1832 10.1093/brain/awv117

76. Nuovo, S., Micalizzi, A., D'Arrigo, S., Ginevrino, M., Biagini, T., Mazza, T. *et al.* (2018) Between SCA5 and SCAR14: delineation of the SPTBN2 p.R480W-associated phenotype European Journal of Human Genetics **26**, 928-929 10.1038/s41431-018-0158-7

77. Mizuno, T., Kashimada, A., Nomura, T., Moriyama, K., Yokoyama, H., Hasegawa, S. *et al.* (2019) Infantile-onset spinocerebellar ataxia type 5 associated with a novel SPTBN2 mutation: A case report Brain Dev **41**, 630-633 10.1016/j.braindev.2019.03.002

78. Accogli, A., St-Onge, J., Addour-Boudrahem, N., Lafond-Lapalme, J., Laporte, A. D., Rouleau, G. A. *et al.* (2020) Heterozygous Missense Pathogenic Variants Within the Second Spectrin Repeat of SPTBN2 Lead to Infantile-Onset Cerebellar Ataxia J Child Neurol **35**, 106-110 10.1177/0883073819878917

79. Nicita, F., Nardella, M., Bellacchio, E., Alfieri, P., Terrone, G., Piccini, G. *et al.* (2019) Heterozygous missense variants of SPTBN2 are a frequent cause of congenital cerebellar ataxia Clin Genet **96**, 169-175 10.1111/cge.13562

80. Rea, G., Tirupathi, S., Williams, J., Clouston, P., andMorrison, P. J. (2020) Infantile Onset of Spinocerebellar Ataxia Type 5 (SCA-5) in a 6 Month Old with Ataxic Cerebral Palsy The Cerebellum **19**, 161-163 10.1007/s12311-019-01085-7

81. Zonta, A., Brussino, A., Dentelli, P., andBrusco, A. (2020) A novel case of congenital spinocerebellar ataxia 5: further support for a specific phenotype associated with the p.(Arg480Trp) variant in SPTBN2 BMJ Case Rep **13**, 10.1136/bcr-2020-238108

82. Sancho, P., Andrés-Bordería, A., Gorría-Redondo, N., Llano, K., Martínez-Rubio, D., Yoldi-Petri, M. E. *et al.* (2021) Expanding the β-III Spectrin-Associated Phenotypes toward Non-Progressive Congenital Ataxias with Neurodegeneration International Journal of Molecular Sciences **22**, 2505 10.3390/ijms22052505

83. Romaniello, R., Citterio, A., Panzeri, E., Arrigoni, F., De Rinaldis, M., Trabacca, A. *et al.* (2021) Novel SPTBN2 gene mutation and first intragenic deletion in early onset spinocerebellar ataxia type 5 Annals of Clinical and Translational Neurology **8**, 956-963 10.1002/acn3.51345

84. Ranum, L. P., Schut, L. J., Lundgren, J. K., Orr, H. T., andLivingston, D. M. (1994) Spinocerebellar ataxia type 5 in a family descended from the grandparents of President Lincoln maps to chromosome 11 Nat Genet **8**, 280-284 10.1038/ng1194-280

85. Stevanin, G., Herman, A., Brice, A., andDürr, A. (1999) Clinical and MRI findings in spinocerebellar ataxia type 5 Neurology **53**, 1355-1357 10.1212/wnl.53.6.1355

86. Bürk, K., Zühlke, C., König, I. R., Ziegler, A., Schwinger, E., Globas, C. *et al.* (2004) Spinocerebellar ataxia type 5: clinical and molecular genetic features of a German kindred Neurology **62**, 327-329 10.1212/01.wnl.0000103293.63340.c1

87. Knierim, E., Gill, E., Seifert, F., Morales-Gonzalez, S., Unudurthi, S. D., Hund, T. J. *et al.* (2017) A recessive mutation in beta-IV-spectrin (SPTBN4) associates with congenital myopathy, neuropathy, and central deafness Hum Genet **136**, 903-910 10.1007/s00439-017-1814-7

88. Häusler, M. G., Begemann, M., Lidov, H. G., Kurth, I., Darras, B. T., andElbracht, M. (2020) A novel homozygous splice-site mutation in the SPTBN4 gene causes axonal neuropathy without intellectual disability European Journal of Medical Genetics **63**, 103826 https://doi.org/10.1016/j.ejmg.2019.103826

89. Tejwani, L., andLim, J. (2020) Pathogenic mechanisms underlying spinocerebellar ataxia type 1 Cell Mol Life Sci **77**, 4015-4029 10.1007/s00018-020-03520-z

90. Dick, K. A., Ikeda, Y., Day, J. W., andRanum, L. P. (2012) Spinocerebellar ataxia type 5 Handb Clin Neurol **103**, 451-459 10.1016/b978-0-444-51892-7.00028-0

91. Rüb, U., Schöls, L., Paulson, H., Auburger, G., Kermer, P., Jen, J. C. *et al.* (2013) Clinical features, neurogenetics and neuropathology of the polyglutamine spinocerebellar ataxias type 1, 2, 3, 6 and 7 Prog Neurobiol **104**, 38-66 10.1016/j.pneurobio.2013.01.001

92. Synofzik, M., andNémeth, A. H. (2018) Recessive ataxias Handb Clin Neurol **155**, 73-89 10.1016/b978-0-444-64189-2.00005-6

93. Bertini, E., Zanni, G., andBoltshauser, E. (2018) Nonprogressive congenital ataxias Handb Clin Neurol **155**, 91-103 10.1016/b978-0-444-64189-2.00006-8

94. Ashizawa, T., Figueroa, K. P., Perlman, S. L., Gomez, C. M., Wilmot, G. R., Schmahmann, J. D. *et al.* (2013) Clinical characteristics of patients with spinocerebellar ataxias 1, 2, 3 and 6 in the US; a prospective observational study Orphanet J Rare Dis **8**, 177 10.1186/1750-1172-8-177

95. Shakkottai, V. G. (2014) Physiologic Changes Associated with Cerebellar Dystonia The Cerebellum **13**, 637-644 10.1007/s12311-014-0572-5

96. Paulson, H. L., Shakkottai, V. G., Clark, H. B., andOrr, H. T. (2017) Polyglutamine spinocerebellar ataxias - from genes to potential treatments Nat Rev Neurosci **18**, 613-626 10.1038/nrn.2017.92

97. Müller, U. (2021) Spinocerebellar ataxias (SCAs) caused by common mutations neurogenetics **22**, 235-250 10.1007/s10048-021-00662-5

98. Seidel, K., Siswanto, S., Brunt, E. R., den Dunnen, W., Korf, H. W., andRüb, U. (2012) Brain pathology of spinocerebellar ataxias Acta Neuropathol **124**, 1-21 10.1007/s00401-012-1000-x

99. Koeppen, A. H. (2011) Friedreich's ataxia: pathology, pathogenesis, and molecular genetics J Neurol Sci **303**, 1-12 10.1016/j.jns.2011.01.010

100. Chen, D.-H., Raskind, W. H., andBird, T. D. (2012) Chapter 36 - Spinocerebellar ataxia type 14 In Handbook of Clinical Neurology, Subramony SH, Dürr A, eds. Elsevier, 555-559

101. Denha, S., DeLaet, N., Abukamil, A., Alexopoulos, A., Keller, A., Atang, A. *et al.* (2024) Molecular consequences of SCA5 mutations in the spectrin-repeat

domains of beta-III-spectrin bioRxiv 2024.2009.2017.613313 10.1101/2024.09.17.613313

102. Ghanekar, S. D., Kuo, S. H., Staffetti, J. S., andZesiewicz, T. A. (2022) Current and emerging treatment modalities for spinocerebellar ataxias Expert Rev Neurother **22**, 101-114 10.1080/14737175.2022.2029703

103. Rebbeck, R. T., Andrick, A. K., Denha, S. A., Svensson, B., Guhathakurta, P., Thomas, D. D. *et al.* (2021) Novel drug discovery platform for spinocerebellar ataxia, using fluorescence technology targeting β-III-spectrin J Biol Chem **296**, 100215 10.1074/jbc.RA120.015417

104. Guhathakurta, P., Rebbeck, R. T., Denha, S. A., Keller, A. R., Carter, A. L., Atang, A. E. *et al.* (2023) Early-phase drug discovery of β-III-spectrin actin-binding modulators for treatment of spinocerebellar ataxia type 5 J Biol Chem **299**, 102956 10.1016/j.jbc.2023.102956

105. García-Ponce, A., Citalán-Madrid, A. F., Velázquez-Avila, M., Vargas-Robles, H., andSchnoor, M. (2015) The role of actin-binding proteins in the control of endothelial barrier integrity Thromb Haemost **113**, 20-36 10.1160/th14-04-0298

106. Korenbaum, E., andRivero, F. (2002) Calponin homology domains at a glance J Cell Sci **115**, 3543-3545 10.1242/jcs.00003

107. Bañuelos, S., Saraste, M., andDjinović Carugo, K. (1998) Structural comparisons of calponin homology domains: implications for actin binding Structure **6**, 1419-1431 10.1016/s0969-2126(98)00141-5

108. Broderick, M. J., andWinder, S. J. (2002) Towards a complete atomic structure of spectrin family proteins J Struct Biol **137**, 184-193 10.1006/jsbi.2002.4465

109. Abramson, J., Adler, J., Dunger, J., Evans, R., Green, T., Pritzel, A. *et al.* (2024) Accurate structure prediction of biomolecular interactions with AlphaFold 3 Nature **630**, 493-500 10.1038/s41586-024-07487-w

110. Avery, A. W., Fealey, M. E., Wang, F., Orlova, A., Thompson, A. R., Thomas, D. D. *et al.* (2017) Structural basis for high-affinity actin binding revealed by a β-III-spectrin SCA5 missense mutation Nat Commun **8**, 1350 10.1038/s41467-017-01367-w

111. Harris, A. R., Belardi, B., Jreij, P., Wei, K., Shams, H., Bausch, A. *et al.* (2019) Steric regulation of tandem calponin homology domain actin-binding affinity Mol Biol Cell **30**, 3112-3122 10.1091/mbc.E19-06-0317

112. Galkin, V. E., Orlova, A., Salmazo, A., Djinovic-Carugo, K., andEgelman, E. H. (2010) Opening of tandem calponin homology domains regulates their affinity for F-actin Nat Struct Mol Biol **17**, 614-616 10.1038/nsmb.1789

113. Iwamoto, D. V., Huehn, A., Simon, B., Huet-Calderwood, C., Baldassarre, M., Sindelar, C. V. *et al.* (2018) Structural basis of the filamin A actin-binding domain interaction with F-actin Nat Struct Mol Biol **25**, 918-927 10.1038/s41594-018-0128-3

114. Avery, A. W., Crain, J., Thomas, D. D., andHays, T. S. (2016) A human β-III-spectrin spinocerebellar ataxia type 5 mutation causes high-affinity F-actin binding Sci Rep **6**, 21375 10.1038/srep21375

115. Bandi, S., Singh, S. M., andMallela, K. M. (2015) Interdomain Linker Determines Primarily the Structural Stability of Dystrophin and Utrophin Tandem Calponin-

Homology Domains Rather than Their Actin-Binding Affinity Biochemistry **54**, 5480-5488 10.1021/acs.biochem.5b00741

116. Singh, S. M., Bandi, S., andMallela, K. M. G. (2017) The N-Terminal Flanking Region Modulates the Actin Binding Affinity of the Utrophin Tandem Calponin-Homology Domain Biochemistry **56**, 2627-2636 10.1021/acs.biochem.6b01117

117. Upadhyay, V., Bandi, S., Panja, S., Saba, L., andMallela, K. M. G. (2020) Tissue-Specificity of Dystrophin–Actin Interactions: Isoform-Specific Thermodynamic Stability and Actin-Binding Function of Tandem Calponin-Homology Domains ACS Omega **5**, 2159-2168 10.1021/acsomega.9b02911

118. Shao, H., Wingert, B., Weins, A., Pollak, M. R., Camacho, C., andWells, A. (2019) Focal segmental glomerulosclerosis ACTN4 mutants binding to actin: regulation by phosphomimetic mutations Scientific Reports **9**, 15517 10.1038/s41598-019-51825-2

119. Djinovic-Carugo, K., Gautel, M., Ylänne, J., andYoung, P. (2002) The spectrin repeat: a structural platform for cytoskeletal protein assemblies FEBS Letters **513**, 119-123 https://doi.org/10.1016/S0014-5793(01)03304-X

120. Broderick, M. J., andWinder, S. J. (2005) Spectrin, alpha-actinin, and dystrophin Adv Protein Chem **70**, 203-246 10.1016/s0065-3233(05)70007-3

121. Winder, S. J. (1997) The membrane-cytoskeleton interface: The role of dystrophin and utrophin Journal of Muscle Research and Cell Motility **18**, 617-629 10.1023/A:1018627705273

122. Grum, V. L., Li, D., MacDonald, R. I., andMondragón, A. (1999) Structures of two repeats of spectrin suggest models of flexibility Cell **98**, 523-535 10.1016/s0092-8674(00)81980-7

123. Lenne, P.-F., Raae, A. J., Altmann, S. M., Saraste, M., andHörber, J. K. H. (2000) States and transitions during forced unfolding of a single spectrin repeat FEBS Letters **476**, 124-128 https://doi.org/10.1016/S0014-5793(00)01704-X

124. Speicher, D. W., Weglarz, L., andDeSilva, T. M. (1992) Properties of human red cell spectrin heterodimer (side-to-side) assembly and identification of an essential nucleation site J Biol Chem **267**, 14775-14782,

125. Ursitti, J. A., Kotula, L., DeSilva, T. M., Curtis, P. J., andSpeicher, D. W. (1996) Mapping the human erythrocyte beta-spectrin dimer initiation site using recombinant peptides and correlation of its phasing with the alpha-actinin dimer site J Biol Chem **271**, 6636-6644 10.1074/jbc.271.12.6636

126. Sjöblom, B., Salmazo, A., andDjinović-Carugo, K. (2008) Alpha-actinin structure and regulation Cell Mol Life Sci **65**, 2688-2701 10.1007/s00018-008-8080-8

127. Speicher, D. W., DeSilva, T. M., Speicher, K. D., Ursitti, J. A., Hembach, P., andWeglarz, L. (1993) Location of the human red cell spectrin tetramer binding site and detection of a related "closed" hairpin loop dimer using proteolytic footprinting J Biol Chem **268**, 4227-4235,

128. Mehboob, S., Luo, B. H., Fu, W., Johnson, M. E., andFung, L. W. (2005) Conformational studies of the tetramerization site of human erythroid spectrin by cysteine-scanning spin-labeling EPR methods Biochemistry **44**, 15898-15905 10.1021/bi051009m

129. Li, X., andBennett, V. (1996) Identification of the spectrin subunit and domains required for formation of spectrin/adducin/actin complexes J Biol Chem **271**, 15695-15702 10.1074/jbc.271.26.15695

130. Henderson, D. M., Lin, A. Y., Thomas, D. D., andErvasti, J. M. (2012) The carboxy-terminal third of dystrophin enhances actin binding activity J Mol Biol **416**, 414-424 10.1016/j.jmb.2011.12.040

CHAPTER TWO

BETA-III-SPECTRIN N-TERMINUS IS REQUIRED FOR HIGH-AFFINITY ACTIN BINDING AND SCA5 NEUROTOXICITY

2.0 Summary

Recent structural studies of β-III-spectrin and related cytoskeletal proteins revealed N-terminal sequences that directly bind actin. These sequences are variable in structure, and immediately precede a conserved actin-binding domain composed of tandem calponin homology domains (CH1 and CH2). Here we investigated in *Drosophila* the significance of the β-spectrin N-terminus, and explored its functional interaction with a CH2-localized L253P mutation that underlies the neurodegenerative disease spinocerebellar ataxia type 5 (SCA5). We report that pan-neuronal expression of an N-terminally truncated β-spectrin fails to rescue lethality resulting from a β-spectrin loss-of-function allele, indicating that the N-terminus is essential to β-spectrin function *in vivo*. Significantly, N-terminal truncation rescues neurotoxicity and defects in dendritic arborization caused by L253P. *In vitro* studies show that N-terminal truncation eliminates L253P-induced high-affinity actin binding, providing a mechanistic basis for rescue. These data suggest that N-terminal sequences may be useful therapeutic targets for small molecule modulation of the aberrant actin binding associated with SCA5 β-spectrin and spectrin-related disease proteins.

2.1 Introduction

β-spectrin, in a heterotetrameric complex with α-spectrin, binds actin filaments to form a spectrin-actin cytoskeleton that lines the cytoplasmic surface of the plasma membrane. Recent studies in neurons showed that the spec- trin-actin cytoskeleton

confers mechanical resiliency to axons (1-3), regulates axon diameter (4,5), organizes microtubule tracks (2,6), assembles and maintains axon initial segments and nodes of Ranvier (7-9), and enables intracellular transport (5, 10). Moreover, the mammalian β-III-spectrin isoform and the *Drosophila* homolog, β-spectrin, are required for morphogenesis and stability of the large, complex dendritic arbors extended by cerebellar Purkinje cells (11–13) and dendritic arborization (da) sensory neurons (14), respectively. Dominant mutations in β-III-spectrin cause the neurodegenerative disease spinocerebellar ataxia type 5 (SCA5) (15), which is characterized by atrophy of the cerebellar cortex containing Purkinje cell dendrites (16). A SCA5 missense mutation, L253P, localizes to the β-III-spectrin actin-binding domain (ABD) and induces a ~ 1000-fold increase in actin affinity (17). In *Drosophila*, this mutation is neurotoxic, and reduces dendrite stability and arbor outgrowth in class IV da neurons (14). The SCA5 L253P mutation highlights the importance of proper binding of β-spectrin to actin to support neuronal structure and function.

β-spectrin proteins bind actin through an ABD composed of two calponin homology domains (CH1 and CH2) in tandem. The two CH domains are conserved evolutionarily in β-spectrins, and in spectrin-related proteins including α-actinin, filamin and utrophin (18). Structural studies of numerous tandem-CH ABDs showed that in the absence of actin, CH1 and CH2 are bound to each other in a compact structural state (19–22). Cryo-EM studies of the β-III-spectrin (23), filamin A (24) or utrophin (25) ABD in complex with actin showed that actin binding is directly mediated by CH1. CH1 engagement with actin requires an ABD conformational “opening” in which CH2 is repositioned to expose an actin-binding site in CH1, and to prevent steric clash between

CH2 and actin. The β-III-spectrin SCA5 L253P mutation, which localizes to CH2, shifts the ABD conformational equilibrium towards the open state23, explaining the increased actin affinity induced by L253P.

Intriguingly, the recent structural studies of tandem-CH ABDs bound to actin revealed N-terminal sequences, immediately preceding CH1, that also bind actin. Unlike the CH domains, these N-terminal sequences vary greatly in amino acid composition and secondary structure. In the actin-bound state, both the β-III-spectrin and utrophin N-termini take the form of an extended helix (23, 25), while the filamin A N-terminus forms a helix-loop structure (24). Truncation of the N-terminus of filamin A (24) or utrophin (26, 27) decreases actin binding. Significantly, truncation of the N-terminal sequence preceding the β-III-spectrin CH domains abolishes actin binding (23). The divergence of N-terminal sequences among spectrin-related proteins suggests the N-termini also confer unique functionality. Indeed, a recent study of the utrophin terminus suggests it directs binding of utrophin to specific actin structures in cells (27). Further, studies of α-actinin (28) and plectin (29) suggest that N-terminal phosphorylation and calmodulin binding regulate actin binding. The *in vivo* significance of the β-III-spectrin N-terminus, in any species, has yet to be established.

Here, using new *Drosophila* transgenic lines, we examine the functional significance of the β-spectrin N-terminus *in vivo*. We further explore the functional interaction of the N-terminus with the SCA5, CH2-localized L253P mutation that induces high-affinity actin binding

2.2 Results

2.2.1 Delineation of the β-III-spectrin N-terminus

Prior cryo-EM analysis showed that the N-terminus of β-III-spectrin forms an extended α-helix that is tightly associated with actin, and is contiguous with helix A of CH1. To clarify the boundary between N-terminus and CH1, the β-III-spectrin sequence was aligned to other tandem-CH ABD proteins to assess amino acid conservation. The alignment shows low conservation of residues in the N-terminal region corresponding to β-III-spectrin residues 1-52, **Figure 2.1A**. In contrast, beginning at β-III-spectrin residue D53, sequence conservation is clearly elevated. Thus, we define D53 as the first residue of the conserved CH1, similar to a prior CH1 demarcation (18); the novel N-terminal α-helix identified by cryo-EM is composed of N-terminal residues S37 to A52, and is contiguous with CH1 helix A that begins at residue D53, **Figure 2.1B**. The N-terminal sequence is well-conserved between human β-III-spectrin and *Drosophila* β-spectrin (**Figure 2.1C**), supporting the functional importance of the N-terminus across species.

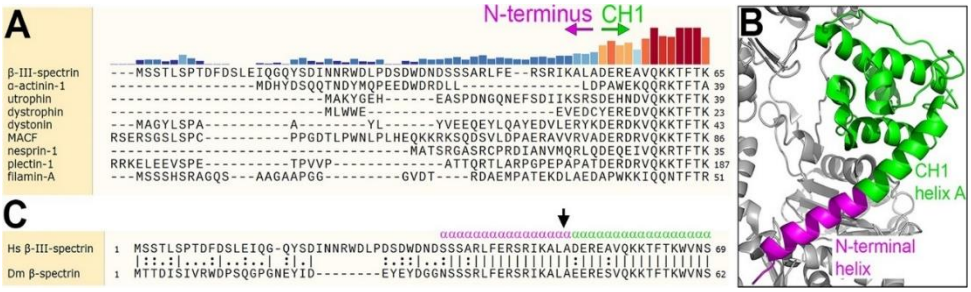

Figure 2.1. Delineation of N-terminus. (A) Alignment of N-terminal amino acid sequences preceding CH1. Tall and dark red bars indicate high conservation, while short and dark blue bars indicate low conservation. Based on increased conservation, we define the first residue of β-III-spectrin CH1 as D53. Amino acids 1–52 constitute the N-terminus. (B) Structure of β-III-spectrin CH1 (green) and N-terminal residues N35-A52 (magenta) in complex with actin (grey) (PDB: 6ANU). N-terminal residues S37-A52 form a helix that is continuous with helix A of CH1. (C) Alignment of human (Hs) and *Drosophila* (Dm) β-spectrin showing high conservation in N-terminal residues. Arrow indicates the site of N-terminal truncation chosen for *Drosophila* ΔN transgenes and binding assays.

2.2.2 N-terminus is required for β-spectrin function and SCA5 toxicity in *Drosophila*

Our prior biochemical truncation studies showed that N-terminal residues 1–51 are required for binding of the β-III-spectrin to actin *in vitro*. To evaluate the importance of the N-terminus to β-spectrin function *in vivo*, new *Drosophila* lines were generated carrying transgenes consisting of an upstream activation sequence (UAS) fused to the *Drosophila* β-spectrin coding sequence, with or without the N-terminal truncation (ΔN; see Figure. 2.1C). The *UAS-βspec* transgenes were inserted into the *attP154* genomic locus (30) for equal expression. Rescue experiments were performed to assess the ability of the *βspec* transgenes to support viability. Males carrying *βspec* transgenes were crossed to females carrying an X-chromosome containing the pan-neuronal driver, *elav-Gal4*, and an ems-induced mutation (em21) in the endogenous *βspec* gene. $\beta spec^{em21}$ is a recessive, loss-of-function allele containing a nonsense mutation in the thirteenth spectrin-repeat domain (31), resulting in low level expression of a truncated β-spectrin

protein, **Figure 2.2**. The *βspec*^{em21} allele causes lethality in males and homozygous females. In contrast, females heterozygous for *βspec*^{em21} are healthy. Pan-neuronal expression of transgenic wild-type β-spectrin (*βspec*^{WT}) rescued adult viability in ~ 25% of male progeny receiving the *βspec*^{em21} mutant X-chromo- some, **Table 2.1**. In contrast, expression of N-terminally truncated β-spectrin (*βspec*$^{\Delta N\text{-}WT}$) failed to rescue *βspec*^{em21} lethality. This indicates that the N-terminus is required for β-spectrin function *in vivo*. In addition, expression of N-terminally truncated β-spectrin (*βspec*$^{\Delta N\text{-}WT}$) in heterozygous *βspec*^{em21} females reduced viability by ~ 30%. This indicates that the N-terminal truncation mutant is mildly neurotoxic. Moreover, raising *Drosophila* incubation temperature from 22 to 25 °C, to increase expression of the N-terminal truncation mutant, reduced survival by ~ 95%, **Table 2.2** This indicates that toxicity of the N-terminal truncation mutant is dose responsive, consistent with a dominant negative mechanism. Additionally, pan-neuronal expression of *βspec*$^{\Delta N\text{-}WT}$ in the absence of *βspec*^{em21}also caused lethality (**Table 2.3**), indicating that *βspec*$^{\Delta N\text{-}WT}$ neurotoxicity is not due to a possible functional interaction with the *βspec*^{em21} protein fragment. Using the rescue assay, we further tested how the N-terminus functionally interacts with the CH2-localized L253P mutation. In agreement with our prior results (14), pan-neuronal expression of β-spectrin carrying the SCA5 missense mutation (L246P in *Drosophila* β-spectrin; *βspec*^{SCA5}) failed to rescue lethality of *βspec*^{em21} males, and dominantly induced lethality in females heterozygous for *βspec*^{em21}, **Table 2.1**. In contrast, the SCA5 mutant with N-terminal truncation (*βspec*$^{\Delta N\text{-}SAC5}$) did not induce lethality in female *βspec*^{em21} heterozygotes (**Table 2.1**), even when the temperature was elevated to increase transgene expression, Table 2. This indicates that the N-terminus is required for L253P-induced

neurotoxicity. Further, the N-terminally truncated SCA5 mutant did not rescue lethality in *βspec*^{em21} males at 22 °C or 25 °C. Altogether, these data suggest that the N-terminally truncated SCA5 mutant is neither toxic nor functional.

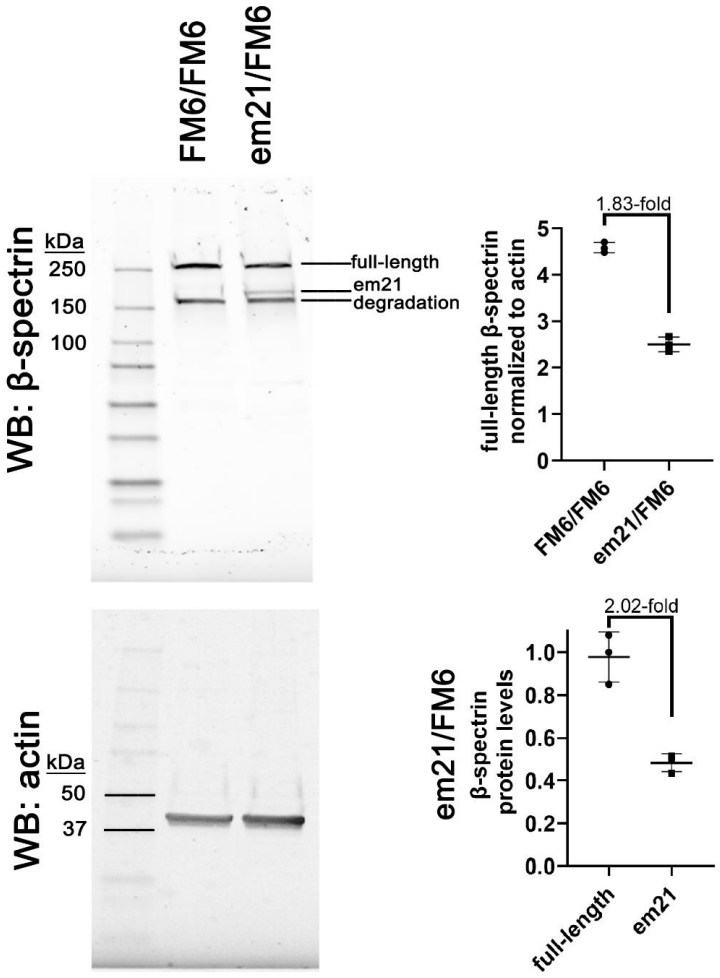

Figure 2.2. The *βspec*^{em21} allele encodes a truncated protein with reduced expression level. *Drosophila* head extracts were prepared from flies homozygous for the *FM6* X-chromosome balancer containing the endogenous, wild-type *βspe*c gene, or flies containing the FM6 balancer in combination with the *βspec*^{em21} mutant X-chromosome (*FM6/βspec*^{em21}). Western blotting of extracts was performed using an antibody specific to *Drosophila* β-spectrin, spectrin-repeat domains 7-11(1). Western blot of *FM6/FM6* extracts shows a two-band pattern: one band at ~250 kDa, corresponding to full-length β-spectrin, and a second band at ~150 kDa, corresponding to a degradation product. In flies containing the *FM6/βspec*^{em21}, an additional band running at ~170 kDa is present. This

170 kDa band corresponds to the truncated em21 protein terminating in spectrin-repeat domain 132. Full-length β-spectrin protein is ~50% lower in abundance in *FM6/βspec*^{em21} extracts relative to *FM6/FM6* extracts, consistent with the 50% reduction in wild-type βspec allele number in *FM6/FM6* versus *FM6/βspec*^{em21} flies. In *FM6/βspec*^{em21} extracts, the full-length β-spectrin protein is ~2-fold more abundant than the truncated em21 protein.

Table 2.1

Rescue of lethal *em21* mutation by *UAS-βspec* transgenes at 22 °C.

Transgene	Progeny class: total number of adults			
	em21, elav-Gal4/Y; transgene/+	***FM6/Y; transgene/+***	***em21, elav-Gal4/+; transgene/+***	***FM6/+; transgene/+***
attP154	0	60	97	68
UAS-βspec^{WT}	42	163	161	162
UAS-βspec$^{\Delta N\text{-}WT}$	0	147	112	162
UAS-βspec^{SCA5}	0	122	0	163
UAS-βspec$^{\Delta N\text{-}SCA5}$	0	130	133	148

Males homozygous for *UAS-βspec* transgenes or the 3rd chromosome *attP154* landing site, were crossed to females carrying the *βspec*^{em21}, *elav-Gal4* recombinant chromosome balanced over the *FM6* chromosome.

Table 2.2

Rescue of lethal *em21* mutation by *UAS-βspec* transgenes at 25°C

transgene	Progeny class: total number of adults			
	em21, elav-Gal4/Y; transgene/+	*FM6/Y; transgene/+*	*em21, elav-Gal4/+; transgene/+*	*FM6/+; transgene/+*
attP154	0	147	172	173
UAS-βspec^{WT}	19	125	145	145
UAS-βspec$^{\Delta N\text{-}WT}$	0	123	9	157
UAS-βspec^{SCA5}	0	88	0	150
UAS-βspec$^{\Delta N\text{-}SCA5}$	0	87	158	138

Males homozygous for *UAS-βspec* transgenes or the 3rd chromosome *attP154* landing site, were crossed to females carrying the *βspec*^{em21}, *elav-Gal4* recombinant chromosome balanced over the *FM6* chromosome.

Table 2.3

Neurotoxicity of *UAS-βspec* transgenes at 25°C

transgene	*elavGal4/+;; transgene/+*		
	Number Pupal cases	Number Adults	% Adults/pupal cases
attP154	247	259	104
UAS-βspec^{WT}	298	292	98.0
UAS-ΔN-βspec^{WT}	381	156	40.9
UAS-βspec^{SCA5}	335	16	4.78
UAS-ΔN-βspec^{SCA5}	338	321	95.0

Males homozygous for *UAS-βspec* transgenes or the 3rd chromosome *attP154* landing site, into which *UAS-βspec* transgenes are inserted, were crossed to females homozygous for *elav-Gal4* transgene.

2.2.3 N-terminal truncation alleviates SCA5-induced dendritic arbor defects

To determine how N-terminal truncation impacts SCA5-induced dendritic arborization defects, *βspec* transgenes were expressed using the *477-Gal4* driver in *Drosophila* class IV da neurons. Relative to neurons expressing $\beta spec^{WT}$, neurons expressing $\beta spec^{SCA5}$ showed reduced arborization characterized by a loss of distal dendrites in Sholl analysis, and decreased total branch length and number of branch points (**Figure 2.3**), consistent with our prior characterization (14). In contrast, neurons expressing $\beta spec^{\Delta N\text{-}SCA5}$ displayed a dendritic arbor morphology indistinguishable from control neurons expressing the wild-type transgene. This indicates that the N-terminus is required for the SCA5 mutation to induce dendritic arbor defects. Moreover, the N-terminally truncated wild-type β-spectrin ($\beta spec^{\Delta N\text{-}WT}$) did not reduce arborization, consistent with mild neurotoxicity observed in rescue assays at 22 °C.

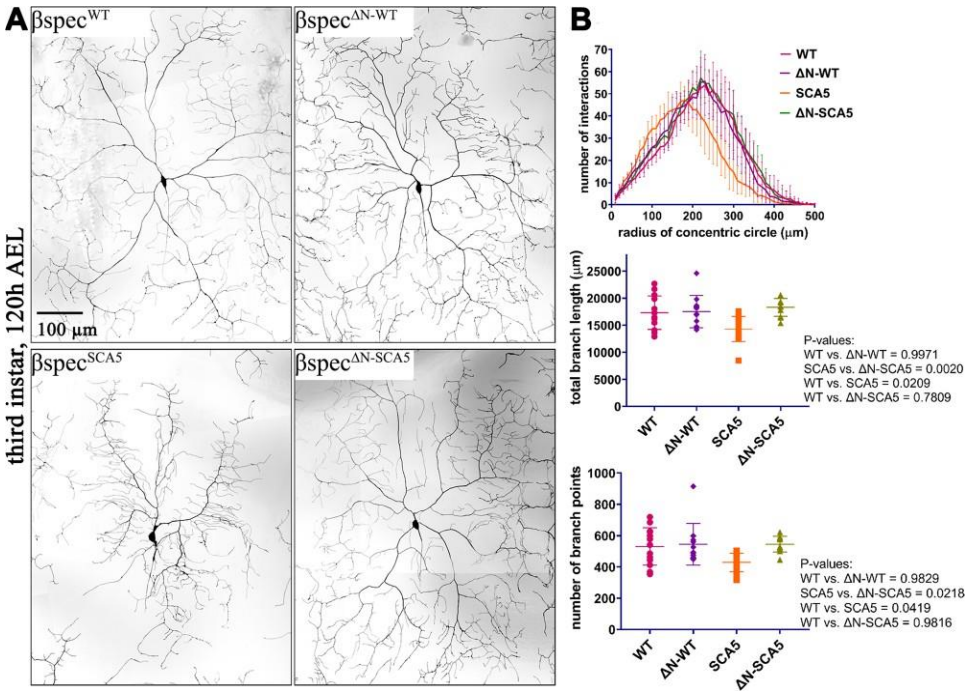

Figure 2.3. N-terminal truncation alleviates SCA5-induced arborization defects. (A) Dendritic arbors of class IV da neurons expressing wild-type *Drosophila* β-spectrin (*βspec*^{WT}), N-terminally truncated β-spectrin (*βspec*$^{\Delta N\text{-}WT}$), SCA5 (L246P) β-spectrin with intact N-terminus (*βspec*^{SCA5}), and N-terminally truncated SCA5 β-spectrin (*βspec*$^{\Delta N\text{-}SCA5}$). Dendritic arbors were documented by fluorescence confocal microcopy in live third instar larvae, 120 h after egg laying (AEL). (B) Top, Sholl analyses showing that *βspec*^{SCA5}, but not *βspec*$^{\Delta N\text{-}WT}$ nor *βspec*$^{\Delta N\text{-}SCA5}$, alter the position of dendritic branches relative to the soma. Middle, quantitation of total branch length showing that only *βspec*^{SCA5} significantly alters total branch length relative to *βspec*^{WT}. Bottom, quantitation showing that only *βspec*^{SCA5} impacts total branch points. n = 11–14 neurons for each genotype. Statistical significance was determined by One-way ANOVA followed by multiple comparisons post hoc test. *P*-values are reported to the right of panels.

2.2.4 N-terminus modulates β-spectrin protein level in neurons

To evaluate the potential impact of N-terminal truncation on β-spectrin protein level, an additional set of *Drosophila* lines were generated containing UAS-transgenes, consisting of β-spectrin, with or without N-terminus, fused at the C-terminus to GFP. The transgenes encoding the β-spectrin-GFP fusion proteins were inserted into the *attP154* genomic locus, as performed for the untagged β-spectrins. In rescue assays,

the β-spectrin-GFP fusions performed similar to their untagged counterparts (**Table 2.4**), indicating that the GFP tag does not interfere with function. To assess relative abundance of wild-type and N-terminally truncated β-spectrins, female *βspec*^{em21} heterozygotes expressing *UAS-βspec*^{GFP} transgenes under the pan-neuronal *elav-Gal4* driver were collected from rescue assays at 18 °C and head extracts prepared. Using a GFP antibody, western blot analysis of *UAS-βspec*$^{WT\text{-}GFP}$ extracts revealed a prominent band running over 250 kDa, consistent with the predicted size (293 kDa) of the full-length β-spectrin-GFP protein, **Figure 2.4**. Significantly, in the soluble fraction, N-terminally truncated wild-type β-spectrin was ~ fivefold more abundant than wild-type β-spectrin with intact N-terminus. This suggests that the inability of the N-terminally truncated β-spectrin to support viability is not due to insufficient protein level. Instead, it suggests that the N-terminus is essential for β-spectrin function in neurons, presumably to enable actin binding. Moreover, the increased steady-state β-spectrin protein level potentially reflects the effect of N-terminal truncation to stabilize wild-type β-spectrin protein, as observed in thermal denaturation studies (23).

Table 2.4

Rescue of lethal *em21* mutation by *UAS-βspec*^{GFP} transgenes

	Progeny class: total number of adults			
transgene	*em21, elav-Gal4/Y; transgene/+*	*FM6/Y; transgene/+*	*em21, elav-Gal4/+; transgene/+*	*FM6/+; transgene/+*
attP154	0	172	192	156
UAS-βspec$^{WT\text{-}GFP}$	32	206	205	173
UAS-βspec$^{\Delta N\text{-}WT\text{-}GFP}$	0	175	3	173
UAS-βspec$^{SCA5\text{-}GFP}$	0	164	0	179
UAS-βspec$^{\Delta N\text{-}SCA5\text{-}GFP}$	0	130	195	216

Males homozygous for *UAS-βspec-GFP* transgenes, or the 3rd chromosome *attP154* landing site, were crossed to females carrying the *βspec*^{em21}, *elav-Gal4* recombinant chromosome balanced over the *FM6* chromosome.

We likewise evaluated the abundance of SCA5 β-spectrin protein, with and without N-terminus. At 18 °C, a fraction of female *βspec*^{em21} heterozygotes expressing the toxic SCA5 mutant β-spectrin survive to adulthood, enabling evaluation of SCA5 mutant protein abundance in head extracts. For SCA5 β-spectrin with intact N-terminus, western blot analysis revealed that soluble SCA5 β-spectrin protein is ~ threefold more abundant than wild-type β-spectrin with intact N-terminus, **Figure 2.4**. SCA5 β-spectrin was also more abundant than wild-type in the insoluble fraction. The increased SCA5 β-spectrin in the insoluble fraction may reflect its high affinity for actin, as the insoluble fraction is enriched in actin. Altogether, the data indicate that the SCA5 mutation, in addition to causing high-affinity actin binding, also causes the mutant β-spectrin protein to accumulate in neurons. It is possible that a high-affinity complex formed between SCA5 β-spectrin and F-actin is resistant to protein turnover. Interestingly, western blotting revealed a fraction of actin with reduced gel mobility in SCA5 β-spectrin head extracts, **Figure 2.4**. Potentially high-affinity binding of SCA5 β-spectrin to F-actin results in post-translational or structural modifications to actin.

Further, the average level of soluble, N-terminally truncated SCA5 β-spectrin protein was 67% lower than wild-type β-spectrin with intact N-terminus, and 89% lower than SCA5 β-spectrin, **Figure 2.4**. In addition, the N-terminally truncated SCA5 β-spectrin did not accumulate in the insoluble fraction, nor cause reduced gel mobility of actin, as observed for SCA5 β-spectrin with intact N-terminus. The lower abundance of the N-terminally truncated SCA5 β-spectrin likely contributes to its the lack of toxicity. However, toxicity was not observed for N-terminally truncated SCA5 β-spectrin when incubation temperature was elevated to increase transgene expression, **Table 2.2**. This

suggests that the lack of toxicity of N-terminally truncated SCA5 β-spectrin is not solely due to reduced protein level. Instead, N-terminal truncation may cause loss of a toxic functional property conferred by the SCA5 mutation.

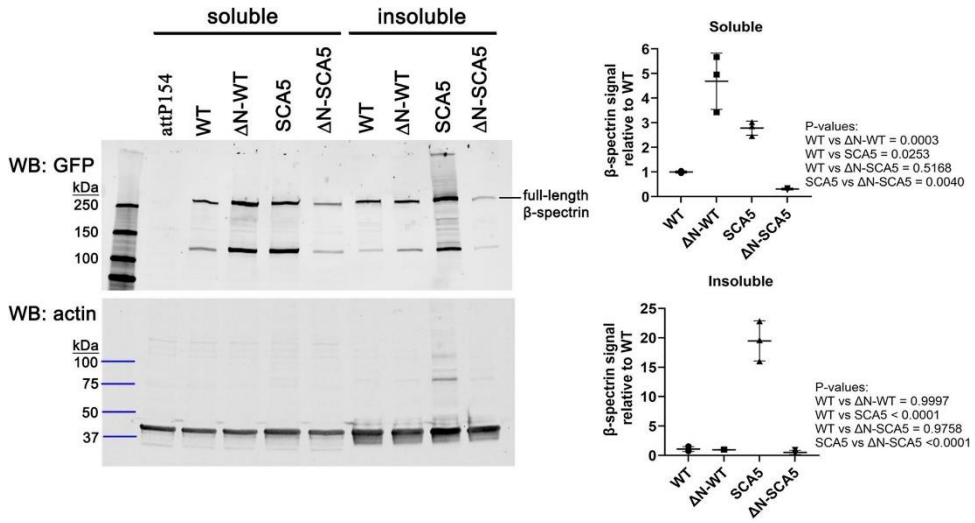

Figure 2.4. N-terminal truncation impacts β-spectrin protein level. *Left*, western blot of head extracts from adult *Drosophila* expressing *UAS-βspec*^{GFP} transgenes under the pan-neuronal driver *elav-Gal4*. As a control, head extracts were also prepared from adult *Drosophila* containing the *attP154* landing site, into which all *UAS-βspec*^{GFP} transgenes were inserted. β-spectrin proteins were identified by probing with a GFP antibody. Total actin was probed as a loading control. The GFP and actin western blot images were cropped to show the regions of the blot containing GFP and actin proteins. The full-size gel images are provided in Figs. S2 and S3. *Right*, quantitation of β-spectrin-GFP protein levels from western blot. Head extracts were prepared a total of three times for each genotype. Statistical analysis was performed by One-way ANOVA followed by multiple comparisons post hoc test. *P*-values are reported to the right of panels.

We evaluated whether the SCA5 mutation or N-terminal truncation impacts the binding of β-spectrin to α-spectrin. Co-immunoprecipitation assays showed that neither the SCA5 mutation nor N-terminal truncation disrupts the co-association of the mutant β-spectrin proteins with α-spectrin in head extracts, **Figure 2.5 and 2.6**. This indicates that the mutant β-spectrin proteins are not impaired in their ability to bind α-spectrin nor assemble into a spectrin heterotetramer.

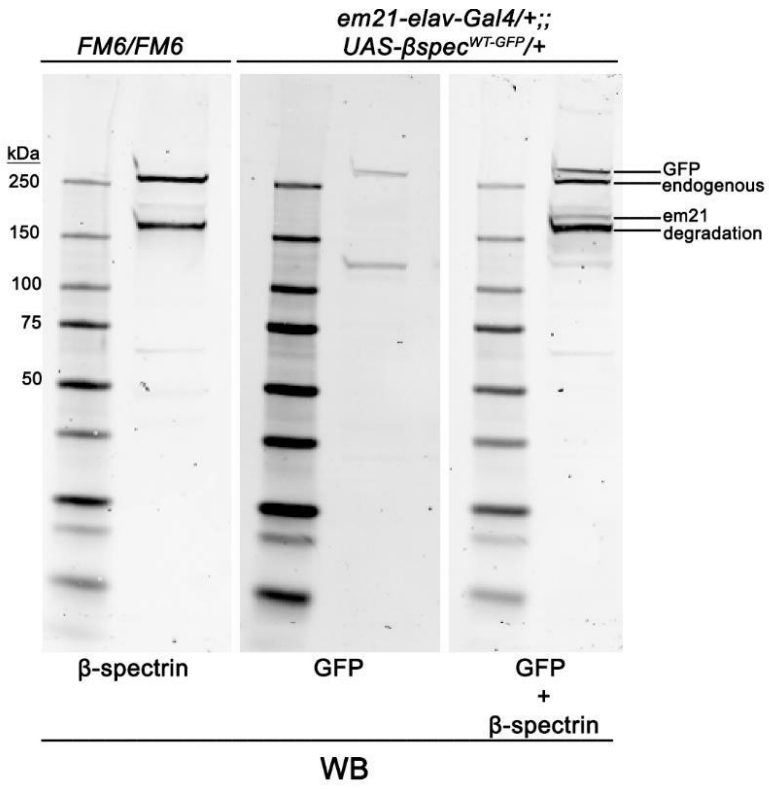

Figure 2.5. β-spectrin-GFP fusion protein runs as a distinct, high molecular weight band relative to endogenous, untagged β-spectrin. Head extracts from *FM6/FM6* or *em21-elav-Gal4/+;;UAS-βspecWT-GFP/+* flies were subjected to SDS-PAGE followed by western blotting using GFP or β-spectrin antibody. *Left*, western blot using β-spectrin antibody of *FM6/FM6* flies expressing endogenous β-spectrin. Full-length endogenous β-spectrin runs near the 250 kDa protein ladder band, in agreement with the predicted molecular weight of 266 kDa. *Middle,* western blot using GFP antibody of *em21-elav-Gal4/+;;UAS-βspecWT-GFP/+* flies shows full-length β-spectrin-GFP runs above the 250 kDa protein ladder band, in agreement with the larger, 293 kDa size of the fusion protein. *Right*, re-probing of the GFP blot (middle panel) with β-spectrin antibody reveals the lower molecular weight endogenous β-spectrin protein. Thus SDS-PAGE resolves β-spectrin-GFP and endogenous β-spectrin proteins as two distinct bands.

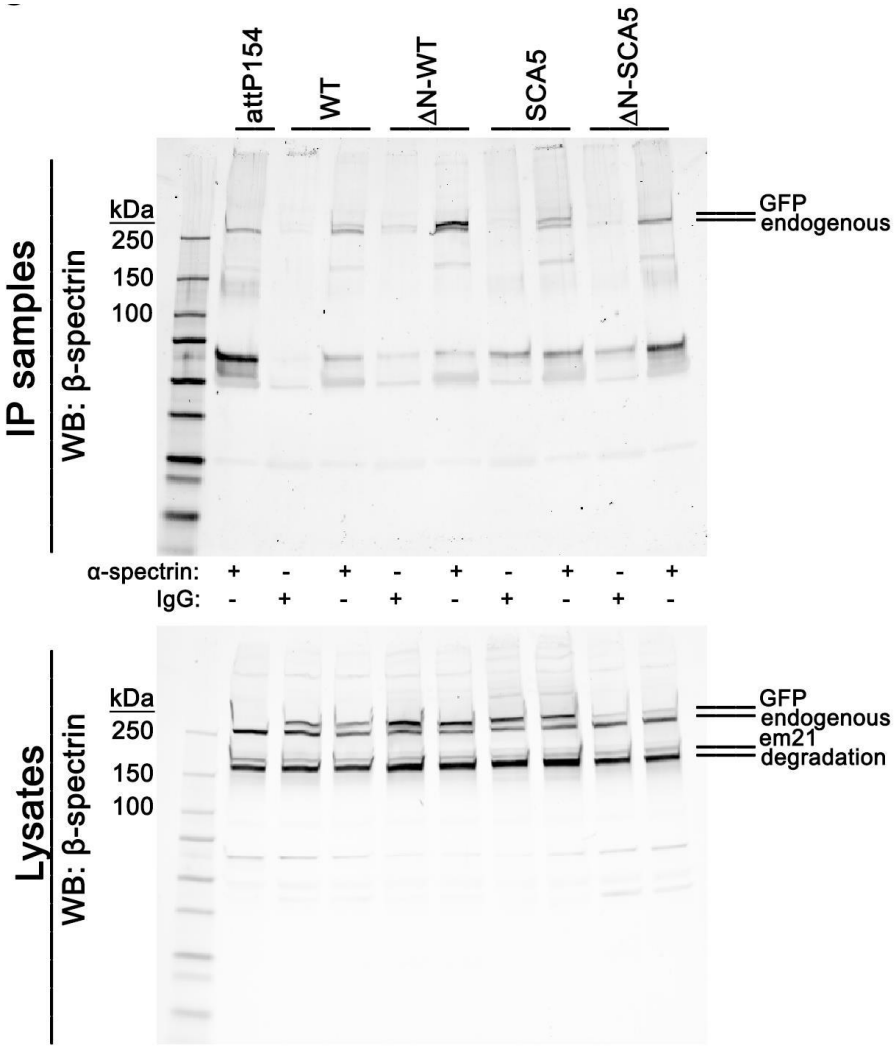

Figure 2.6. SCA5 and N-terminally truncated β-spectrin mutants bind α-spectrin. Head lysates were prepared from *em21-elav-Gal4/+;;attP154/+* control flies or *em21-elav-Gal4/+;;UAS-βspecGFP/+* flies expressing different β-spectrin-GFP fusion proteins. Immunoprecipitation was performed using α-spectrin or control IgG antibodies. In co-IP samples, endogenous β-spectrin (~250 kDa) is enriched in α-spectrin antibody samples relative to control IgG samples. Higher molecular weight wild-type, SCA5 and ΔN-β-spectrin-GFP fusion proteins are likewise enriched in the α-spectrin antibody co-IP samples relative to IgG control. ΔN-SCA5 β-spectrin-GFP, which is present at low abundance in lysate, is present as a faint band in the α-spectrin antibody co-IP sample, but not in controls (IgG or attP154).

2.2.5 L253P causes protein destabilization independent of the N-terminus

To assess how N-terminal truncation impacts the folded state and stability of the SCA5 mutant β-spectrin, circular dichroism spectroscopy was performed. As previously reported, the β-III-spectrin L253P ABD with intact N-terminus showed a pronounced α-helical absorption profile consistent with a well-folded ABD, **Figure 2.7A**. Further, thermal denaturation studies showed that the L253P ABD unfolded in a cooperative, two-state transition with a melting temperature (Tm) of 44.9 °C, **Figure 2.7B**. This Tm is 14.8 °C lower than the Tm of the wild-type ABD with intact N-terminus (59.7 °C). The circular dichroism absorption spectra of the N-terminally truncated L253P ABD similarly showed an α-helical absorption profile indicating a well-folded protein, **Figure 2.7 A**. Significantly, the N-terminally truncated L253P ABD unfolded with a Tm of 46.1 °C. Thus, the N-terminally truncated L253P ABD, like the L253P ABD with intact N-terminus, is highly destabilized relative to wild-type. Notably, N-terminal truncation of the L253P ABD or wild-type ABD raised the Tm by ~ 1 °C relative to the L253P or wild-type ABD with intact N-terminus, respectively. We previously reported a 1 °C increase in Tm for the N-terminally truncated wild-type ABD (23), and suggested that this reflects the loss of an N-terminus that is structurally disordered when not bound to actin.

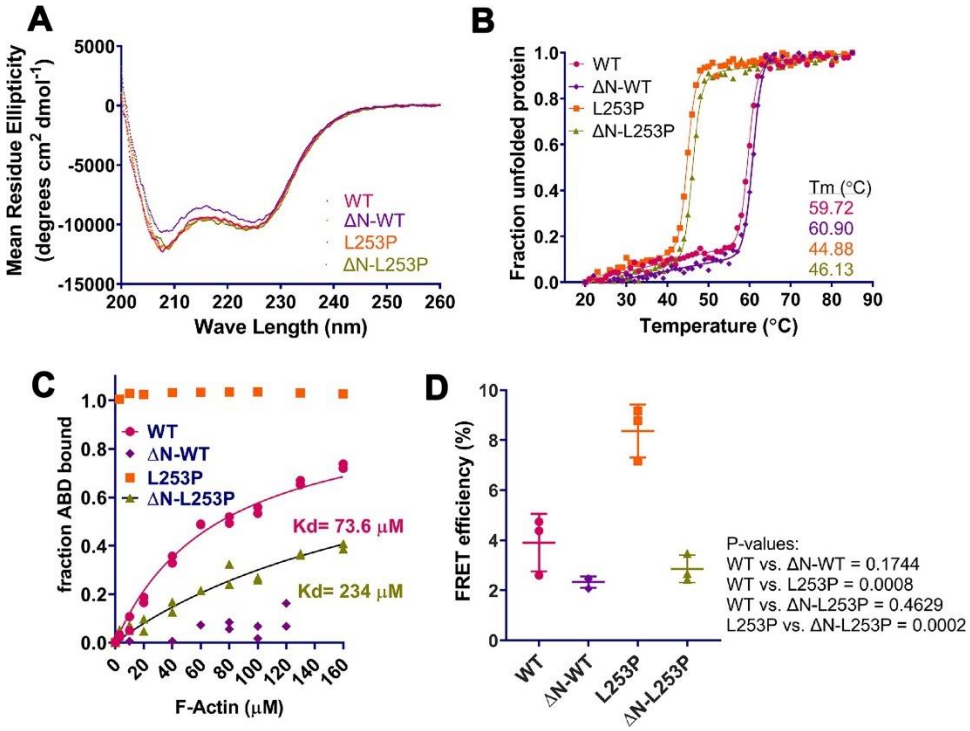

Figure 2.7. Structural and functional characterization of N-terminally truncated ABDs. (A) Circular dichroism (CD) absorption spectra for wild-type and L253P β-III-spectrin ABDs, with or without N-terminus. All ABDs show pronounced α-helical absorption profiles characterized by minima at 208 and 222 nm. (B) CD thermal denaturation curves generated by monitoring absorption at 222 nm. All ABDs unfolded with a cooperative, two-state transition, indicating well-folded proteins. Introduction of L253P decreases the Tm's by ~ 15 °C. In contrast, N-terminal truncation increases the Tm's by ~ 1 °C. (C) *In vitro* co-sedimentation assays showing that N-terminally truncated human β-III-spectrin ABD with L253P mutation (ΔN-L253P) binds actin with Kd of 234 μM (95% confidence interval: 215.5–253.8 μM), compared to the L253P ABD which is entirely bound at all actin concentrations, or to the wild-type ABD with intact N-terminus (WT) that binds actin with a Kd of 73.6 μM (95% confidence interval: 68.0–79.3 μM). Duplicate data points are plotted for each actin concentration. (D) FRET assays monitoring the binding of ABDs to F-actin in live HEK293 cells. L253P increases FRET relative to wild-type. N-terminal truncation blocks L253P-induced actin binding. n = 3. Statistical significance determined by One-way ANOVA followed by multiple comparison post hoc test. P-values are reported to the right of the panel.

2.2.6 N-terminus is required for L253P-induced high-affinity actin binding

To determine whether N-terminal truncation impacts L253P-induced high-affinity actin binding, *in vitro* co-sedimentation assays were performed. Consistent with high-affinity binding previously reported (17), the L253P ABD with intact N-terminus was

entirely bound to F-actin at all actin concentrations tested (3–140 μM), **Figures 2.7C, 2.8 and 2.9.** In contrast, the N-terminally truncated L253P ABD bound actin with very low affinity (Kd = 234 μM). Indeed, the actin-binding affinity of the N-terminally truncated L253P ABD is ~ 3000-fold lower than the affinity of the L253P ABD with intact N-terminus (Kd = 75 nM; (17), and threefold lower than the affinity of the wild-type ABD with intact N-terminus (74 μM). The binding affinity of the N-terminally truncated L253P ABD is higher than that of the N-terminally truncated wild-type ABD, which did not bind actin with measurable affinity.

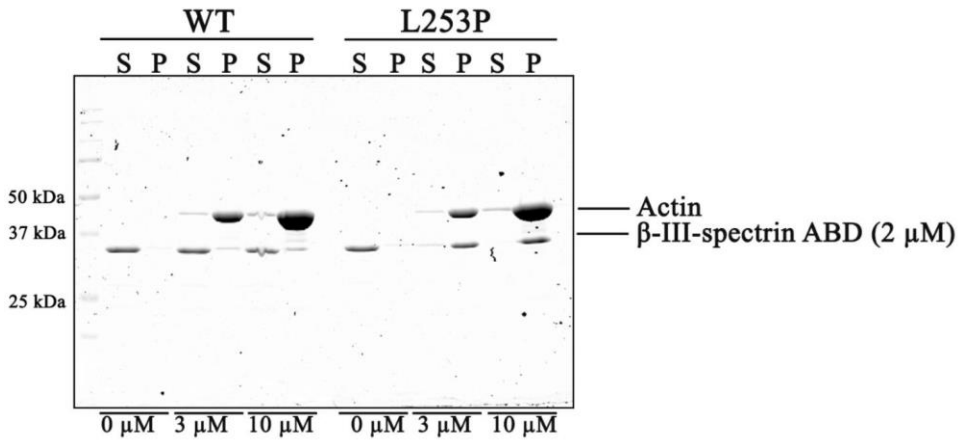

Figure 2.8. Sedimentation of L253P ABD is dependent on F-actin. Actin co-sedimentation reactions were performed for wild-type (WT) and L253P mutant ABD with varying amounts of F-actin. After ultracentrifugation to pellet F-actin, supernatant (S) and pellet (P) samples were collected, followed by SDS-PAGE and Coomassie blue staining. In the absence of F-actin, wild-type and L253P ABDs (2 μM) are present in the supernatant samples, and only a trace amount of either ABD is detected in the pellet samples. In reactions containing 3 or 10 μM F-actin, almost all L253P ABD is in the pellet, consistent with high-affinity binding. In contrast, in reactions containing 3 or 10 μM F-actin, only a small amount of wild-type ABD shifts to the pellet, consistent with low affinity binding. For all reactions containing F-actin, the majority of F-actin is present in the pellet. The trace amount of actin in the supernatant may reflect the G-actin that is in equilibrium with F-actin.

To confirm the *in vitro* co-sedimentation data, we employed a recently developed Förster resonance electron transfer (FRET) assay that detects the binding of the β-III-spectrin ABD to F-actin in live cells (32). In this assay, HEK293T cells are transfected with a DNA construct consisting of the ABD fused to GFP, and a second construct consisting of the actin-binding peptide Lifeact fused to mCherry. FRET between GFP and mCherry results from the formation of a ternary complex consisting of the ABD-GFP and Lifeact-mCherry bound to an actin filament. Co-expression of the wild-type ABD and Lifeact-mCherry resulted in an average FRET efficiency of 3.9%, **Figure 2.7D**. In contrast, the L253P mutant ABD showed an increased FRET efficiency of 8.4%, indicating that the L253P mutation causes increased actin binding in live cells. Significantly, N-terminal truncation of the wild-type ABD or L253P ABD lowered the FRET efficiency to 2.1% and 2.4%, respectively. Altogether, the biochemical and live cell FRET binding assays demonstrate that the N-terminus is required for the L253P mutation to induce high-affinity actin binding.

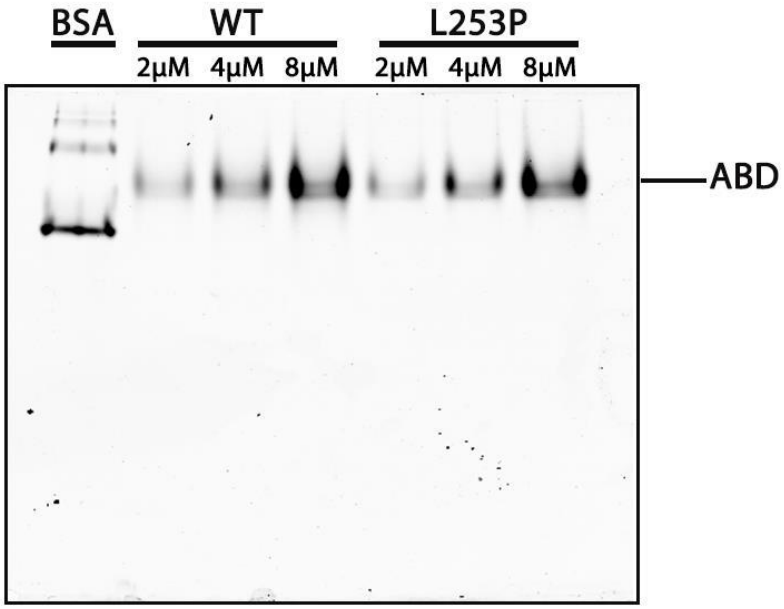

Figure 2.9. Wild-type and L253P ABDs show similar band patterns on native gel. Wild-type or L253P ABD, at different concentrations (2, 4 or 8 μM), were loaded onto a 12% native polyacrylamide gel. Following electrophoresis, Coomassie blue staining was performed. The wild-type and L253P ABD proteins show similar band patterns. This suggests that the wild-type and L253P ABD proteins are in a similar monomeric/oligomeric state. In contrast, bovine serum albumin (BSA) separates into distinct bands, as previously described (3).

2.3 Discussion

The binding of β-spectrin to actin is required for the formation of the plasma membrane-associated spectrin cytoskeleton that is implicated in numerous neuronal functions. Here we investigated the *in vivo* functional significance of the β-III-spectrin N-terminus, which flanks the conserved tandem-CH ABD, and was recently discovered by cryo-EM, to bind actin. Using *Drosophila*, we demonstrated that the N-terminus is essential for β-spectrin function in neurons. Moreover, we showed that the N-terminus is required for neurotoxicity and dendritic arborization defects induced by L253P. We further demonstrated that the N-terminus is required for L253P-induced high-affinity

actin binding, which provides a mechanistic explanation for how N-terminal truncation rescues SCA5 neurotoxicity.

The requirement of the N-terminus for L253P-induced high-affinity actin binding emphasizes the critical role of the N-terminus in the actin-binding mechanism. The N-terminus supports β-spectrin actin binding, at least in part, through its direct interaction with actin. The N-terminus is also destabilizing, **Figure 2.7**. Structural instability conferred by the N-terminus may promote the conformational opening of the CH1-CH2 interface that is required for CH1 to bind actin. Potentially the N-terminus supports actin-binding by additional mechanisms. The N-terminal helix is continuous with CH1 helix A (**Figure 2.1**), which makes contacts with CH2 residues, including L253. Possibly binding of the N-terminus to actin alters CH1-CH2 contacts to facilitate opening of the CH1-CH2 interface. In addition, the N-terminus may be a site of regulation for β-spectrin actin-binding activity. Several amino acids in the β-spectrin N-terminus have been reported to be phosphorylated (33, 34). Phosphorylation of the α-actinin N-terminus reduces actin binding (28). Potentially β-spectrin phosphorylation modulates the function of the N-terminus to promote actin binding.

Here we showed that the SCA5 L253P mutation, in addition to causing high-affinity actin binding, also causes the mutant β-spectrin protein to accumulate in neurons, Figure 2.4. It is possible that this accumulation also contributes to SCA5 neurotoxicity. In contrast, the N-terminally truncated SCA5 mutant did not accumulate, and instead showed decreased abundance relative to wild-type. N-terminal truncation, by itself, is not destabilizing. Rather, we showed that N-terminal truncation increases protein stability (**Figure 2.7**), and that the N-terminally truncated wild-type β-spectrin was more abundant

than wild-type β-spectrin with intact N-terminus, **Figure 2.4**. On the other hand, the L253P mutation is strongly destabilizing, in the presence or absence of the N-terminus, **Figure 2.7**. L253P destabilization may reflect solvent exposure of hydrophobic residues at the CH1-CH2 interface. For example, an X-ray crystal structure of filamin A showed that CH1 residue W142 is buried at the CH interface in the "closed", actin-unbound state (35). Cryo-EM of the filamin ABD-actin complex showed that in the "open" conformation, W142 makes hydrophobic contacts with actin (24), avoiding solvent exposure. Actin binding may stabilize the L253P ABD by burying hydrophobic residues that would otherwise be solvent exposed. In contrast, the N-terminally truncated L253P ABD has very low affinity for actin, and thus remains destabilized and prone to misfolding and protein turnover.

A currently pursued therapeutic strategy for SCA5 is to identify small molecules that bind the L253P β-III-spectrin ABD and reduce its binding to actin (32). The critical role of the N-terminus in actin binding suggests that small molecules that target the N-terminus may effectively reduce actin binding, similar to N-terminal truncation. In addition, it is possible that the large difference in stability of L253P β-III-spectrin versus wild-type may be leveraged to selectively target mutant β-III-spectrin. We suggest that the reduced protein level of N-terminally truncated SCA5 β-spectrin, but not N-terminally truncated wild-type β-spectrin, is due to enhanced protein turnover of a destabilized SCA5 β-spectrin that cannot bind actin. Thus, a small molecule that reduces actin binding may enhance turnover of the destabilized L253P β-III-spectrin, but not the more stable wild-type protein.

2.4 Materials and Methods

2.4.1 *Drosophila* stocks

All stocks were maintained on standard food. The following stocks were obtained from the Bloomington *Drosophila* Stock Center: *477-Gal4/CyO, ppk-CD4-tdTom (10a)/TM6, Tb,* and *elav-Gal4 (C155). attP154* transgenic flies were kindly provided by Norbert Perrimon, Harvard Medical School, Boston. The $\beta spec^{em21}$ line was obtained from Ronald Dubreuil, University of Illinois at Chicago, Chicago. We previously generated *UAS-*$\beta spec^{WT}$ and *UAS-*$\beta spec^{SCA5}$ fly lines (14).

2.4.2 Generation of UAS-βspec$^{\Delta N}$transgenic fly lines

A multi-step protocol was followed to fuse mEGFP to the 3′ end of the fly β-spectrin coding sequence. PCR were performed to amplify a 3′ region of the fly β-spectrin coding sequence, using pUASTattB-β-spectrin wild-type as template, together with forward primer, AAACGCCGGCGAGGGTCACGAAGG and the reverse primer, CTCCTCGCCCTTGCTCACCATCTTTTTCTTTAAAGTAAAAAACG. The reverse primer contains sequence complementary to the 3′ end of the β-spectrin coding sequence and sequence complementary to the 5′ end of mEGFP. A second PCR was performed to amplify mEGFP using the forward primer, ATGGTGAGCAAGGGCGAGGAG and the reverse primer, AAATCTAGACTCGTTCTTCTCTTGCTTATGGTTGCGTTACGGCTGTTACTTTACTTGTACAGCTCGTCCATGCC. The reverse primer includes a short β-spectrin 3'UTR sequence, attached to the 3′ end of the mEGFP coding sequence. The mEGFP DNA used as template in the PCR was synthesized by IDT DNA Technologies. A third PCR was performed to fuse the PCR products generated in the first two PCRs. In the third PCR, the

PCR products from the first two PCRs were used as template, and combined with the forward primer, AAAGGTACCCGCCGGCGAGGGTCACGAAGG, containing KpnI and MreI restriction sites, and the reverse oligo AAATCTAGACTCGTTCTTCTCTTGCTTATGGTTGCGTTACGGCTGTTACTTTAC TTGTACAGCTCGTCCATGCC, containing XbaI site. The resulting PCR product was a fusion of the 3′ coding sequence and mEGFP. The fusion DNA was inserted KpnI-XbaI into pcDNA3.1 digested with the same restriction enzymes, to generate the intermediate construct termed pcDNA3.1-fly-β-spec CT-GFP. The β-spectrin 3′ coding sequence with GFP fusion was subcloned from pcDNA3.1-fly-β-spec CT-GFP into pUASTattB-β-spectrin constructs using MreI and XbaI restriction enzymes. The final pUASTattB-β-spectrin-mEGFP constructs were sequence verified and transgenesis performed using the *attP154* landing site at BestGene, Inc.

2.4.3 Rescue experiments

Female flies containing a recombinant X chromosome *βspec*^{em21}*, elav-Gal4,* balanced over *FM6,* were crossed to male flies homozygous for *UAS-βspec* transgenes, or *attP154* landing site, on the third chromosome. All classes of adult progeny were scored. Fly incubation temperature ranged from 18 to 25 °C, as indicated in the Tables containing rescue assay data

2.4.4 Dendritic arbor analysis

In Figure 2.3, female flies carrying *477-Gal4; ppk-CD4-tdTom/TM6* transgene were crossed to *UAS-βspec* males at 22 °C. Eggs were collected from grape juice plates containing yeast paste every 4 h. Third-instar female larvae 120 h after egg laying (AEL) were imaged using HC PL APO 20x/0.80 NA dry objective and a Leica DMi8 inverted

microscope equipped with X-Light V2 spinning-disc (CrestOptics), LDI laser unit (89 North), and Photometrics Prime 95B CMOS camera. Z-stack images of class IV da neurons were obtained from A3 and A4 abdominal segments (1–3 neurons per larva) and processed to generate maximum intensity projections using Metamorph software. Reconstructions of the arbors were generated using Photoshop 21.0.1. Sholl analysis, and total branch length and branch point quantitation were performed as previously described using ImageJ software (14, 36). Statistical analyses on total branch length and number of branch points were performed in Prism 8 (GraphPad) using unpaired two-tailed t test ($n = 10$ for $\beta spec^{WT}$ and $\beta spec^{SCA5}$, $n = 11$ for $\beta spec^{\Delta N\text{-}WT}$ and $\beta spec^{\Delta N\text{-}SCA5}$).

2.4.5 Western blot analysis

Males homozygous for *UAS-βspec-GFP* transgenes or *attP154* landing site were crossed to females containing $\beta spec^{em21}$*, elav-Gal4/FM6.* Flies were incubated on standard food at 18 °C. Adult female progeny containing $\beta spec^{em21}$*, elav-Gal4* and *UAS- βspec-GFP* transgenes were collected and stored at − 80 °C. To separate fly heads from bodies, a microtube containing flies was frozen in liquid nitrogen and then vigorously shaken. Heads were collected and homogenized using a G-tube with pestle (Bio Plas, Inc) in RIPA buffer (0.05 M HEPES, 0.001 M EDTA, 0.5 M lithium chloride, Complete protease inhibitor cocktail, no EDTA (Roche), 1% IGEPAL CA-630, and 0.7% DOC) at a ratio of 2 µL buffer per head. The supernatants containing soluble proteins were mixed with 4X Laemmli sample buffer (Bio-Rad) after centrifugation at 17,000 RCF and 4 °C for 15 min. The pellets (insoluble fraction) were resuspended in 1X sample buffer. SDS-PAGE was performed on soluble and insoluble protein samples using 12% SDS-acrylamide gels. Proteins were transferred from gels to Immobilon-FL membranes

(Millipore). Membranes were blocked with 1% casein (Hammersten; Alfa Aesar) in 1 × PBS-L (9 g NaCl, 2 g Na_2HPO_4, 0.83 g $NaH_2PO_4 \cdot H_2O$, dissolved in 1 L H_2O) for 1 h at room temperature. Then the membranes were probed overnight at 4 °C with the following primary antibodies diluted in 1 × PBS-L with 1% casein and 0.1% Tween 20: 1:2000 α-actin JLA20 (Developmental Studies Hybridoma Bank), 1:2000 α-GFP (Millipore) or 1:1000 *Drosophila* β-spectrin antibody. Primary antibody solution was removed, and membranes washed with 1 × PBS plus 0.1% Tween 20. The membranes were probed for 1 h with the following secondary antibodies: α-mouse IRDye 800CW (LI-COR Biosciences), α-rabbit IRDye 680RD (LI-COR Biosciences), or α-guinea pig IRDye 680RD (LI-COR Biosciences), diluted to 1:5000 in 1xPBS-L with 1% Casein, 0.1% Tween 20, and 0.01% SDS. Secondary antibodies were removed, and membrane washed with 1 × PBS plus 0.1% Tween 20. Membranes were imaged on a Sapphire scanner (Azure) using 680 nm and 800 nm channels. Protein band fluorescence intensities were quantified in ImageStudio lite (LI-COR Biosciences) by drawing rectangular boxes of uniform size around each protein band. Local fluorescence background signal was subtracted using the median pixel intensity measured under the upper and lower bounds of each measurement box.

2.4.6 Co-immunoprecipitation assay

Drosophila head extracts were prepared as described above. After homogenization and clarification by centrifugation, a Bradford assay was performed to determine lysate protein concentrations. A sample of each lysate (80–100 µg) was collected and mixed with 2 × Laemmli sample buffer. Remaining lysate supernatants were clarified by inversion with Protein A agarose resin for 1 h at 4 °C. Then ~ 500 µg

total lysate protein was incubated with either 10 µg anti-*Drosophila* α-spectrin 3A9 (Developmental Studies Hybridoma Bank) or 10 µg normal mouse IgG (Millipore) antibodies for 1 h at 4 °C, with inversion. Protein A agarose beads equilibrated with RIPA buffer was then added to lysate/antibody mixtures and incubated with inversion overnight at 4 °C. Then, Protein A agarose beads were pelleted at 760×*g* for 1 min and washed 3 × with RIPA buffer. The protein samples were eluted by boiling the beads with 1X Laemmli sample buffer for 5 min at 85 °C.

2.4.7 Protein expression and purification

The coding sequences for L253P β-III-spectrin ABD with or without N-terminus were PCR amplified from pET-30a-ABD L253P (17) using the following forward primers for intact N-terminus AAACACCTGCAAAAAGGTATGAGCAGCACGCTGTCACCC or truncated N-terminus AAACACCTGCAAAAAGGTGCAGATGAACGAGAAGCTGTGC, and the reverse primer AAATCTAGACTACTTCATCTTGGAGAAGTAATGGTAGTAAG. PCR products were digested with AarI and XbaI restriction enzymes and ligated into the compatible ends in pE-SUMOpro (LifeSensors) generated by BsaI digestion. The final constructs, pE-SUMO-ABD L253P and pE-SUMO-A52-ABD L253P, together with the previously generated pE-SUMO-ABD WT and pE-SUMO-A52-ABD WT constructs (23), were transformed into Rosetta 2 (DE3) *E. coli* (Novagen). Bacteria were gown in 1 L of LB broth with ampicillin (100 µg/mL) and chloramphenicol (34 µg/mL) and SUMO-ABD protein expression induced with 0.5 mM IPTG, for 6 h, at 300 rpm and room temperature. Bacteria were pelleted at 4000 rpm and 4 °C for 30 min, and pellets stored at − 20 °C until further use. Protein extraction and purification proceeded as

described previously (23), except that a final gel filtration chromatography step was not performed due to high purity of ABD protein. Buffer exchange was performed by dialysis in 10 mM Tris, pH 7.5, 150 mM NaCl, 2 mM, $MgCl_2$, and 1 mM DTT using Slide-A-Lyzer, 10,000 MWCO cassettes (Thermo Scientific).

2.4.8 Circular dichroism spectroscopy

Purified ABD proteins were diluted to 200 ng/µL in buffer containing 10 mM Tris, pH 7.5, 150 mM NaCl, 2 mM, $MgCl_2$, and 1 mM DTT. Circular dichroism absorption spectra and thermal denaturation data were collected in a Jasco J-810 spectropolarimeter with Peltier temperature controller, as described previously (23). Raw absorption data was converted to mean residue ellipticity using an equation described previously (23). For thermal denaturation absorption data measured at 222 nm, melting temperatures were calculated in Prism 8 (GraphPad) using nonlinear regression to fit a two-state transition equation previously described (23).

2.4.9 Actin co-sedimentation binding assays

Actin was purified from rabbit muscle acetone powder acquired from Pel-Freez Biologicals. To extract actin, acetone powder was incubated in pre-chilled water (1 g / 20 mL) for 30 min followed by vacuum-filtration using Whatman #4 filter paper. One Complete protease inhibitor cocktail, without EDTA, mini tablet (Roche) was added to the filtrate. Actin was then polymerized to F-actin by addition of 30 mM KCl for 1 h at room temperature. F-actin was pelleted by centrifugation at 80,000 RPM at 4 °C, for 30 min, in a TLA-100.3 rotor (Beckman). Supernatants were decanted and F-actin depolymerized by resuspension and homogenization in G-buffer containing 5 mM Tris, pH 7.5, 0.5 mM ATP, and 0.2 mM $CaCl_2$. Homogenized actin was clarified by

centrifugation at 70,000 RPM and 4 °C for 10 min in a TLA-100.3 rotor. Actin was polymerized to F-actin by addition of 2 mM $MgCl_2$ for 30 min at room temperature. F-actin was pelleted at 80,000 RPM for 30 min at 4 °C in a TLA-100.3 rotor. The F-actin was resuspended and homogenized in F-buffer containing 10 mM Tris, pH 7.5, 150 mM NaCl, 0.5 mM ATP, 2 mM $MgCl_2$, 1 mM DTT. Immediately before binding assays, ABD proteins were clarified by centrifugation at 40,000 RPM for 30 min at 4 °C in a TLA-100.3 rotor. ABD and F-actin concentrations were determined by Bradford assay. Binding reactions were performed by combining 2 µM ABD with varying concentrations for F-actin (3–160 µM), and incubating reactions for 30 min at room temperature. To pellet F-actin and actin-bound ABD, binding reactions were centrifuged at 50,000 RPM, for 30 min at 25 °C, in a TLA-100 rotor (Beckman). Supernatants containing unbound ABD protein were sampled and mixed with 1X Laemmli sample buffer. In Figure 2.8, pellet samples were also resuspended in 1X Laemmli sample buffer. Supernatant samples were separated by SDS-PAGE and gels stained using Coomassie Brilliant Blue R-250 solution. Destained gels were imaged using the 680 nm channel of an Azure Sapphire imager. ABD band intensities were quantified from fluorescent gel images using Image Studio Lite version 5.2 software. Raw fluorescence intensity data were converted to ABD protein concentration using a standard curve generated from a Coomassie stained gel loaded with varying amounts of ABD protein. Dissociation constants (Kd) were determined in Prism 8 (GraphPad) by nonlinear regression to fit a one site specific binding equation with Bmax constrained to 1, as described previously (17).

2.4.10 Native-PAGE

ABD and BSA proteins were clarified by centrifugation at 40,000 RPM for 30 min at 4 °C in a TLA-100.3 rotor. ABD and BSA concentrations were determined by Bradford assay. Varying concentrations of ABD proteins (2–8 μM) were prepared in F-buffer containing 10 mM Tris, pH 7.5, 150 mM NaCl, 0.5 mM ATP, 2 mM $MgCl_2$, 1 mM DTT. BSA protein was prepared at concentration of 2 μM, also in F-buffer. Samples were mixed with 2X Native Sample Buffer (Bio-Rad). Native-PAGE was performed using a 12% acrylamide gel and ice-cold Tris–glycine buffer (Bio-Rad). Gels were stained using Coomassie Brilliant Blue R-250 solution. The destained gel was imaged using the 785 nm channel of an Azure 600 imager.

2.4.11 Live cell FRET binding assays

Mammalian cell DNA constructs were generated to express ABD proteins fused at the C-terminus to mEGFP, to be used as FRET donors. For these constructs, the mEGFP coding sequence was PCR amplified using the forward primer CTTGGTACCACCATGGTGAGC, containing a KpnI site, and the reverse primer AAATCTAGACTACTTGTACAGCTCGTCCATGCC, containing a XbaI site, followed by digestion and ligation into pcDNA3.1, resulting in the intermediate construct pcDNA3.1-mEGFP. For PCR amplification of the ABD coding sequence, the forward primer AAAAAGCTTACCACCATGAGCAGCACGCTGTCACCC, or AAAAAGCTTACCACCATGGCAGATGAACGAGAAGCTGTGC, for full-length or N-terminally truncated ABD, respectively, was used with the reverse primer AAAGGTACCCTTCATCTTGGAGAAGTAATGG. The amplified ABD sequences were digested with HindIII and KpnI, and ligated 5′ of mEGFP in pcDNA3.1-mEGFP.

The final FRET donor constructs pcDNA3.1-β-III-spectrin ABD-mEGFP with or without the N-terminal truncation were sequence verified. The pcDNA3.1-Lifeact-mCherry FRET acceptor construct was previously described (32). HEK293T cells were acquired from the American Tissue Culture Collection (ATTC) and were transiently transfected using Lipofectamine 3000 (ThermoFisher Scientific) with either pcDNA3.1-β-III-spectrin ABD-mEGFP donor construct (D), or co-transfected with pcDNA3.1-β-III-spectrin ABD-mEGFP and pcDNA3.1-Lifeact-mCherry donor and acceptor constructs (DA), in 6-well microplates. Cells were harvested 24 h after transfection by dissociation with TrypLE (Gibco), followed by TrypLE inactivation in 1 × DMEM (4.5 g/L D-glucose and 110 mg/L sodium pyruvate) supplemented with 10% FBS (Gibco) and 1% penicillin/streptomycin (Gibco), and then washing in 1 × DPBS (Gibco). Fluorescence lifetime measurements were performed using time-correlated single photon counting method in a FS5 spectrofluorometer equipped with an EPL-472 pulse laser with 5 MHz frequency (Edinburgh Instruments). mEGFP emission signals were detected at 510 nm until the fluorescence decay reached 1000 photon counts within a 50 ns time window. The lifetime (τ) of mEGFP in D and DA samples was obtained by fitting the fluorescence decay data using Fluoracle software (Edinburgh Instruments) reconvolution analysis with instrument response function correction. The FRET efficiency was calculated using the equation:

$$E = 1 - \frac{\tau DA}{\tau D} \quad (1)$$

2.4.12 Sequence alignments

For **Figure 2.1**, amino acid sequences of β-spectrin and related proteins were aligned using Clustal Omega 1.2.4 algorithm in SnapGene 5.1.7.

References

1. Hammarlund M, Jorgensen EM, Bastiani MJ. Axons break in animals lacking beta-spectrin. J. Cell Biol. 2007;176:269–275. doi: 10.1083/jcb.200611117.
2. Krieg M, et al. Genetic defects in beta-spectrin and tau sensitize C. elegans axons to movement-induced damage via torque-tension coupling. Elife. 2017 doi: 10.7554/eLife.20172.
3. Dubey S, et al. The axonal actin-spectrin lattice acts as a tension buffering shock absorber. Elife. 2020 doi: 10.7554/eLife.51772.
4. Costa AR, et al. The membrane periodic skeleton is an actomyosin network that regulates axonal diameter and conduction. Elife. 2020 doi: 10.7554/eLife.55471.
5. Lorenzo DN, et al. betaII-spectrin promotes mouse brain connectivity through stabilizing axonal plasma membranes and enabling axonal organelle transport. Proc. Natl. Acad. Sci. U S A. 2019;116:15686–15695. doi: 10.1073/pnas.1820649116.
6. Qu Y, Hahn I, Webb SE, Pearce SP, Prokop A. Periodic actin structures in neuronal axons are required to maintain microtubules. Mol. Biol. Cell. 2017;28:296–308. doi: 10.1091/mbc.E16-10-0727.
7. Komada M, Soriano P. [Beta]IV-spectrin regulates sodium channel clustering through ankyrin-G at axon initial segments and nodes of Ranvier. J. Cell Biol. 2002;156:337–348. doi: 10.1083/jcb.200110003.
8. Voas MG, et al. alphaII-spectrin is essential for assembly of the nodes of Ranvier in myelinated axons. Curr. Biol. 2007;17:562–568. doi: 10.1016/j.cub.2007.01.071.

9. Liu CH, et al. beta spectrin-dependent and domain specific mechanisms for Na(+) channel clustering. Elife. 2020 doi: 10.7554/eLife.56629.

10. Lorenzo DN, et al. Spectrin mutations that cause spinocerebellar ataxia type 5 impair axonal transport and induce neurodegeneration in Drosophila. J. Cell Biol. 2010;189:143–158. doi: 10.1083/jcb.200905158.

11. Perkins EM, et al. Loss of beta-III spectrin leads to Purkinje cell dysfunction recapitulating the behavior and neuropathology of spinocerebellar ataxia type 5 in humans. J. Neurosci. 2010;30:4857–4867. doi: 10.1523/JNEUROSCI.6065-09.2010.

12. Gao Y, et al. beta-III spectrin is critical for development of purkinje cell dendritic tree and spine morphogenesis. J. Neurosci. 2011;31:16581–16590. doi: 10.1523/JNEUROSCI.3332-11.2011.

13. Fujishima K, Kurisu J, Yamada M, Kengaku M. betaIII spectrin controls the planarity of Purkinje cell dendrites by modulating perpendicular axon-dendrite interactions. Development. 2020 doi: 10.1242/dev.194530.

14. Avery AW, Thomas DD, Hays TS. b-III-spectrin spinocerebellar ataxia type 5 mutation reveals a dominant cytoskeletal mechanism that underlies dendritic arborization. Proc. Natl. Acad. Sci. USA. 2017;114:E9376–E9385. doi: 10.1073/pnas.1707108114.

15. Ikeda Y, et al. Spectrin mutations cause spinocerebellar ataxia type 5. Nat. Genet. 2006;38:184–190. doi: 10.1038/ng1728.

16. Burk K, et al. Spinocerebellar ataxia type 5: Clinical and molecular genetic features of a German kindred. Neurology. 2004;62:327–329. doi: 10. 1212/01. wnl.0000103293 .6334 0.c1.

17. Avery AW, Crain J, Thomas DD, Hays TS. A human beta-III-spectrin spinocerebellar ataxia type 5 mutation causes high-affinity F-actin binding. Sci. Rep. 2016;6:21375. doi: 10.1038/srep21375.

18. Banuelos S, Saraste M, Carugo KD. Structural comparisons of calponin homology domains: Implications for actin binding. Structure. 1998;6:1419–1431. doi: 10.1016/s0969-2126(98)00141-5.

19. Norwood FL, Sutherland-Smith AJ, Keep NH, Kendrick-Jones J. The structure of the N-terminal actin-binding domain of human dystrophin and how mutations in this domain may cause Duchenne or Becker muscular dystrophy. Structure. 2000;8:481–491. doi: 10.1016/s0969-2126(00)00132-5.

20. Borrego-Diaz E, et al. Crystal structure of the actin-binding domain of alpha-actinin 1: Evaluating two competing actin-binding models. J. Struct. Biol. 2006;155:230–238. doi: 10.1016/j.jsb.2006.01.013.

21. Keep NH, et al. Crystal structure of the actin-binding region of utrophin reveals a head-to-tail dimer. Structure. 1999;7:1539–1546. doi: 10.1016/s0969-2126(00)88344-6.

22. Franzot G, Sjoblom B, Gautel M, Carugo KD. The crystal structure of the actin binding domain from alpha-actinin in its closed conformation: Structural insight into phospholipid regulation of alpha-actinin. J. Mol. Biol. 2005;348:151–165. doi:10.1016 /j.jmb.2005.01.002.

23. Avery AW, et al. Structural basis for high-affinity actin binding revealed by a beta-III-spectrin SCA5 missense mutation. Nat. Commun. 2017;8:1350. doi: 10.1038/s41467-017-01367-w.

24. Iwamoto DV, et al. Structural basis of the filamin A actin-binding domain interaction with F-actin. Nat. Struct. Mol. Biol. 2018;25:918–927. doi: 10.1038/s41594-018-0128-3.

25. Kumari A, Kesarwani S, Javoor MG, Vinothkumar KR, Sirajuddin M. Structural insights into actin filament recognition by commonly used cellular actin markers. EMBO J. 2020;39:e104006. doi: 10.15252/embj.2019104006.

26. Singh SM, Bandi S, Mallela KMG. The N-terminal flanking region modulates the actin binding affinity of the utrophin tandem Calponin-homology domain. Biochemistry. 2017;56:2627–2636. doi: 10.1021/acs.biochem.6b01117.

27. Harris AR, et al. Steric regulation of tandem calponin homology domain actin-binding affinity. Mol. Biol. Cell. 2019;30:3112–3122. doi: 10.1091/mbc.E19-06-0317.

28. Shao H, et al. Focal segmental glomerulosclerosis ACTN4 mutants binding to actin: Regulation by phosphomimetic mutations. Sci. Rep. 2019;9:15517. doi: 10.1038/s41598-019-51825-2.

29. Song JG, et al. Structural insights into Ca2+-calmodulin regulation of Plectin 1a-integrin beta4 interaction in hemidesmosomes. Structure. 2015;23:558–570. doi: 10.1016/j.str.2015.01.011.

30. Markstein M, Pitsouli C, Villalta C, Celniker SE, Perrimon N. Exploiting position effects and the gypsy retrovirus insulator to engineer precisely expressed transgenes. Nat. Genet. 2008;40:476–483. doi: 10.1038/ng.101.

31. Dubreuil RR, Wang P, Dahl S, Lee J, Goldstein LS. Drosophila beta spectrin functions independently of alpha spectrin to polarize the Na, K ATPase in epithelial cells. J. Cell Biol. 2000;149:647–656. doi: 10.1083/jcb.149.3.647.

32. Rebbeck RT, et al. Novel drug discovery platform for spinocerebellar ataxia, using fluorescence technology targeting beta-III-spectrin. J. Biol. Chem. 2021;296:100215. doi: 10.1074/jbc.RA120.015417.

33. Bian Y, et al. An enzyme assisted RP-RPLC approach for in-depth analysis of human liver phosphoproteome. J. Proteom. 2014;96:253–262. doi: 10.1016/j.jprot.2013.11.014.

34. Trinidad JC, et al. Global identification and characterization of both O-GlcNAcylation and phosphorylation at the murine synapse. Mol. Cell Proteom. 2012;11:215–229. doi: 10.1074/mcp.O112.018366.

35. Clark AR, Sawyer GM, Robertson SP, Sutherland-Smith AJ. Skeletal dysplasias due to filamin A mutations result from a gain-of-function mechanism distinct from allelic neurological disorders. Hum. Mol. Genet. 2009;18:4791–4800. doi:10.1093 /hm g/ dd p 442.

36. Neisch AL, Avery AW, Machamer JB, Li MG, Hays TS. Methods to identify and analyze gene products involved in neuronal intracellular transport using Drosophila. Methods Cell Biol. 2016;131:277–309. doi: 10.1016/bs.mcb.2015.06.015.

CHAPTER THREE

MOLECULAR CONSEQUENCES OF SCA5 MUTATIONS IN THE SPECTRIN-REPEAT DOMAINS OF β-III-SPECTRIN

3.0 Summary

Spinocerebellar ataxia type 5 (SCA5) mutations in the protein β-III-spectrin cluster to the N-terminal actin-binding domain (ABD) and the central spectrin-repeat domains (SRDs). We previously reported that a common molecular consequence of ABD-localized SCA5 mutations is increased actin binding. However, little is known about the molecular consequences of the SRD-localized mutations. It is known that the SRDs of β-spectrin proteins interact with α-spectrin to form an α/β-spectrin dimer. In addition, it is known that SRDs neighbouring the β-spectrin ABD enhance actin binding. Here, we tested the impact of the SRD-localized R480W and the E532_M544del mutations on the binding of β-III-spectrin to α-II-spectrin and actin. Using multiple experimental approaches, we show that both the R480W and E532_M544del mutants can bind α-II-spectrin. However, E532_M544del causes partial uncoupling of complementary SRDs in the α/β-spectrin dimer. Further, the R480W mutant forms large intracellular inclusions when co-expressed with α-II-spectrin in cells, supporting that R480W mutation grossly disrupts the α-II/β-III-spectrin physical complex. Moreover, actin-binding assays show that E532_M544del, but not R480W, increases β-III-spectrin actin binding. Altogether, these data support that SRD-localized mutations alter key interactions of β-III-spectrin with α-II-spectrin and actin.

3.1 Introduction

Mutations in the *SPTBN2* gene encoding the protein β-III-spectrin are associated with multiple neurological disorders including spinocerebellar ataxia type 5 (SCA5) and spinocerebellar ataxia autosomal recessive type 14 (SCAR14) (also known as spectrin-associated autosomal recessive cerebellar ataxia type 1 (SPARCA1)). SCA5 is caused by autosomal dominant missense or in-frame deletion mutations (1-6). Three SCA5 mutations were initially described in large kindreds of different nationalities (American, French and German) (1). Within these families, ataxic symptoms began in the third or fourth decade of life, on average, and were associated with cerebellar degeneration (7-9). In contrast, SCAR14/SPARCA1 is a recessive disorder, typically caused by mutations that truncate the β-III-spectrin protein (10-12). SCAR14/SPARCA1 causes cerebellar atrophy, severe infantile onset of ataxia and global motor and cognitive impairments. Recent clinical studies have also reported infants or adolescents, carrying *de novo* heterozygous dominant SPTBN2 missense mutations, presenting with severe symptoms that mimic SCAR14 (13-23). These cases have been referred to as infantile SCA5 or SPTBN2-associated nonprogressive cerebellar ataxia (NPCA) (21). The association of these mutations with severe, early onset symptoms suggests a strong disruption to spectrin function. However, our current understanding of the molecular mechanisms of SCA5 pathogenesis is limited.

β-III-spectrin is a cytoskeletal protein with prominent expression in the soma and dendrites of cerebellar Purkinje neurons (24). β-III-spectrin is comprised of an N-terminal actin-binding domain (ABD), a central region containing 17 spectrin-repeat domains (SRDs), and a C-terminal pleckstrin homology domain (PH). β-spectrin proteins are

known to form an antiparallel dimer with α-spectrin (25). Two heterodimers then associate to form a heterotetramer, which can cross-link actin filaments through the terminal β-spectrin ABDs (26-28). In cultured neurons, β-III-spectrin, like other neuronal β-spectrin proteins, was shown to form a sub-plasma membrane cytoskeleton composed of spectrin tetramers and actin filaments (29). Prior studies on erythrocyte β-I-spectrin and the broadly expressed β-II-spectrin indicate that dimerization critically depends on a high affinity, electrostatic interaction between N-terminal SRDs 1-2 of β-spectrin and the C-terminal SRDs 20-21 of α-spectrin (30-33). Following this nucleating interaction, the dimer is further stabilized by weak interactions between complementary SRDs that laterally associate along the two spectrin molecules (25, 30, 32, 33). It is also known that SRDs proximal to the ABD can enhance β-spectrin actin binding. Specifically, it was shown that a β-II-spectrin protein fragment containing the ABD and SRD1 has increased actin-binding affinity compared to the ABD by itself (34).

SCA5 mutations cluster within the N-terminal ABD and neighboring SRDs. We previously showed that many ABD-localized mutations, including L253P (German family), cause increased actin binding (35, 36). The magnitude of the increase in binding varies among the mutations, and we suggested a correlation between magnitude of actin-binding affinity and age of onset/severity of symptoms. In contrast to the ABD-localized mutations, very little is known about the molecular consequences of the SRD-localized mutations. However, the position of the SCA5 mutations within the N-terminal SRDs suggests that they interfere with heterodimerization or actin binding.

Here, we explored the molecular consequences of two SRD-localized SCA5 mutations: R480W, located in SRD2, and E532_M544del, located in SRD3. The

R480W missense mutation is a de novo mutation reported in four unrelated patients with infantile onset of symptoms including global developmental delay that leads to ataxia and intellectual disability (13-15, 20). E532_M544del was clinically characterized in the American SCA5 family that descends from the paternal grandparents of the United States President Abrahem Lincoln (7). E532_M544del causes an in-frame deletion of 13 amino acids in SRD3 and is associated with late onset SCA5. We performed biochemical and cell-based experiments to assess the impact of the mutations on β-III-spectrin folded state, dimerization with α-II-spectrin, and actin binding. Our findings support that both mutations alter how β-III-spectrin physically associates with α-II-spectrin, and that the E532_M544del mutation additionally impacts actin binding.

3.2 Results

3.2.1 Impact of R480W and E532_M544del on β-III-spectrin folded state and conformation

Numerous SCA5-associated missense and in-frame deletion mutations localize to SRDs 2-6 of β-III-spectrin, **Figure 3.1A**. However, little is known about the molecular consequences of these mutations. Here we investigated the molecular consequences of the SRD2-localized R480W and SRD3-localized E532_M544del mutations. To study the impact of these mutations *in vitro*, we purified β-III-spectrin proteins containing the N-terminal ABD and first seven SRDs (amino acids 1-1066), **Figure 3.1B**. For tandem affinity purification, the β-III-spectrin proteins were fused to an N-terminal His-SUMO tag and a C-terminal FLAG tag. The N-terminal His-SUMO tag was removed using Ulp1 protease, and the resulting purified β-III-spectrin proteins run at the expected molecular weight (~122 kDa) following SDS-PAGE, **Figure 3.1B**. Both the N-terminal ABD and

SRDs are known to adopt highly α-helical folds (37-39). X-ray crystallography and cryo-EM structural data for spectrin proteins showed that the SRD consists of three α-helices (termed A, B, and C), bundled into an anti-parallel coiled-coil structure. This coiled-coil structure confers an overall rod-like shape to the SRD (40-44). Consecutive SRDs are linked to each other by a continuous helix formed by helix C of the first SRD and helix A of the second. To experimentally assess the folded state of the purified β-III-spectrin proteins, circular dichroism (CD) spectroscopy was performed. The wild-type protein shows a pronounced α-helical absorption profile characterized by two negative peaks near 208 and 222 nm, **Figure 3.1C**. This absorption profile is thus consistent with the known α-helical fold of both the ABD and SRDs. Both R480W and E532_M544del mutant β-III-spectrin proteins also exhibit α-helical absorption profiles, indicating that the mutant proteins are also rich in α-helical content.

To assess how the mutations impact the stability of the β-III-spectrin proteins, thermal denaturation studies were performed while monitoring the CD peak absorption at 222 nm. Wild-type β-III-spectrin unfolded in a single sharp transition between two states, with a Tm of 44.0 ±0.2 °C, **Figure 3.1D**. This melt curve is indicative of highly cooperative unfolding. Similarly, the melt curves for R480W and E532_M544del mutants show single step transitions with similar Tm values (44.9 ±0.3 °C for R480W and 44.2 ±0.7 °C for E532_M544del). The E532_M544del melt profiles repeatedly showed a less sharp/more gradual transition to the unfolded state, compared to wild-type and R480W mutant. This slight flattening of the melt curve suggests a modest reduction in cooperative unfolding (45) for the E532_M544del protein.

Complementing our CD structural studies, AlphaFold structure prediction software (46) was used to assess the impact of the R480W or E532_M544del mutation on the local SRD structure and overall protein conformation. In the wild-type protein, R480 localizes to helix B of SRD2. In contrast, the 13 amino acids deleted by E532_M544del mutation localize to the N-terminus of SRD3 helix A, **Figure 3.1E**. The R480W mutant structure shows no loss in secondary structure relative to wild-type. Further, the predicted wild-type and R480W structures adopt similar overall conformations. In contrast, the E532_M544del mutation is predicted to replace the α-helical structure at the N-terminus of SRD3 helix A with an unstructured loop. The E532_M544del mutation thus eliminates the helical linker connecting SRD2 and SRD3. As a result, the unstructured loop introduces a hinge point, increasing conformational flexibility, such that the C-terminus of the protein can fold back towards the N-terminus. This loss of structured linker between SRD2 and SRD3 may account for partial reduction in cooperative unfolding of the E532_M544del mutant in our CD denaturation studies.

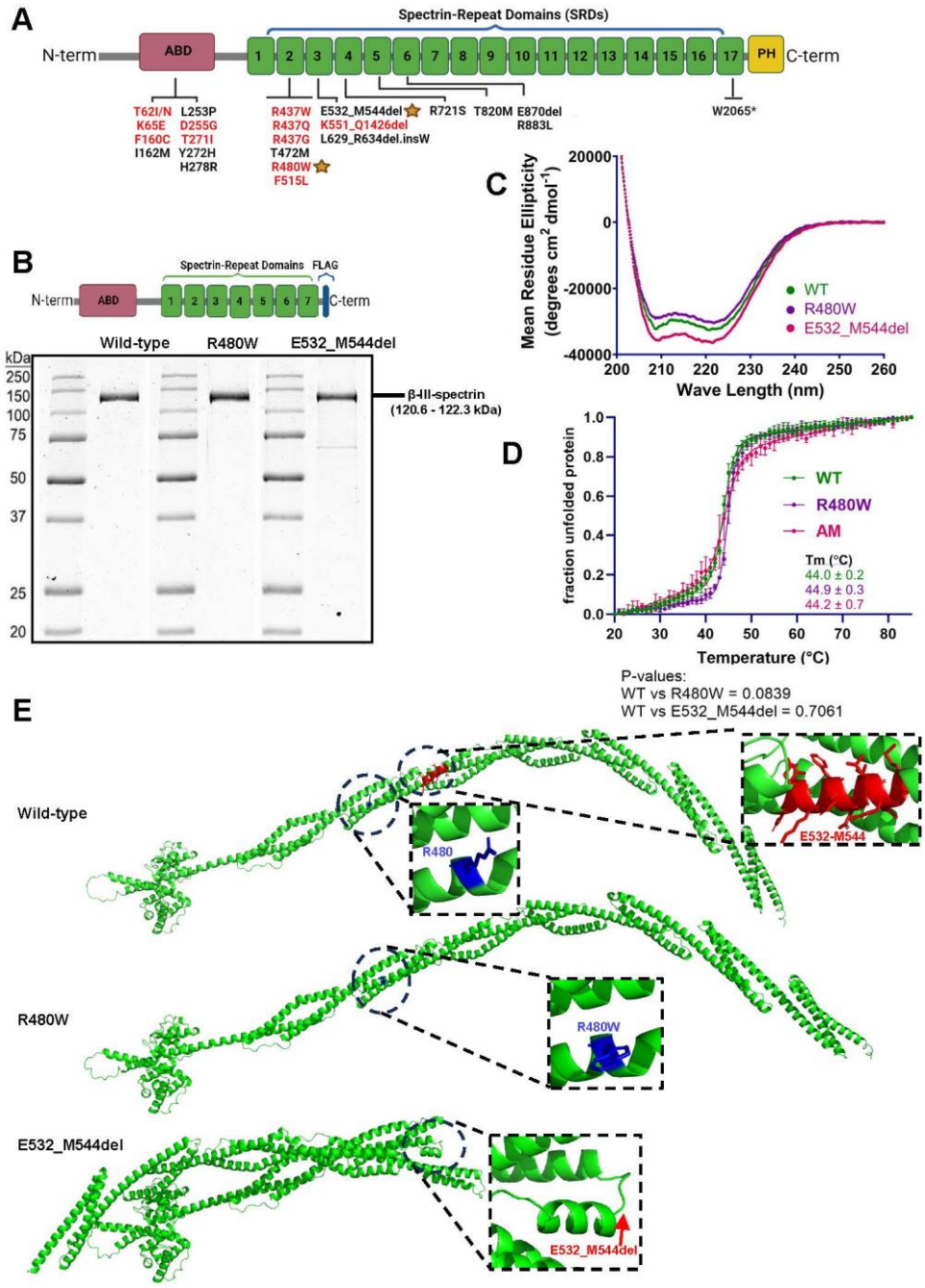

Figure 3.1. Structural analyses of R480W and E532_M544del β-III-spectrin proteins. (A) Domain diagram showing the N-terminal ABD, central 17 SRDs and C-terminal PH domain of β-III-spectrin. Many SCA5 mutations cluster in the ABD and the proximal SRDs (SRDs 2-6). Mutations in red are associated with early onset SCA5 and in black are associated with late onset SCA5. Y272H and W2065* were found together in a patient with early onset SCA5, as compound heterozygous variants Y272H/W2065* (18). SRD2-localized R480W and SRD3-localized E532_M544del mutations, which we characterized in this study, are marked with yellow stars. Domain diagrams were generated using BioRender.com (B) Top, domain diagram of the N-terminal fragment

(amino acids 1-1066) of β-III-spectrin used in this study for *in vitro* biophysical and binding studies. The β-III-spectrin fragment is fused at the C-terminus to a FLAG epitope tag for purification purposes. Bottom, SDS-PAGE gel showing the purified β-III-spectrin proteins. The wild-type, R480W and E532_M544del mutant proteins run at the expected molecular weight (120.6-122.3 kDa). (C) Representative CD α-helical absorption profiles measured over the range of 200-260 nm. (D) CD melting curves measured at 222 nm. Each curve is the average of three independent denaturation curves and error bars are equal to standard deviation. Tm values equal the average of three Tm values fitted in the three replicate denaturation curves, with error given as standard deviation. Statistical significance was determined by Ordinary one-way ANOVA tests followed by Dunnett's multiple comparisons test, n = 3. (E) AlphaFold structural predictions of wild-type and mutant β-III-spectrin proteins (1-1066 amino acids). R480 is located to helix B of SRD2 while E532-M544 residues are located at the start of SRD3 helix A. E532_M544del mutation is predicted to induce a disorder region to the continuous α-helix formed by SRD2 helix C and SRD3 helix A.

3.2.2 R480 and E532-M544 residues are predicted to localize to the α/β dimer interface

Prior biochemical studies using N-terminal β-II-spectrin fragments and C-terminal α-II-spectrin fragments showed that β-II-spectrin SRDs 1-2 and α-II-spectrin SRDs 20-21 are necessary and sufficient for heterodimerization (33). A similar conclusion was drawn using N-terminal and C-terminal fragments of β-I-spectrin and α-I-spectrin, respectively (30,33). The high-affinity binding of β-spectrin SRDs 1-2 to α-spectrin SRDs 20-21 is thought to nucleate the pairing of additional β-spectrin and α-spectrin SRDs, strengthening the dimer. To explore whether the SRD-localized SCA5 mutations impact dimerization, we used AlphaFold to predict the structure of an α-II/β-III-spectrin dimer consisting of β-III-spectrin SRDs 1-4 and α-II-spectrin SRDs 18-21, **Figure 3.2A**. In this structure, β-III-spectrin SRD2-localized R480 is closely positioned to α-II-spectrin SRD20 residues, **Figure 3.2B**. A closer inspection shows that the R480 sidechain guanidinium group is predicted to form a charge-polar contact with the sidechain of α-II-spectrin residue N2109, and a salt bridge with α-II-spectrin E2108 sidechain, **Figure**

3.2B. In addition, R480 is predicted to interact with both R437 and Y477 within β-III-spectrin SRD2. These contacts are supported by a recent cryo-EM structure of the blood α-I/β-I-spectrin dimer (44). In the α-I/β-I-spectrin dimer, the β-III-spectrin R480 equivalent, R477, interacts with α-I-spectrin N2059, equivalent of α-II-spectrin N2109, **Figure 3.2C**. The equivalent residue to E2108 in α-I-spectrin (E2058) was not shown to interact with β-I-spectrin R477. However, the structure resolved similar interactions within β-I-spectrin, as R477 contacted R434 and Y474 (equivalent to β-III-spectrin R437 and Y477). Altogether, these analyses support that β-III-spectrin R480 participates in direct interactions with α-II-spectrin. This suggests that the R480W mutation is in position to alter binding of β-III-spectrin to α-II-spectrin.

We similarly assessed the position of SRD3 amino acids E532-M544. In the AlphaFold structure, these 13 amino acids are positioned near the interface with α-II-spectrin SRD19, **Figure 3.2D**. However, no direct interaction of these residues with α-II-spectrin is predicted. Moreover, the resolution of the equivalent region in α-I/β-I-spectrin dimer is poor, precluding a direct comparison in the experimentally derived structure.

In sum, while E532-M544 residues are not predicted to directly contact α-II-spectrin, the position of the residues at the dimer interface supports that their deletion could disrupt dimer assembly.

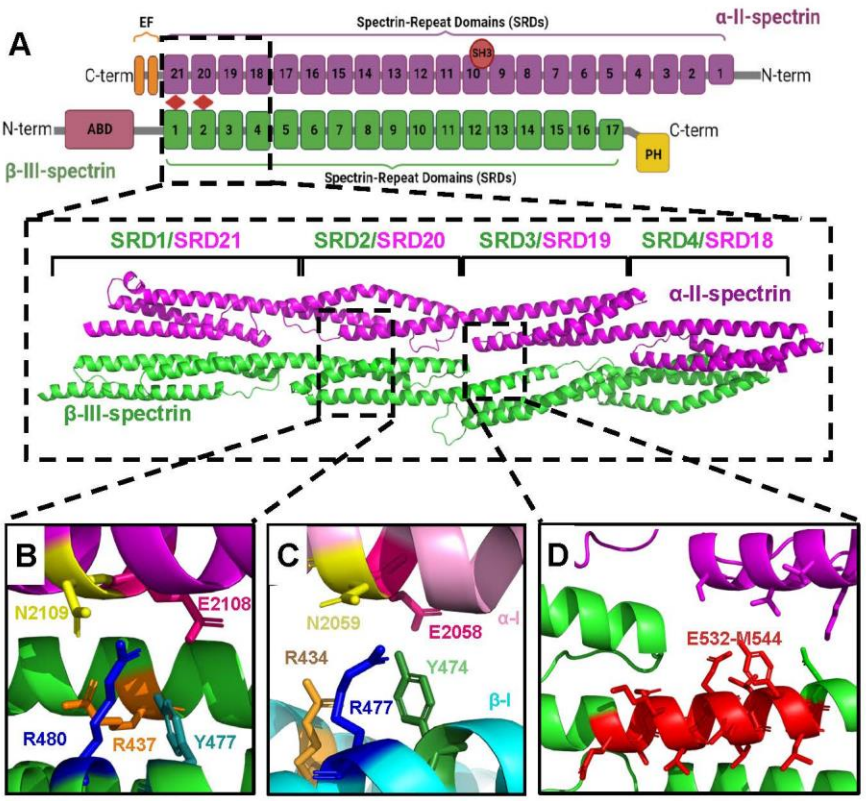

Figure 3.2. α/β-spectrin dimer structure. (A) Top, domain diagram of α-II/β-III-spectrin dimer. By analogy to other spectrin proteins, high affinity binding of N-terminal β-III-spectrin SRDs 1-2 to C-terminal α-II-spectrin SRDs 20-21, nucleate formation of an anti-parallel dimer in which complementary α-II/ β-III-spectrin SRDs laterally associate. Domain diagram generated using BioRender.com. Bottom, AlphaFold predicted structure showing the lateral association of SRDs 1-4 of β-III-spectrin with SRDs 18-21 of α-II-spectrin. Each SRD consists of a 3-helix bundle (helices A, B, and C). Consecutive SRDs are linked by a continuous helix formed by helix C of the first SRD and helix A of the next SRD. (B) Close-up view showing the location of R480 residue in SRD2 helix B and its predicted contacts in α-II-spectrin. R480 is predicted to interact with N2109 and E2108 residues on SRD20 of α-II-spectrin. Within β-III-spectrin, R480 is closely positioned to R437 and Y477. (C) Cryo-EM structure (PDB: 8IAH) of the erythrocyte α-I/β-I-spectrin dimer. The β-III-spectrin R480 equivalent in β-I-spectrin is R477. β-I-spectrin R477 is closely positioned to similar residues in β-I-spectrin and α-I-spectrin, supporting the accuracy of the AlphaFold model in panel B. (D) Close-up view showing the predicted location of E532-M544 residues at the N-terminus of SRD3 helix A of β-III-spectrin. E532-M544 residues are positioned at the interface with α-II-spectrin, although direct binding (< 4 Å) of these amino acids to α-II-spectrin is not predicted.

3.2.3 E532_M544del partially opens α/β dimer interface

Several experimental approaches were taken to assess the impact of the R480W and E532_M544del mutations on binding of β-III-spectrin to α-II-spectrin. In one approach, we performed a cell-based FRET assay that provides a readout of dimerization. In this assay, HEK293T cells are transfected with a β-III-spectrin fragment (amino acids 1-1066), fused at the C-terminus to GFP (β-III-spectrin-GFP), together with the complementary fragment of α-II-spectrin (amino acids 1545-2473), fused at the N-terminus to mCherry (mCh-α-II-spectrin), **Figure 3.3A**. Binding of these fragments is predicted to bring the C-terminal GFP of β-III-spectrin in close apposition to the N-terminal mCherry attached to α-II-spectrin. Indeed, cells co-expressing wild-type β-III-spectrin with α-II-spectrin generate an ~8% FRET efficiency, **Figure 3.3A**. In contrast, control cells expressing GFP (no β-III-spectrin fusion) together with mCherry-α-II-spectrin produced only a ~2% FRET efficiency. Similar to wild-type, the R480W mutant produced an ~8% FRET efficiency, suggesting that R480W does not impact formation of the dimer. In contrast, E532_M544del decreased FRET efficiency to a similar level as the GFP control, suggesting a strong decrease in dimerization.

To confirm the decrease in dimer formation caused by E532_M544del, the co-association of the β-III-spectrin and α-II-spectrin proteins was assessed by co-immunoprecipitation (co-IP) binding assays. In the co-IP assays, the β-III-spectrin-GFP and mCh-α-II-spectrin proteins (same fragments used for FRET assays described above) were expressed in HEK293T cells. Wild-type and mutant β-III-spectrin proteins were immunoprecipitated using GFP antibody, and the co-associated α-II-spectrin protein levels were quantified on western blots, **Figure 3.3B**. Surprisingly, a similar amount of

mCh-α-II-spectrin is present across the wild-type, R480W and E532_M544del mutant IP samples. This suggests that neither mutation causes a strong reduction in binding affinity of β-III-spectrin to α-II-spectrin.

We further tested binding of β-III-spectrin to α-II-spectrin using a biochemical, native PAGE mobility shift assay. Purified β-III-spectrin fragments (amino acids 1-1066), **Figure 3.1B**, were incubated with the complementary α-II-spectrin fragment (amino acids 1545–2473). In native PAGE, control samples containing 0.5 μM α-II-spectrin or β-III-spectrin show that the α-II-spectrin protein migrates faster and in a more well-defined band compared to the β-III-spectrin proteins, **Figure 3.3C**. Of the β-III-spectrin proteins, the E532_M544del mutant is most poorly resolved, supporting that the mutant adopts an altered conformation(s) compared to wild-type or R480W, in agreement with our AlphaFold prediction. In samples containing β-III-spectrin combined with α-II-spectrin, the α-II-spectrin and β-III-spectrin proteins shift up (migrate more slowly) to form a new single intense band, representing a physical complex between β-III-spectrin and α-II-spectrin. For wild-type and R480W, the α-II/β-III-spectrin complex bands migrate at a similar position, located just above the β-III-spectrin band observed in the wild-type or R480W β-III-spectrin only control. In contrast, for E532_M544del, the α-II/β-III-spectrin band migrates more slowly (at a higher position in the gel), suggesting a distinct conformation for the E532_M544del α-II/β-III-spectrin complex. Because the α-II-spectrin band was well-defined and well-separated, the extent of β-III-spectrin binding to α-II-spectrin was determined by quantifying depletion of the α-II-spectrin band upon addition of β-III-spectrin. Notably, as a further loading control, the spectrin proteins were analysed by denaturing SDS-PAGE, **Figure 3.3C, bottom left**. Quantitation of α-II-

spectrin band depletion, relative to the amount of β-III-spectrin loaded, shows that the wild-type and mutant β-III-spectrin proteins bind a similar amount of α-II-spectrin. This *in vitro* assay is thus consistent with the similar binding of wild-type and mutant β-III-spectrin proteins to α-II-spectrin measured by our cell-based co-IP assays.

We further explored the interaction of the wild-type and E532_M544del β-III-spectrin (SRDs 1-4) with the α-II-spectrin (SRDs 18-21) using AlphaFold-Multimer (47). For wild-type, β-III-spectrin SRDs 1-4 lay alongside and antiparallel to α-II-spectrin SRDs 18-21, **Figure 3.3D**. In contrast, for E532_M544del, only β-III-spectrin SRDs 1-2 are in contact with α-II-spectrin. Following the E532_M544del mutation, SRDs 3-4 are positioned away from α-II-spectrin. This suggests that the E532_M544del mutation does not disrupt nucleation mediated by binding of β-III-spectrin SRDs 1-2 to α-II-spectrin SRDs 20-21. However, the E532_M544del disrupts the coupling of β-III-spectrin SRDs to α-II-spectrin SRDs outside of the high affinity nucleation site. This structure prediction explains why E532_M544del mutation abolishes binding in our FRET assay that requires association of the β-III-spectrin C-terminal SRDs with α-II-spectrin, but does not impact overall binding in the co-IP and native PAGE assays. Further the predicted open confirmation of the E532_M544del α-II/β-III-spectrin dimer explains the slower migration of complex, relative to wild-type or R480W, in native PAGE.

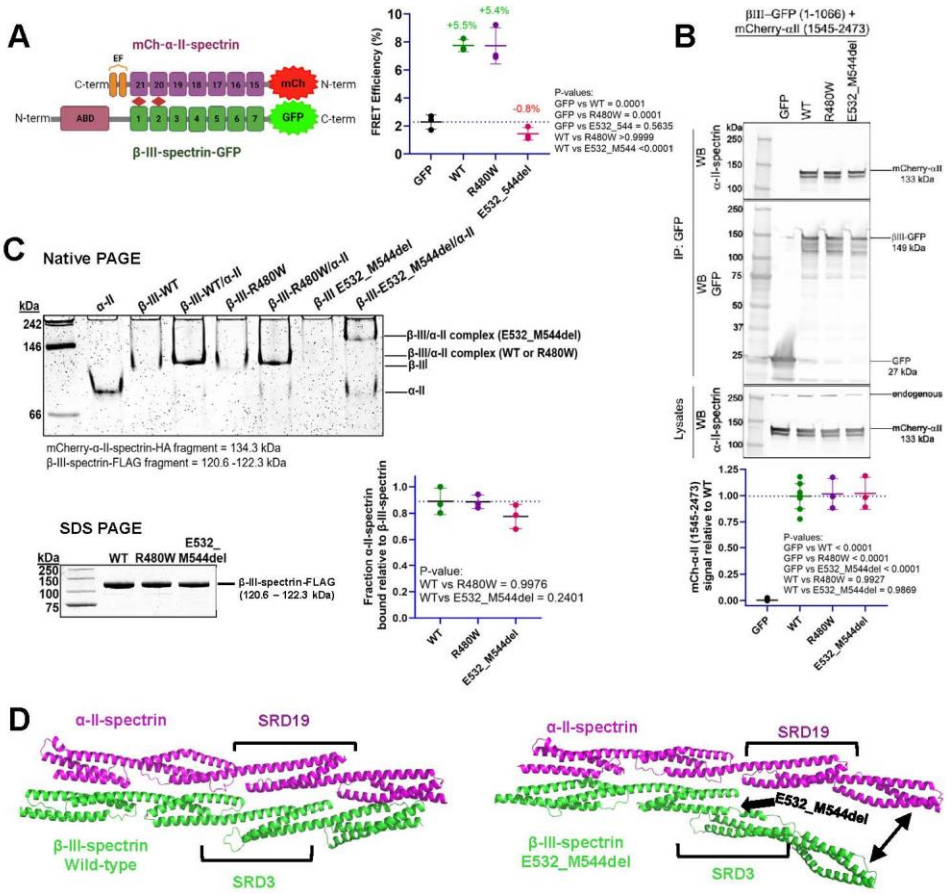

Figure 3.3. Cell-based, biochemical and *in silico* analyses of the impact of R480W and E532_M544del mutations on α-II-spectrin binding. (A) Live-cell FRET binding assays. Left, the FRET donor consists of β-III-spectrin fragment (amino acids 1-1066) fused at the C-terminus to GFP. The FRET acceptor contains α-II-spectrin fragment (amino acids 1545-2473) fused at the N-terminus to mCherry. Right, FRET binding data. (B) HEK293T cell co-immunoprecipitation (co-IP) assay using the β-III-spectrin and α-II-spectrin FRET assay protein fragments. Top, representative western blot of co-IP and lysate samples. Bottom, quantitation of α-II-spectrin protein in co-IP samples. (C) *In vitro* native PAGE mobility shift assay using purified, recombinant β-III-spectrin (amino acids 1-1066) and α-II-spectrin (amino acids 1545-2473) proteins. Top, representative native gel (Coomassie blue stained) showing the migration patterns of the α-II-spectrin C-terminal fragment in the absence of β-III-spectrin, β-III-spectrin N-terminal fragments in the absence of α-II-spectrin, and α-II/β-III-spectrin complexes. Protein concentration for β-III-spectrin or α-II-spectrin equaled 0.5 µM. Bottom left, SDS-PAGE denaturing gel loaded with the individual β-III-spectrin proteins used in the native-PAGE binding assay. Bottom right, quantitation of depletion of the fast-running α-II-spectrin band in native PAGE binding assays, showing that both mutants bind a similar amount of α-II-spectrin compared to wild-type. (D) AlphaFold-Multimer predicted structures of the N-terminal SRDs 1-4 of β-III-spectrin bound to the complementary C-terminal SRDs 18-21 of α-II-spectrin for β-III-spectrin wild-type (left) versus the E532_M544del mutant

(right). E532_M544del is predicted to open the interface between β-III-spectrin and α-II-spectrin beginning at the site of the mutation in SRD3. Statistical significance was determined using the Ordinary one-way ANOVA test followed by Tukey's multiple comparisons test for FRET and co-IP assays and Dunnett's multiple comparisons test for native PAGE assay, n = 3 independent experiments.

3.2.4 R480W and E532_M544del β-III-spectrin proteins co-localize with α-II-spectrin at the plasma membrane and cytoplasmic inclusions

Previously we showed in transfected HEK293T cells that full-length wild-type β-III-spectrin is predominantly localized to the plasma membrane (48). To determine whether the R480W or E532_M544del mutation impacts the subcellular localization of β-III-spectrin or α-II-spectrin, HEK293T cells were co-transfected with full-length, GFP-tagged β-III-spectrin proteins (GFP-β-III-spectrin) and full-length, mCherry-tagged α-II-spectrin (α-II-spectrin-mCherry). In agreement with our prior observation, wild-type β-III-spectrin shows prominent localization to the plasma membrane. Further, α-II-spectrin co-localizes with wild-type β-III-spectrin at the plasma membrane (Pearson correlation coefficient ~0.7), **Figure 3.4**. In contrast, in control cells expressing α-II-spectrin with a plasma membrane GFP tagged marker (PM-GFP), α-II-spectrin localization appears diffuse in the cytoplasm and less cortically localized (Pearson correlation coefficient ~0.5). This suggests that β-III-spectrin recruits α-II-spectrin to the plasma membrane. The R480W and E532_M544del mutants also show pronounced co-localization with α-II-spectrin at the cell cortex (with Pearson correlation coefficients of ~0.9), supporting that both mutants interact with α-II-spectrin for recruitment to the plasma membrane. Notably, for the R480W mutant, in addition to co-localizing with α-II-spectrin at the plasma membrane, large, spherical cytoplasmic inclusions are present that contain both

the β-III-spectrin mutant and α-II-spectrin, **Figure 3.4A**. Altogether, these data support that both full-length mutant proteins bind α-II-spectrin in cells.

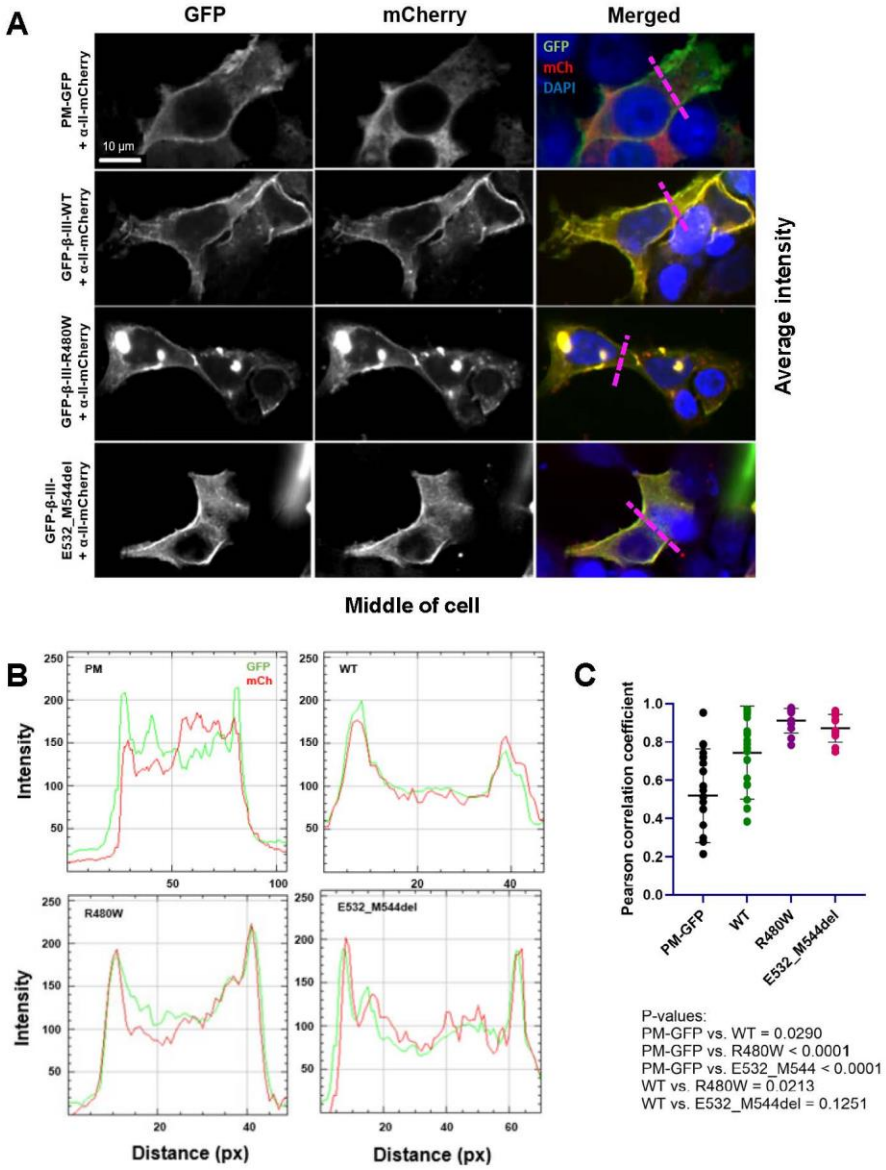

Figure 3.4. Wild-type and mutant β-III-spectrin proteins recruit α-II-spectrin to the plasma membrane. (A) Representative images of HEK293T cells co-expressing full-length GFP-tagged β-III-spectrin and mCherry-tagged α-II-spectrin. Each image is the average intensity of three z-stack planes in the middle of the cell. Wild-type β-III-spectrin localizes primarily to plasma membrane. α-II-spectrin shows pronounced co-localization with wild-type β-III-spectrin at the plasma membrane. In contrast, in cells expressing the plasma membrane-targeted GFP (PM-GFP), α-II-spectrin shows little plasma membrane localization and is instead diffusely localized in the cytoplasm. This suggests that wild-type β-III-spectrin recruits α-II-spectrin to the plasma membrane. Like

wild-type, R480W and E532_M544del mutants also localize to plasma membrane and recruit α-II-spectrin to the plasma membrane. In addition to plasma membrane localization, R480W is also present in large cytoplasmic inclusions that contain α-II-spectrin. (B) Representative line scans of GFP and mCherry fluorescence intensities measured along the pink dash lines crossing the plasma membrane of the cells shown in A. Wild-type and mutant β-III-spectrin show peak intensities at the cell membrane which overlap with the α-II-spectrin peak intensities. In contrast, in PM-GFP control cells, α-II-spectrin intensities appear flatter along the measured distance. (C) Co-localization quantitation using Pearson correlation coefficient. GFP and mCherry fluorescence intensities were measured along lines crossing the plasma membrane, as shown in panel A. R480W and E532_M544del show similar or slightly higher Pearson correlation coefficients compared to wild-type. Statistical significance is determined using Brown-Forsythe and Welch ANOVA tests followed by Dunnett's T3 multiple comparisons test, n= 11-25.

To determine if the R480W inclusions form in the absence of α-II-spectrin co-expression, the R480W mutant was expressed with and without α-II-spectrin in HEK293T cells. Interestingly, in cells not expressing α-II-spectrin, the R480W mutant shows little localization to inclusions, **Figure 3.5A, B**. The few R480W inclusions present appear small and irregularly shaped, similar to the occasional inclusions observed in cells expressing wild-type or the E532_M544del mutant (in the absence of α-II-spectrin). Indeed, in the absence of α-II-spectrin co-expression, the percentage of cells showing β-III-spectrin inclusions was similar among wild-type, R480W and the E532_M544del mutant (~50%), **Figure 3.5B**. This supports that neither mutation causes internal accumulation of β-III-spectrin, which may result from possible protein destabilization/unfolding. This is consistent with our CD data showing that the mutations do not cause protein destabilization. In contrast, when α-II-spectrin is co-expressed, ~100% of cells expressing the R480W mutant show inclusions. These inclusions appear larger and more spherical compared to the inclusions observed for R480W in the absence of α-II-spectrin, **Figure 3.5A**. Also, with α-II-spectrin co-expression, for E532_M544del,

the percentage of cells showing inclusions (~70%) was higher than for wild-type (~40%), **Figure 3.5B**. Like R480W, the E532_M544del inclusions contained α-II-spectrin. However, unlike R480W inclusions, the E532_M544del inclusions appeared small and less regularly shaped (not round).

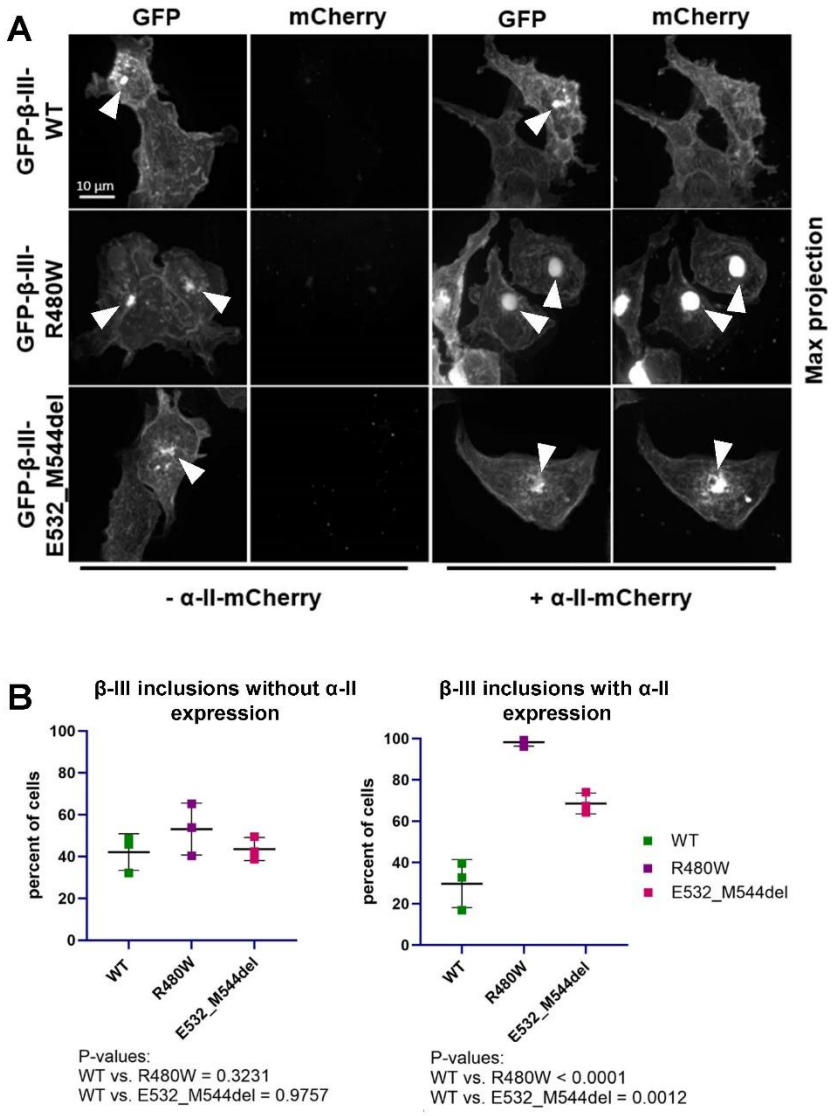

Figure 3.5. R480W and E532_M544del mutants form inclusions when co-expressed with α-II-spectrin. (A) Representative z-stack max projection images of HEK293T cells showing inclusions containing full-length GFP-β-III-spectrin protein, in the absence (left) or presence (right) of α-II-spectrin-mCherry. In the absence of α-II-spectrin co-expression, wild-type and mutant β-III-spectrin inclusions (white arrows) appear similarly small and irregularly shaped. Co-expression of α-II-spectrin does not change

the appearance of wild-type β-III-spectrin inclusions. In contrast, co-expression of α-II-spectrin causes the R480W mutant to localize to large, spherical inclusions that contain α-II-spectrin. (B) Quantitation of cells containing spectrin inclusions. In the absence of α-II-spectrin expression, approximately 40-50% of cells show inclusions for wild-type or mutant β-III-spectrin (left). In contrast, with α-II-spectrin co-expression (right), ~30% of wild-type β-III-spectrin cells show inclusions. The number of cells showing inclusions increases to ~95% when R480W mutant is co-expressed with α-II-spectrin and to ~70% when α-II-spectrin is co-expressed with E532_M544del mutant. Statistical significance was determined using Ordinary one-way ANOVA followed by Dunnett's multiple comparisons test, data represent three independent experiments, with 77-180 cells scored per wild-type or mutant sample, in each replicate.

Altogether, these data support that both R480W and E532_M544del proteins physically associate with α-II-spectrin in cells. However, the incorporation of both mutants into inclusions, by a mechanism dependent on α-II-spectrin co-expression, supports that both mutations disrupt the α-II/β-III-spectrin complex. In particular, the striking large and spherical inclusions observed for R480W suggest that the mutation grossly alters the α-II/β-III-spectrin complex in a way that is not captured by our FRET, co-IP nor native PAGE binding assays.

3.2.5 E532_M544del increases β-III-spectrin actin binding

A shared molecular consequence for many ABD-localized SCA5 mutations is increased actin-binding affinity (35,36). Previously, it was shown for β-II-spectrin that attachment of the proximal SRDs to the N-terminal ABD enhances actin binding (34). This indicates that the SRDs might contribute to actin binding by a direct or indirect mechanism. Due to proximity of R480W and E532_M544del to the N-terminal ABD, we tested the impact of the R480W and E532_M544del mutations on actin binding. Co-sedimentation assays were performed using a fixed concentration (0.5 μM) of purified β-III-spectrin proteins (amino acids 1-1066) and increasing concentrations of F-actin (0-120

μM). Wild-type β-III-spectrin binds actin with Kd = 24.6 ± 12.0 μM, **Figure 3.6A**. This affinity is higher than the ABD by itself (Kd ~75 μM) (35,49), supporting a role for the β-III-spectrin SRDs to enhance actin binding. The R480W mutant binds actin with a Kd of 34.9 ± 14.4 μM, indicating that the mutation has no significant impact on β-III-spectrin actin binding. In contrast, over the same actin concentrations, E532_M544del is completely bound to actin. This supports that E532_M544del causes a large increase in actin binding, likely with a sub-micromolar Kd.

Previously, we showed that the L253P mutation, which causes high-affinity actin binding (Kd ~75 nM), causes the full-length β-III-spectrin protein to be absent from lamellipodia and filopodium-like protrusions in HEK293T cells (48). We suggested that increased actin binding limits the pool of free β-III-spectrin available to enter dynamic membrane extensions. To test whether the E532_M544del mutant shows a similar mislocalization to the cellular protrusions, the full-length E532_M544del β-III-spectrin mutant was co-expressed with a mCherry-tagged membrane marker (mCherry-Mem) in HEK293T cells. As reported previously (48), the wild-type β-III-spectrin is detected in filopodium-like and lamellipodia plasma membrane extensions, **Figure 3.6B**. The presence of wild-type β-III-spectrin in these membrane extensions causes cells stained for β-III-spectrin to have a highly textured or "rough" surface. Similar to wild-type, the R480W mutant is present in membrane extensions. In contrast, the E532_M544del mutant is absent from filopodium-like and lamellipodia extensions counter-labelled with mCherry-Mem. The lack of the E532_M544del mutant in cell surface extensions causes cells stained for β-III-spectrin to have a cell surface that appears untextured or "smooth". Indeed, ~85% of cells expressing the E532_M544del mutant show a smooth cell surface,

compared to ~10% of cells for wild-type or R480W. These data support that the E532_M544del mutant binds actin with increased affinity in cells, consistent with our *in vitro* actin co-sedimentation assays.

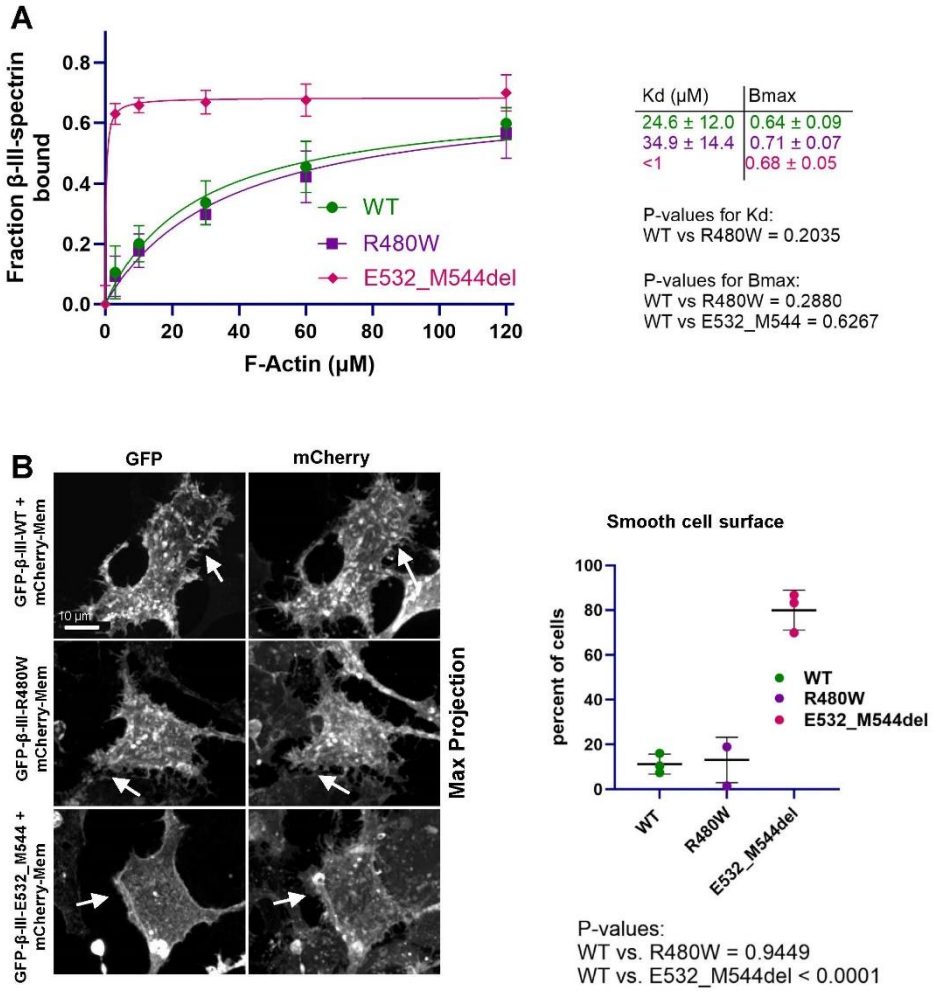

Figure 3.6. E532_M544del mutation increases β-III-spectrin binding to actin. (A) *In vitro* actin co-sedimentation binding data. Statistical analysis of Kd was performed by unpaired t test. For Bmax, Ordinary one-way ANOVA followed by Dunnett's multiple comparisons test was used for statistical analysis, n = 4-9 (B) Left, representative z-stack max projection images of HEK293T co-expressing GFP tagged full-length β-III-spectrin proteins and plasma membrane targeted mCherry (mCherry-Mem). Both wild-type and R480W β-III-spectrin proteins localize to filopodia and lamellipodia-like cellular protrusions (white arrow). As a result, images of wild-type and R480W β-III-spectrin proteins give cells a highly textured or "rough" cell surface, similar to images of the mCherry-Mem. The E532_M544del mutant also localizes to the cell cortex. However, the

E532_M544del mutant shows reduced localization to filopodia and lamellipodia-like cellular protrusions (labeled with mCherry-Mem). Thus, images of the E532_M544del mutant show a less textured, "smooth" cells surface. Right, quantitation of percentage of cells showing "smooth" cell surface based on β-III-spectrin localization. Approximately 85% of cells expressing the E532_M544del mutant appear smooth compared to ~20% of cells expressing R480W or wild-type. Statistical significance was determined using Ordinary one-way ANOVA followed by Dunnett's multiple comparisons test, data represent three independent experiments, with 79-145 cells scored per wild-type or mutant sample, in each replicate.

3.3 Discussion

Multiple SCA5 mutations localize to the β-III-spectrin SRDs. However, little is known about the molecular consequences of these mutations. Here we assessed the molecular impact of the SRD2-localized R480W mutation, which is associated with early onset and severe symptoms. We also characterized the SRD3-localized E532_M544del mutation that is associated with late onset and relatively mild symptoms. Based on the position of these mutations in the N-terminal SRDs, we hypothesized that they would impact actin binding and dimerization with α-II-spectrin. Our results support that these mutations differentially impact the association of β-III-spectrin with actin and α-II-spectrin. R480W has no impact on actin binding. However, R480W causes the formation of large intracellular inclusions containing the mutant β-III-spectrin and α-II-spectrin. The R480W mutant forms these inclusions only when it is co-expressed with α-II-spectrin, suggesting that R480W grossly alters the α-II/β-III-spectrin complex. In contrast to R480W, the E532_M544del mutation causes β-III-spectrin to bind actin with increased affinity. E532_M544del additionally alters the physical association of β-III-spectrin with α-II-spectrin. Specifically, the E532_M544del mutation causes a loss in

coupling of β-III-spectrin SRDs, beginning with SRD3, to the complementary SRDs of α-II-spectrin.

The R480W mutation is located in SRD2, a domain known to be required for nucleating α/β-spectrin dimer through electrostatic interactions (31,32). Our AlphaFold modelling of the α-II/β-III-spectrin nucleation site and the recent cryo-EM analyses of the erythrocyte α-I/β-I-spectrin dimer support that R480 directly contacts α-II-spectrin (44). Thus, we expected that substitution of R480 with a hydrophobic tryptophan residue would alter dimer formation. However, we did not detect a decrease or increase in binding of R480W β-III-spectrin to α-II-spectrin in FRET, co-IP nor native PAGE mobility shift assays, using N-terminal and C-terminal fragments of β-III-spectrin and α-II-spectrin, respectively. Thus, any change in binding of the R480W mutant to α-II-spectrin is below the sensitivity of these assays. Strikingly, co-expression of α-II-spectrin with the R480W β-III-spectrin mutant induces the formation of large, spherical cytoplasmic inclusions containing both the R480W mutant and α-II-spectrin. The dependence of R480W inclusion formation on the co-expression of α-II-spectrin supports that the α-II/β-III-spectrin complex is grossly altered by R480W, even though the mutation did not otherwise cause a detectable change in binding of the two proteins in our other experiments.

The spherical shape of the R480W inclusions is reminiscent of phase-separated condensates. Interestingly, α-II/β-II-spectrin phase-separated condensates were recently suggested to be present in developing neurites (50). Spectrin condensate formation appeared to be mediated by the spectrin-repeat domains (50). Thus, it is possible that the R480W mutation traps the α-II/β-III-spectrin complex in a biomolecular condensate that

is relevant to normal spectrin biology in neurons. Of note, the inclusions caused by R480W appear distinct from the inclusions we previously observed for L253P, which appear as a cluster of small vesicles (48). We suggest that the formation of the R480W inclusions contributes to SCA5 pathogenesis and the associated early onset, severe symptoms. By forming these intracellular accumulations, R480W likely reduces the amount of β-III-spectrin and α-II-spectrin at the plasma membrane, where the wild-type protein normally localizes. In future work, it will be important to study the R480W mutation in an animal model or primary neurons at endogenous spectrin protein levels to determine if R480W causes inclusion formation.

Interestingly, R480 is closely positioned to β-III-spectrin residue R437. These two arginine residues share Y477 as a contact within β-III-spectrin, and both arginine residues contact α-II-spectrin. Several R437 missense mutations have been reported that cause severe symptoms similar to those caused by R480W (16-18). Thus, it will be important to test whether R437 mutations also cause inclusion formation.

Our data show that SRD3-localized E532_M544del impacts β-III-spectrin interaction with both actin and α-II-spectrin. Our co-IP and native PAGE binding experiments with the N-terminal β-III-spectrin fragment (amino acids 1-1066) and complementary C-terminal α-II-spectrin fragment (amino acids 1545-2473) show that the E532_M544del mutant can bind α-II-spectrin. However, our FRET data indicate that the mutation decreases the apposition/coupling of α-II/β-III-spectrin SRDs outside of the high-affinity dimer nucleation site. Our AlphaFold modelling suggests that the E532_M544del introduces a disordered region at the N-terminal half of SRD3 helix A. This disordered region likely acts as a hinge, increasing conformational flexibility of the

E532_M544del mutant and interfering with the pairing of downstream α-II/β-III-spectrin SRDs. The E532_M544del mutant can still form a dimer at the nucleation site (SRDs 1-2 of β-III-spectrin), but the C-terminal SRDs do not associate with α-II-spectrin. This unique dimer conformation is supported by our FRET data and the slower migration of the E532_M544del α-II/β-III-spectrin complex in native PAGE compared to wild-type. The uncoupling of SRDs in the spectrin heterodimer would further be expected to interfere with the co-association of two dimers to form a tetramer. A loss in tetramer formation would impede the actin cross-linking function of β-III-spectrin.

We also found that the E532_M544del mutant causes increased actin binding. The mechanism by which E532_M544del increases actin binding is not clear. It is possible that the E532_M544del causes direct binding of SRDs to actin or that the mutation allosterically enhances actin binding of the N-terminal ABD. In addition, our AlphaFold model showed that the E532_M544del mutation allows the C-terminus to fold back onto the β-III-spectrin N-terminus. It is possible that a novel contact between SRDs and the N-terminal ABD enhances binding of the ABD to actin.

Numerous ABD-localized mutations, including L253P, increase actin binding (35,36). As we reported for L253P (48), the E532_M544del mutation decreases the localization of β-III-spectrin to filopodium-like and lamellipodia cellular protrusions in HEK293T cells. Further, our prior experiments in *Drosophila* showed that the L253P mutation decreases β-spectrin localization to dendritic extensions (48). Fujishima et al confirmed in cultured Purkinje neurons that the L253P mutation decreases β-III-spectrin dendritic localization (51). Fujishima et al further showed that the E532_M544del mutant was also restricted to the soma and absent from Purkinje cell dendrites (51). We suggest

that increased actin binding decreases the mobile pool of β-III-spectrin, reducing expansion of the spectrin cytoskeleton into dendrites.

A SCA5 mouse model was previously reported in which a human E532_M544del β-III-spectrin transgene was expressed in Purkinje neurons (52). This SCA5 mouse is ataxic and exhibits thinning of the cerebellar molecular layer containing Purkinje cell dendrites. Interestingly, mGluR1α receptor clustering was found to be reduced in Purkinje cell dendritic spines. This is consistent with a knockout mouse study showing that β-III-spectrin is required for normal spine density and morphology, and the proper localization of other membrane proteins involved in glutamate signalling (53). In the SCA5 mouse model, the E532_M544del mutant β-III-spectrin appears present in dendritic arbores, although quantitation of dendritic localization of the mutant versus wild-type protein was not performed. It is possible that the E532_M544del slows, but does not completely block, the entry of β-III-spectrin into dendrites. We think it is likely that quantitative analysis of the E532_M544del mutant subcellular localization, as performed by Fujishima et al. with cultured neurons (51), will reveal a reduction of dendrite-localized β-III-spectrin in the SCA5 mouse model, at least at early developmental time points. We suggest that either a reduction in E532_M544del mutant localization to dendrites, and/or impaired α-II/β-III-spectrin heterodimer/tetramer formation, is responsible for the decrease in clustering of mGluR1α in dendritic spines.

A second late onset SCA5 mutation that localizes to SRD3 also causes an in-frame deletion (L629_R634delinsW; French family). Similar to E532_M544del, the L629_R634delinsW mutant showed reduced localization in the dendrites of cultured Purkinje neurons (51). This similar mislocalization suggests that the L629_R634delinW

mutation also increases actin binding. Moreover, AlphaFold predicts that L629_R634delinsW introduces a disordered region that acts as flexible hinge near the linker connecting SRD3 to SRD4. Thus, we expect that L629_R634delinsW, like E532_M544del, will also disrupt coupling SRDs in the α-II/β-III-spectrin dimer.

3.4 Materials and methods

3.4.1 Expression constructs

GFP and mCherry intermediate constructs. To fuse GFP at the N-terminus of full-length β-III-spectrin, pcDNA3.1-mEGFP-N intermediate construct was generated as follow: the coding sequence for mEGFP was PCR amplified using pcDNA3.1-mEGFP (49) as a template, the forward primer AAA GGT ACC ATG GTG AGC AAG GGC GAG GAG CTG TTC A and the reverse primer AAA GAA TTC CTT GTA CAG CTC GTC CAT GCC GAG AGT GAT. The PCR product was digested with KpnI and EcoRI restriction enzymes and ligated into pcDNA3.1(+) vector. To fuse GFP tag at the C-terminus of β-III-spectrin fragment proteins (amino acids 1-1066), pcDNA3.1-mEGFP-C intermediate construct was generated as follow: the coding sequence for mEGFP was PCR amplified using pcDNA3.1-mEGFP (49) as a template, the forward primer GGT ACC ACC ATG GTG AGC AAG GGC GAG GAG CTG TTC ACC GGG GTG GTG CC and the reverse primer AAA TCT AGA CTC GTT CTT CTC TTG CTT ATG GTT GCG TTA CGG CTG TTA CTT TAC TTG TAC AGC TCG TCC ATG CC. The reverse primer introduces a stop codon at the 3' sequence of mEGFP. The PCR product was digested with KpnI and XbaI, and inserted into pcDNA3.1(+) vector.

To fuse mCherry tag at the C-terminus of full-length α-II-spectrin, pcDNA3.1-mCherry-C intermediate construct was generated as follow: the coding sequence for

mCherry was PCR amplified using LifeAct-mCherry construct (a gift from Micheal Davidson; Addgene plasmid #54491) as a template , the forward primer AAA CTC GAG ATG GTG AGC AAG GGC GAG GAG GAT AAC ATG GCC ATC ATC AAG GAG TTC AT and the reverse primer AAA TCT AGA TTA CTT GTA CAG CTC GTC CAT GCC GCC GGT G. The reverse primer introduces a stop codon at the 3' sequence of mCherry. The PCR product was digested with XhoI and XbaI, and ligated into pCDNA3.1(+) vector. To fuse mCherry at the N-terminus of α-II-spectrin fragment protein (amino acids 1545-2473), pcDNA3.1-mCherry-N intermediate construct was generated as follow: the coding sequence for mCherry was PCR amplified using LifeAct-mCherry construct (a gift from Micheal Davidson; Addgene plasmid #54491) as a template, the forward primer AAA CTC GAG ATG GTG AGC AAG GGC GAG GAG GAT AAC ATG GCC ATC ATC AAG GAG TTC AT and the reverse primer AAA CTC GAG TTA CTT GTA CAG CTC GTC CAT GCC GCC GGT G. The PCR product was digested with KpnI and XhoI, and inserted into pcDNA3.1(+) vector.

The (N) and (C) at the end of pcDNA3.1-mEGFP/mCherry intermediate constructs refer to whether GFP/mCherry is fused to the N-terminus (N) or the C-terminus (C) of the spectrin proteins.

Bacteria expression constructs. For N-terminal β-III-spectrin-FLAG fragment proteins (amino acids 1-1066), the wild-type (1-3198 bp) and E532_M544del (1-3159 bp) coding sequences were PCR amplified using pcDNA3.1-myc-β-III-spectrin (48) and pUASp-hSPAM (54) as templates, respectively, the forward primer AAA CAC CTG CAA AAA GGT ATG AGC AGC ACG CTG TCA CCC and the reverse primer AAA TCT AGA TTA CTT GTC GTC ATC GTC TTT GTA GTC CCG CCG CGC CTC CCC

CAG CGA C. The reverse primer contains FLAG epitope sequence to attach FLAG tag at C-terminus of β-III-spectrin proteins (amino acids 1-1066). The PCR products were digested with AarI and XbaI, and were ligated into BasI digested pE-SUMOpro (LifeSensors). This ligation resulted in pE-SUMO-β-III-spectrin-FLAG wild-type (1-3198 bp) or E532_M544del (1-3159 bp) mutant construct. pE-SUMO-β-III-spectrin (1-3198 bp) with R480W mutation was generated with site-directed mutagenesis using pE-SUMO-β-III-spectrin-FLAG wild-type (1-3198 bp) as a template, the sense primer ACA TCG TGG CCT ACA GCG GCT GGG TGC AGG CAG TGG ACG CC and the anti-sense primer GGC GTC CAC TGC CTG CAC CCA GCC GCT GTA GGC CAC GAT GT.

For C-terminal mCherry-α-II-spectrin-HA (amino acids 1545-2473) protein, the 3' coding sequence (4742-7419 bp) of α-II-spectrin was PCR amplified using pcDNA3.1-mCherry-α-II-spectrin (4742-7419 bp) (described below for HEK293T cell expression constructs) as template, the forward primer AAA CAC CTG CAA AAA GGT ATG GTG AGC AAG GGC GAG GAG G and the reverse primer AAA TCT AGA CTA AGC GTA ATC TGG AAC ATC GTA TGG GTA AAC GTT CAC GAA AAG CGA. The forward primer anneals to the 5' sequence of mCherry, and
amplifies the mCherry sequence fused to a coding sequence corresponding to the C-terminal region of α-II-spectrin (4742-7419 bp). The reverse primer inserts HA epitope coding sequence at the 3' sequence of α-II-spectrin. The PCR product was digested with AarI and XbaI and inserted into pE-SUMOpro vector (LifeSensors) digested with BsaI.

HEK293T cell expression constructs. Full-length pcDNA3.1-mEGFP-β-III-spectrin wild-type and E532_M544del constructs were generated in two steps. First, the

5’ coding sequence (1-2025 bp) for β-III-spectrin wild-type and E532_M544del were PCR amplified using pcDNA3.1-myc-β-III-spectrin template for wild-type (48), pUASp-hSPAM template for E532_M544del (54), the forward primer AAA GAA TTC ATG AGC AGC ACG CTG TCA CCC ACA G and the reverse primer AAA TCT AGA ACC GGT CAG GTC TCG GCC. The PCR products were digested with EcoRI and XbaI restriction enzymes, and inserted into pcDNA3.1-mEGFP-N intermediate construct digested with the same enzymes. This insertion resulted in pcDNA3.1-mEGFP-β-III-spectrin (1-2025 bp) intermediate wild-type and E532_M544del constructs. Second, the 3’ coding sequence (2026-7173 bp) of β-III-spectrin was digested with AgeI and XbaI from the pcDNA3.1-myc-β-III-spectrin construct, and ligated into pcDNA3.1-mEGFP-β-III-spectrin (1-2025 bp) intermediate construct digested with the same restriction enzymes. R480W mutation was introduced using site-directed mutagenesis with the pcDNA3.1-mEGFP-β-III-spectrin (1-2025 bp) intermediate construct as a template, the sense primer ACA TCG TGG CCT ACA GCG GCT GGG TGC AGG CAG TGG ACG CC and the anti-sense primer GGC GTC CAC TGC CTG CAC CCA GCC GCT GTA GGC CAC GAT GT. The PCR resulted in pcDNA3.1-mEGFP-β-III-spectrin (1-2025 bp) intermediate construct with R480W mutation. The β-III-spectrin sequence containing R480W mutation was digested with EcoRI and AgeI from the intermediate construct, and inserted into EcoRI and AgeI digested pcDNA3.1-mEGFP-β-III-spectrin construct generated above.

Full-length pcDNA3.1-α-II-spectrin-mCherry was generated in four steps. First, the SbfI recognition sequence in mCherry was mutated using pcDNA3.1-mCherry-C intermediate construct as a template, the forward primer CAG GAC TCC TCC CTG

CAA GAC GGC GAG TTC ATC and the reverse primer GAT GAA CTC GCC GTC TTG CAG GGA GGA GTC CTG. This resulted in pcDNA3.1-mCherry-C construct with mutated SbfI site (pcDNA3.1-mCherry-C-ΔSbfI). Second, the 5' coding sequence (1-3932 bp) of α-II-spectrin was PCR amplified using pF1KB5523-α-II-spectrin (provided) as a template, the forward primer AAA GGT ACC ATG GAC CCA AGT GGG GTC AAA GTG C and the reverse primer AAA GAA TTC CCT GCA GGT CTT CTG GTG AC. The PCR products were digested with KpnI and EcoRI, and were inserted into pcDNA3.1-mCherry-C-ΔSbfI construct digested with the same enzymes. This insertion resulted in pcDNA3.1-α-II-spectrin-mCherry-C-ΔSbfI (1-3932 bp). Third, the 3' sequence (3933-7419 bp) of α-II-spectrin was PCR amplified using pF1KB5523-α-II-spectrin (provided) as a template, the forward primer AAA CCT GCA GGA AAA GTC CAC AGA GTT AAA C and the reverse primer AAA CTC GAG AAC GTT CAC GAA AAG CGA GCG. The PCR product was digested with SbfI and XhoI, and was inserted into pcDNA3.1-α-II-mCherry-C-ΔSbfI (1-3932 bp) construct digested with the same enzymes. After sequencing the final product (pcDNA3.1-α-II-spectrin-mCherry-ΔSbfI), an insertion mutation was found within mCherry sequence. Thus, mutated mCherry sequence was corrected by swapping in the correct mCherry sequence, obtained from pcDNA3.1-mCherry-C, using XhoI and BsrGI.

For N-terminal β-III-spectrin-GFP proteins (amino acids 1-1066) used for FRET and co-IP experiments, the 5' sequence of β-III-spectrin wild-type (1-3198 bp) was PCR amplified using the full-length pcDNA3.1-myc-β-III-spectrin (48) as a template, the forward primer AAA GCT AGC ATG AGC AGC ACG CTG TCA CCC and the reverse primer AAA GGT ACC CCG CCG CGC CTC CCC CAG CGA C. The PCR product

was digested with NheI and KpnI, and was inserted into pcDNA3.1-mEGFP-C intermediate construct digested with the same enzymes. The final product of this insertion is pcDNA3.1-β-III-spectrin-mEGFP (amino acids 1-1066). For R480W and E532_M544del β-III-spectrin-GFP (amino acids 1-1066) proteins, HindIII and AgeI digestion was performed to isolate β-III-spectrin sequence containing R480W or E532_M544del from pE-SUMO-β-III-spectrin-FLAG constructs generated above. The digestion products were inserted into pcDNA3.1-β-III-spectrin-mEGFP (amino acids 1-1066) digested with the same enzymes. The final products are pcDNA3.1-β-III-spectrin-mEGFP (amino acids 1-1066) R480W and E532_M544del constructs. For mCherry-α-II-spectrin (amino acids 1545-2473) proteins, the 3' coding sequence (4742-7419 bp) of α-II-spectrin was PCR amplified using pF1KB5523-α-II-spectrin (company) as a template, the forward primer AAA CTC GAG GGA GAA TCT CAA ACC CTC C and the reverse primer AAA TCT AGA TTA AAC GTT CAC GAA AAG CGA G. The PCR products were digested with XhoI and XbaI, and inserted into pcDNA3.1-mCherry-N digested with same enzymes. This insertion resulted in pcDNA3.1-mCherry-α-II-spectrin (amino acids 1545-2473) construct.

PM-GFP was a gift from Tobias Meyer, Stanford University, Stanford, CA (Addgene plasmid #21213). mCherry-Mem was purchased from Addgene (Plasmid #55779). PCR amplifications were performed using iProof-HF polymerase (BioRad). Site-directed mutagenesis was performed using PfuUltra polymerase (Agilent). All constructs were sequence verified. The NCBI reference cDNA sequence for β-III-spectrin is NM_006946.4 and α-II-spectrin is NM_001375314.2.

3.4.2 Protein expression and purification

For N-terminal β-III-spectrin-FLAG (amino acids 1-1066) expression, pE-SUMO-β-III-spectrin-FLAG constructs were transformed into Rosetta2 (DE3) *E. coli* (Sigma). After transformation, single colonies were grown overnight at 250 rpm and 37 °C in a 50 mL LB broth (Miller) supplemented with 100 µg/mL ampicillin and 34 µg/mL chloramphenicol antibiotics. Each overnight culture was expanded into four flasks each containing 250 mL LB broth (Miller) supplemented with the same antibiotics, and grown at 37°C and 250 rpm until the culture OD_{550} reached 0.5-0.7. Protein expression was induced with 0.3 mM IPTG (Fisher bioreagents), and incubated at 16 °C and 250 rpm for 16-24 hours before pelleting.

For purification, the bacteria pellets were resuspended in lysis buffer (50 mM Tris pH 7.5, 300 mM NaCl, 25% sucrose, 1X cOmplete, EDTA-free protease inhibitors (Roche) and 4:1 (w/v) Lysozyme (GoldBio)), and agitated at 4 °C for 30 minutes. Further protein extraction was achieved with sonication at 15 seconds on and 45 seconds off cycles for total time of 3 minutes at 45% amplitude, using a Branson 250 sonifier with tip size of ½ inch. Lysate supernatants were collected after centrifugation at 40,905 x g and 4°C using Sorvall SS-34 rotor for 30 minutes. The supernatants were clarified using 0.45 µm disk filters, and loaded into Poly-Prep chromatography column (BioRad) packed with equilibrated Ni-NTA agarose beads (Invitrogen). Following three washes with 50 mM Tris pH 7.5, 300 mM NaCl and 20 mM imidazole buffer, SUMO-β-III-spectrin-FLAG proteins were eluted off the columns with 50 mM Tris pH 7.5, 300 mM NaCl and 150 mM imidazole buffer. After adding 1:1 volume ratio of 25 mM Tris pH 7.5, 150 mM NaCl, and 5 mM 2-Mercaptoethanol buffer to the eluted proteins, SUMO tag was

digested with 1:100 mass ratio of Ulp1 SUMO protease to total eluted protein for 30 minutes at 4°C. Then, digested proteins were loaded into 10,000 MWCO Slide-A-Lyzer cassettes (Thermo Scientific) for buffer exchange into 50 mM Tris pH 7.5 and 150 mM NaCl, and incubated at 4 °C stirring for 4-6 hours to remove 2-mercaptoethanol. After dialysis, the proteins were loaded into Poly-Prep columns packed with equilibrated anti-FLAG M2 affinity gel beads (Sigma) at 4 °C. After several washes with 50 mM Tris pH 7.5 and 150 mM NaCl buffer, β-III-spectrin-FLAG (amino acids 1-1066) proteins were eluted with 10 mM Tris pH 7.5, 150 mM NaCl and 200 ng/µL FLAG peptide (Sigma) buffer. Final buffer exchange into 10 mM Tris pH 7.5, 150 mM NaCl, 2 mM $MgCl_2$ and 1 mM DTT buffer was performed using 10,000 MWCO Slide-A-Lyzer cassettes stirring overnight at 4 °C. Pure β-III-spectrin-FLAG proteins were supplemented with 25% sucrose before snap-freezing and storage at -80 °C.

Similar expression protocol was followed for C-terminal mCherry-αII-spectrin-HA (amino acids 1545-2473) fragment. For protein purification, SUMO-mCherry-α-II-spectrin-HA protein was purified by Ni-NTA beads, followed by cleavage of the His-SUMO tag using Ulp1 protease. The digest was then loaded onto a GE S100 size exclusion column equilibrated in 10 mM HEPES pH 7.5, 150 mM NaCl, 2 mM $MgCl_2$ and 1 mM DTT buffer, and fractions containing mCherry-α-II-spectrin-HA collected.

3.4.3 Circular dichroism spectroscopy

Purified β-III-spectrin-FLAG fragment proteins (amino acids 1-1066) were thawed and clarified at 100,000 x g and 4 °C for 15 minutes using TLA 100.3 rotor (Beckman). Bradford assay was performed to determine the protein concentration. β-III-spectrin-FLAG proteins (amino acids 1-1066) were diluted to a final concentration of 150

ng/mL in 10 mM Tris pH 7.5, 150 mM NaCl, 2 mM $MgCl_2$, 1 mM DTT buffer. Jasco J-810 spectropolarimeter with Peltier temperature controller was used to collect absorption profiles and thermal denaturation data as was described previously (38). Absorption data were reported as mean residue ellipticity (degrees cm^2 $dmol^{-1}$) after converting the raw data (38). Thermal denaturation data were measured at 222 nm, and melting temperatures were calculated as described previously using Prims 10 (GraphPad) and non-linear regression to fit a two-state transition equation (38).

3.4.4 Live-cell FRET assay

HEK293T cells (ATTC) were either transfected with 0.5 µg pcDNA3.1-β-III-spectrin-mEGFP (amino acids 1-1066) FRET donor constructs (D) only, or co-transfected with 2 µg pcDNA3.1-mCherry-α-II-spectrin (amino acids 1545-2473) FRET acceptor construct (A) following Lipofectamine 3000 protocol (ThermoFisher Scientific) in a 6-well plate. Twenty-Four hours following transfection, cells were harvested and prepared for GFP fluorescence lifetime measurement as previously described (49). FS5 spectrofluorometer equipped with an EPL-472 pulse laser with 5 MHz frequency (Edinburgh Instruments) was used to collect and calculate GFP lifetime (τ) in donor (D) and donor acceptor (DA) samples. FRET efficiency was calculated using the following equation:

$$E = 1 - \frac{\tau DA}{\tau D} \quad (1)$$

3.4.5 Co-immunoprecipitation assay

For β-III-spectrin-GFP (amino acids 1-1066) and mCherry-α-II-spectrin (amino acids 1545-2473) co-immunoprecipitation (co-IP) assay, 0.5 µg of pcDNA3.1-β-III-

spectrin-mEGFP constructs were co-transfected with 2 µg pcDNA3.1-mCherry-α-II-spectrin in HEK293T cells in a 6-well plate, using Lipofectamine 3000, as described for FRET assays. Twenty-four hours post transfection, cells were washed once with 1X DPBS (Gibco), resuspended in ice-chilled lysis buffer (10 mM Tris pH 7.5, 150 mM NaCl, 320 mM sucrose, 2 mM EDTA, 1% Triton X-100, 0.5% IGEPAL CA-630, 0.1% SDS, 1X cOmplete mini, EDTA-free protease inhibitor (Roche)) and incubated on ice for 30 minutes with gentle swirling every 10 minutes. Supernatants were collected after spinning the lysates at 16,000 x g and 4 °C for 10 minutes. A small volume of clarified supernatants was mixed with 4x Laemmli sample buffer (BioRad) and saved at -20 °C for lysate/input analysis on western blots.

To precipitate β-III-spectrin-GFP proteins, GFP-Trap magnetic agarose (Chromotek) beads were first equilibrated with 10 mM Tris pH 7.5, 150 mM NaCl, 2 mM EDTA buffer, and then were incubated with the supernatant samples rotating at 4 °C for 1 hour. After several washes with 10 mM Tris pH 7.5, 150 mM NaCl, 2 mM EDTA buffer, IP samples were eluted into 4x Laemmli sample buffer and heated to 95 °C for 5 minutes.

For western blot analysis, IP and lysate/input samples were resolved by SDS-PAGE and transferred to Immobilon-FL membranes (Millipore). Membranes were blocked with 1X PBS-L (48) containing 1% casein (Hammarsten; Affymetrix). Primary antibodies were diluted in 1X PBS-L, 1% casein and 0.1% Tween 20 buffer, and incubated with the membranes overnight at 4 °C. Primary antibodies included: anti-GFP (1:2000; Millipore), anti-α-II-spectrin C-11 (1:200; Santa Cruz); anti-mCherry (1:2000; Invitrogen). Membranes were washed with 1X PBS-L containing 0.1% Tween 20. Secondary antibodies were diluted to 1:5000 in 1X PBS-L supplemented with 1% Casein,

0.1% Tween 20 and 0.01% SDS, and incubated with the membranes for 1 hour at room temperature. Secondary antibodies used include anti-mouse IRDye 800CW (LI-COR Biosciences) and anti-rabbit IRDye 680RD (LI-COR Biosciences). Membranes were washed with 1X PBS-L containing 0.1% Tween 20 and imaged on a Sapphire scanner (Azure) using 680 nm and 800 nm channels. Fluorescence protein band intensities were quantified using ImageStudio Lite (LI-COR Bioscience) as described previously (49).

3.4.6 Fluorescence subcellular localization assays

Glass coverslips (22 x 22 mm; #1.5; Thermo Fisher Scientific) were cleaned with 70% ethanol, placed in 6-well plate and washed with Ultrapure water (Gibco). The coverslips were incubated with 0.1 mg/mL poly-D-lysine, 70–150 kDa (Sigma) solution for 20 minutes at room temperature. Poly-D-lysine solution was discarded, coverslips washed multiple times with Ultrapure water and sterilized under UV light for 1 hour. HEK293T cells were plated on the coated glass coverslips at 0.3x 106 cells per well, and incubated for 2-4 hours at 37°C and 5% CO2. The cells were co-transfected with Lipofectamine 3000 and 0.5 µg full-length pcDNA3.1-mEGFP-β-III-spectrin or 0.25 µg PM-GFP with or without 0.5 µg full-length pcDNA3.1-α-II-spectrin-mCherry, or with 0.25 µg mCherry-Mem. Twenty-four hours post transfection, the cells were washed with 1X DPBS and fixed with 4% paraformaldehyde in 1X DPBS for 15-30 minutes at room temperature. The cells were washed again with 1X DPBS, and mounted on a 1 mm microscope slide (VWR) using Prolong Diamond antifade with DAPI (Invitrogen). After 24 hours, the cells were imaged using a HC PL APO 63x/1.40-0.60 OIL oil-immersion objective on a Leica DMi8 inverted microscope equipped with X-Light V2 spinning-disk (CrestOptics), LDI laser unit (89 North) and Photometrics Prime 95B CMOS camera. Z-

stack images were processed using ImageJ (NIH) or Photoshop software (Adobe). Representative intensity vs distance profiles were obtained using ImageJ line tool and RGB Profile plugin. Pearson correlation coefficient was calculated in Prism 10 (GraphPad) after measuring GFP and mCherry intensities using the Line and Plot Profile tools in ImageJ. Images of cells expressing GFP-β-III-spectrin proteins were visually scored for inclusions or smooth cell surface.

3.4.7 Actin co-sedimentation assay

Purified β-III-spectrin-FLAG proteins (amino acids 1-1066) were thawed and clarified at 43,000 rpm using TLA-100.3 rotor (Beckman). Actin was extracted from rabbit muscle acetone powder (Pal-Freez Biologicals) and polymerized into F-actin as described previously (49). Bradford assay was performed to measure the concentration of the proteins. β-III-spectrin-FLAG proteins were diluted to 0.5 μM and mixed with varying concentrations of F-actin (3-120 μM) in F-buffer (10 mM Tris pH 7.5, 150 mM NaCl, 0.5 mM ATP, 2 mM MgCl2, 1 mM DTT). For standard curve, β-III-spectrin-FLAG proteins were diluted to 0.5 μM and 0.175 μM. The samples were incubated at room temperature for 30 minutes. Then, the samples were centrifuged at 50,000 rpm and 25 °C for 30 minutes using TLA-100 rotor (Beckman) to pellet F-actin and bound β-III-spectrin-FLAG proteins. Supernatant samples containing unbound β-III-spectrin-FLAG proteins were collected and mixed with 4x Laemmli sample buffer. Supernatant samples were separated by SDS-PAGE using 12% acrylamide gels. Gels were stained with Coomassie R-250, and imaged using a Sapphire fluorescence scanner (Azure). Fluorescence protein band intensities were quantified using ImageStudio Lite software (LICOR) and dissociation constant (Kd) and Bmax calculated in Prism 10 (GraphPad)

using the equation: Y = Bmax*X/(Kd + X), where Y is the bound protein fraction and X is the free F-actin fraction (55).

References

1. Ikeda, Y., Dick, K. A., Weatherspoon, M. R., Gincel, D., Armbrust, K. R., Dalton, J. C. *et al.* (2006) Spectrin mutations cause spinocerebellar ataxia type 5 Nat Genet **38**, 184-190 10.1038/ng1728
2. Bian, X., Wang, S., Jin, S., Xu, S., Zhang, H., Wang, D. *et al.* (2021) Two novel missense variants in SPTBN2 likely associated with spinocerebellar ataxia type 5 Neurol Sci **42**, 5195-5203 10.1007/s10072-021-05204-3
3. Liu, L. Z., Ren, M., Li, M., Ren, Y. T., Sun, B., Sun, X. S. *et al.* (2016) A Novel Missense Mutation in the Spectrin Beta Nonerythrocytic 2 Gene Likely Associated with Spinocerebellar Ataxia Type 5 Chin Med J (Engl) **129**, 2516-2517 10.4103/0366-6999.191834
4. Cho, E., andFogel, B. L. (2013) A Family with Spinocerebellar Ataxia Type 5 Found to Have a Novel Missense Mutation within a SPTBN2 Spectrin Repeat The Cerebellum **12**, 162-164 10.1007/s12311-012-0408-0
5. Fogel, B. L., Lee, H., Deignan, J. L., Strom, S. P., Kantarci, S., Wang, X. *et al.* (2014) Exome sequencing in the clinical diagnosis of sporadic or familial cerebellar ataxia JAMA Neurol **71**, 1237-1246 10.1001/jamaneurol.2014.1944
6. Wang, Y., Koh, K., Miwa, M., Yamashiro, N., Shindo, K., andTakiyama, Y. (2014) A Japanese SCA5 family with a novel three-nucleotide in-frame deletion mutation in the SPTBN2 gene: a clinical and genetic study J Hum Genet **59**, 569-573 10.1038/jhg.2014.74

7. Ranum, L. P., Schut, L. J., Lundgren, J. K., Orr, H. T., andLivingston, D. M. (1994) Spinocerebellar ataxia type 5 in a family descended from the grandparents of President Lincoln maps to chromosome 11 Nat Genet **8**, 280-284 10.1038/ng1194-280

8. Stevanin, G., Herman, A., Brice, A., andDürr, A. (1999) Clinical and MRI findings in spinocerebellar ataxia type 5 Neurology **53**, 1355-1357 10.1212/wnl.53.6.1355

9. Bürk, K., Zühlke, C., König, I. R., Ziegler, A., Schwinger, E., Globas, C. *et al.* (2004) Spinocerebellar ataxia type 5: clinical and molecular genetic features of a German kindred Neurology **62**, 327-329 10.1212/01.wnl.0000103293.63340.c1

10. Lise, S., Clarkson, Y., Perkins, E., Kwasniewska, A., Sadighi Akha, E., Schnekenberg, R. P. *et al.* (2012) Recessive mutations in SPTBN2 implicate β-III spectrin in both cognitive and motor development PLoS Genet **8**, e1003074 10.1371/journal.pgen.1003074

11. Elsayed, S. M., Heller, R., Thoenes, M., Zaki, M. S., Swan, D., Elsobky, E. *et al.* (2014) Autosomal dominant SCA5 and autosomal recessive infantile SCA are allelic conditions resulting from SPTBN2 mutations European Journal of Human Genetics **22**, 286-288 10.1038/ejhg.2013.150

12. Yıldız Bölükbaşı, E., Afzal, M., Mumtaz, S., Ahmad, N., Malik, S., andTolun, A. (2017) Progressive SCAR14 with unclear speech, developmental delay, tremor, and behavioral problems caused by a homozygous deletion of the SPTBN2 pleckstrin homology domain Am J Med Genet A **173**, 2494-2499 10.1002/ajmg.a.38332

13. Jacob, F. D., Ho, E. S., Martinez-Ojeda, M., Darras, B. T., andKhwaja, O. S. (2013) Case of infantile onset spinocerebellar ataxia type 5 J Child Neurol **28**, 1292-1295 10.1177/0883073812454331

14. Parolin Schnekenberg, R., Perkins, E. M., Miller, J. W., Davies, W. I., D'Adamo, M. C., Pessia, M. *et al.* (2015) De novo point mutations in patients diagnosed with ataxic cerebral palsy Brain **138**, 1817-1832 10.1093/brain/awv117

15. Nuovo, S., Micalizzi, A., D'Arrigo, S., Ginevrino, M., Biagini, T., Mazza, T. *et al.* (2018) Between SCA5 and SCAR14: delineation of the SPTBN2 p.R480W-associated phenotype European Journal of Human Genetics **26**, 928-929 10.1038/s41431-018-0158-7

16. Mizuno, T., Kashimada, A., Nomura, T., Moriyama, K., Yokoyama, H., Hasegawa, S. *et al.* (2019) Infantile-onset spinocerebellar ataxia type 5 associated with a novel SPTBN2 mutation: A case report Brain Dev **41**, 630-633 10.1016/j.braindev.2019.03.002

17. Accogli, A., St-Onge, J., Addour-Boudrahem, N., Lafond-Lapalme, J., Laporte, A. D., Rouleau, G. A. *et al.* (2020) Heterozygous Missense Pathogenic Variants Within the Second Spectrin Repeat of SPTBN2 Lead to Infantile-Onset Cerebellar Ataxia J Child Neurol **35**, 106-110 10.1177/0883073819878917

18. Nicita, F., Nardella, M., Bellacchio, E., Alfieri, P., Terrone, G., Piccini, G. *et al.* (2019) Heterozygous missense variants of SPTBN2 are a frequent cause of congenital cerebellar ataxia Clin Genet **96**, 169-175 10.1111/cge.13562

19. Rea, G., Tirupathi, S., Williams, J., Clouston, P., andMorrison, P. J. (2020) Infantile Onset of Spinocerebellar Ataxia Type 5 (SCA-5) in a 6 Month Old with Ataxic Cerebral Palsy The Cerebellum **19**, 161-163 10.1007/s12311-019-01085-7

20. Zonta, A., Brussino, A., Dentelli, P., andBrusco, A. (2020) A novel case of congenital spinocerebellar ataxia 5: further support for a specific phenotype associated with the p.(Arg480Trp) variant in SPTBN2 BMJ Case Rep **13**, 10.1136/bcr-2020-238108

21. Sancho, P., Andrés-Bordería, A., Gorría-Redondo, N., Llano, K., Martínez-Rubio, D., Yoldi-Petri, M. E. *et al.* (2021) Expanding the β-III Spectrin-Associated Phenotypes toward Non-Progressive Congenital Ataxias with Neurodegeneration Int J Mol Sci **22**, 10.3390/ijms22052505

22. Romaniello, R., Citterio, A., Panzeri, E., Arrigoni, F., De Rinaldis, M., Trabacca, A. *et al.* (2021) Novel *SPTBN2* gene mutation and first intragenic deletion in early onset spinocerebellar ataxia type 5 Annals of Clinical and Translational Neurology **8**, 956-963 10.1002/acn3.51345

23. Spagnoli, C., Frattini, D., Gozzi, F., Rizzi, S., Salerno, G. G., Cimino, L. *et al.* (2021) Infantile-Onset Spinocerebellar Ataxia Type 5 (SCA5) with Optic Atrophy and Peripheral Neuropathy Cerebellum **20**, 481-483 10.1007/s12311-020-01214-7

24. Ohara, O., Ohara, R., Yamakawa, H., Nakajima, D., andNakayama, M. (1998) Characterization of a new beta-spectrin gene which is predominantly expressed in brain Brain Res Mol Brain Res **57**, 181-192 10.1016/s0169-328x(98)00068-0

25. Speicher, D. W., Weglarz, L., andDeSilva, T. M. (1992) Properties of human red cell spectrin heterodimer (side-to-side) assembly and identification of an essential nucleation site J Biol Chem **267**, 14775-14782,

26. Shotton, D. M., Burke, B. E., andBranton, D. (1979) The molecular structure of human erythrocyte spectrin. Biophysical and electron microscopic studies J Mol Biol **131**, 303-329 10.1016/0022-2836(79)90078-0

27. Cohen, C. M., andLangley, R. C., Jr. (1984) Functional characterization of human erythrocyte spectrin alpha and beta chains: association with actin and erythrocyte protein 4.1 Biochemistry **23**, 4488-4495 10.1021/bi00314a039

28. Xu, K., Zhong, G., andZhuang, X. (2013) Actin, spectrin, and associated proteins form a periodic cytoskeletal structure in axons Science **339**, 452-456 10.1126/science.1232251

29. Han, B., Zhou, R., Xia, C., andZhuang, X. (2017) Structural organization of the actin-spectrin-based membrane skeleton in dendrites and soma of neurons Proc Natl Acad Sci U S A **114**, E6678-e6685 10.1073/pnas.1705043114

30. Ursitti, J. A., Kotula, L., DeSilva, T. M., Curtis, P. J., andSpeicher, D. W. (1996) Mapping the human erythrocyte beta-spectrin dimer initiation site using recombinant peptides and correlation of its phasing with the alpha-actinin dimer site J Biol Chem **271**, 6636-6644 10.1074/jbc.271.12.6636

31. Begg, G. E., Harper, S. L., Morris, M. B., andSpeicher, D. W. (2000) Initiation of Spectrin Dimerization Involves Complementary Electrostatic Interactions between Paired Triple-helical Bundles Journal of Biological Chemistry **275**, 3279-3287 10.1074/jbc.275.5.3279

32. Li, D., Harper, S., andSpeicher, D. W. (2007) Initiation and propagation of spectrin heterodimer assembly involves distinct energetic processes Biochemistry **46**, 10585-10594 10.1021/bi7007905

33. An, X., Guo, X., Yang, Y., Gratzer, W. B., Baines, A. J., andMohandas, N. (2011) Inter-subunit interactions in erythroid and non-erythroid spectrins Biochim Biophys Acta **1814**, 420-427 10.1016/j.bbapap.2010.12.010

34. Li, X., andBennett, V. (1996) Identification of the spectrin subunit and domains required for formation of spectrin/adducin/actin complexes J Biol Chem **271**, 15695-15702 10.1074/jbc.271.26.15695

35. Avery, A. W., Crain, J., Thomas, D. D., andHays, T. S. (2016) A human β-III-spectrin spinocerebellar ataxia type 5 mutation causes high-affinity F-actin binding Sci Rep **6**, 21375 10.1038/srep21375

36. Atang, A. E., Keller, A. R., Denha, S. A., andAvery, A. W. (2023) Increased Actin Binding Is a Shared Molecular Consequence of Numerous SCA5 Mutations in β-III-Spectrin Cells **12**, 10.3390/cells12162100

37. Bañuelos, S., Saraste, M., andDjinović Carugo, K. (1998) Structural comparisons of calponin homology domains: implications for actin binding Structure **6**, 1419-1431 10.1016/s0969-2126(98)00141-5

38. Avery, A. W., Fealey, M. E., Wang, F., Orlova, A., Thompson, A. R., Thomas, D. D. *et al.* (2017) Structural basis for high-affinity actin binding revealed by a β-III-spectrin SCA5 missense mutation Nat Commun **8**, 1350 10.1038/s41467-017-01367-w

39. Yan, Y., Winograd, E., Viel, A., Cronin, T., Harrison, S. C., andBranton, D. (1993) Crystal structure of the repetitive segments of spectrin Science **262**, 2027-2030 10.1126/science.8266097

40. Grum, V. L., Li, D., MacDonald, R. I., andMondragón, A. (1999) Structures of two repeats of spectrin suggest models of flexibility Cell **98**, 523-535 10.1016/s0092-8674(00)81980-7

41. Kusunoki, H., Minasov, G., Macdonald, R. I., andMondragón, A. (2004) Independent movement, dimerization and stability of tandem repeats of chicken brain alpha-spectrin J Mol Biol **344**, 495-511 10.1016/j.jmb.2004.09.019

42. Mehboob, S., Song, Y., Witek, M., Long, F., Santarsiero, B. D., Johnson, M. E. *et al.* (2010) Crystal structure of the nonerythroid alpha-spectrin tetramerization site reveals differences between erythroid and nonerythroid spectrin tetramer formation J Biol Chem **285**, 14572-14584 10.1074/jbc.M109.080028

43. Ipsaro, J. J., Huang, L., andMondragón, A. (2009) Structures of the spectrin-ankyrin interaction binding domains Blood **113**, 5385-5393 10.1182/blood-2008-10-184358

44. Li, N., Chen, S., Xu, K., He, M. T., Dong, M. Q., Zhang, Q. C. *et al.* (2023) Structural basis of membrane skeleton organization in red blood cells Cell **186**, 1912-1929.e1918 10.1016/j.cell.2023.03.017

45. Lebon, F., Bignotti, F., Penco, M., Gangemi, R., Longhi, G., andAbbate, S. (2003) Detection by circular dichroism of conformational transitions in pH and thermosensitive copolymers based on N-isopropylacrylamide and N-methacryloyl-L-leucine Chirality **15**, 251-255 10.1002/chir.10188

46. Abramson, J., Adler, J., Dunger, J., Evans, R., Green, T., Pritzel, A. *et al.* (2024) Accurate structure prediction of biomolecular interactions with AlphaFold 3 Nature **630**, 493-500 10.1038/s41586-024-07487-w

47. Evans, R., O'Neill, M., Pritzel, A., Antropova, N., Senior, A., Green, T. *et al.* (2021) Protein complex prediction with AlphaFold-Multimer Cold Spring Harbor Laboratory,

48. Avery, A. W., Thomas, D. D., andHays, T. S. (2017) β-III-spectrin spinocerebellar ataxia type 5 mutation reveals a dominant cytoskeletal mechanism that underlies dendritic arborization Proc Natl Acad Sci U S A **114**, E9376-e9385 10.1073/pnas.1707108114

49. Denha, S. A., Atang, A. E., Hays, T. S., andAvery, A. W. (2022) β-III-spectrin N-terminus is required for high-affinity actin binding and SCA5 neurotoxicity Sci Rep **12**, 1726 10.1038/s41598-022-05762-2

50. Brown, J. W., Bullitt, E., Sriswasdi, S., Harper, S., Speicher, D. W., andMcKnight, C. J. (2015) The Physiological Molecular Shape of Spectrin: A Compact Supercoil Resembling a Chinese Finger Trap PLOS Computational Biology **11**, e1004302 10.1371/journal.pcbi.100430251.

51. Boyer, N. P., Sharma, R., Wiesner, T., Delamare, A., Pelletier, F., Leterrier, C. *et al.* (2024) Spectrin condensates provide a nidus for assembling the periodic axonal structure Cold Spring Harbor Laboratory,

52. Cousin, M. A., Creighton, B. A., Breau, K. A., Spillmann, R. C., Torti, E., Dontu, S. *et al.* (2021) Pathogenic SPTBN1 variants cause an autosomal dominant

neurodevelopmental syndrome Nat Genet **53**, 1006-1021 10.1038/s41588-021-00886-z

53. Fujishima, K., Kurisu, J., Yamada, M., andKengaku, M. (2020) βIII spectrin controls the planarity of Purkinje cell dendrites by modulating perpendicular axon-dendrite interaction Development **147**, dev194530 10.1242/dev.194530

54. Armbrust, K. R., Wang, X., Hathorn, T. J., Cramer, S. W., Chen, G., Zu, T. *et al.* (2014) Mutant -III Spectrin Causes mGluR1 Mislocalization and Functional Deficits in a Mouse Model of Spinocerebellar Ataxia Type 5 Journal of Neuroscience **34**, 9891-9904 10.1523/jneurosci.0876-14.2014

55. Gao, Y., Perkins, E. M., Clarkson, Y. L., Tobia, S., Lyndon, A. R., Jackson, M. *et al.* (2011) β-III spectrin is critical for development of purkinje cell dendritic tree and spine morphogenesis J Neurosci **31**, 16581-16590 10.1523/jneurosci.3332-11.2011

56. Lorenzo, D. N., Li, M. G., Mische, S. E., Armbrust, K. R., Ranum, L. P., andHays, T. S. (2010) Spectrin mutations that cause spinocerebellar ataxia type 5 impair axonal transport and induce neurodegeneration in Drosophila J Cell Biol **189**, 143-158 10.1083/jcb.200905158

57. Pollard, T. D. (2010) A guide to simple and informative binding assays Mol Biol Cell **21**, 4061-4067 10.1091/mbc.E10-08-0683

CHAPTER FOUR

CONCLUSION

4.0 The N-Terminus

Here we will summarize key findings and interpretations of our studies of the β-spectrin N-terminus, and discuss remaining questions and future directions. We examined the significance of the N-terminal sequence preceding the conserved, tandem-CH ABD, to β-spectrin function in neurons. Previously we showed *in vitro* that N-terminal truncation abolishes actin binding of the wild-type β-III-spectrin ABD (1). Actin binding is required for β-spectrin proteins to crosslink actin filaments and to form a sub-plasma membrane spectrin-actin cytoskeleton in neurons (2, 3). Thus, we predicted that the N-terminus would be required for β-spectrin function in neurons. In viability rescue assays, using the *elav-Gal4* pan-neuronal driver, we showed that the N-terminus is essential for β-spectrin function in neurons. In these assays, expression of a wild-type β-spectrin transgene with intact N-terminus rescued ~25% of the flies homozygous for the recessive lethal $\beta spec^{em21}$ loss-of-function allele. In contrast, the expression of the N-terminally truncated wild-type β-spectrin transgene did not rescue $\beta spec^{em21}$ lethality. We also showed that the inability of the N-terminally truncated wild-type transgene to rescue lethality was not due to low β-spectrin protein level. On the contrary, the N-terminally truncated wild-type protein was 5-fold more abundant than wild-type protein, in *Drosophila* head extracts. This increase in protein level may reflect the 1 °C increase in thermostability that we observe in CD denaturation studies of the purified β-III-spectrin ABD lacking the N-terminus, compared to ABD with intact N-terminus (1, 4).

Altogether, these experiments highlighted that the N-terminus is essential for β-spectrin function in neurons, likely to support spectrin actin-binding activity.

We also showed that expression of the N-terminally truncated wild-type transgene is mildly neurotoxic when expressed broadly in neuronal tissue with *elav-Gal4*, causing a ~33% reduction in viability of flies heterozygous for $\beta spec^{em21}$ ($\beta spec^{em21}$ heterozygotes are otherwise healthy), or in a wild-type genetic background (no $\beta spec^{em21}$). This suggests that the N-terminally truncated β-spectrin may function as a dominant negative mutant *in vivo*. How would the N-terminally truncated β-spectrin act as a dominant negative? One possibility is that the mutant is incorporated into spectrin heterotetramer containing endogenous wild-type β-spectrin and α-spectrin. Incorporation of the transgenic N-terminally truncated β-spectrin into the endogenous spectrin heterotetramer would "poison" the heterotetramer by blocking the actin crosslinking activity of the heterotetramer. We also tested whether the N-terminally truncated β-spectrin dominantly interferes with dendritic arborization. For these experiments, β-spectrin transgenes were specifically expressed in class IV dendritic arborization (da) neurons using the *477-Gal4* driver. However, we did not observe dendritic arbor defects in class IV da neurons expressing the truncated β-spectrin. This is consistent with the mild neurotoxicity observed when the mutant is expressed with the pan-neuronal *elav-Gal4* driver. We expect that we would observe dendritic defects if expression of the truncated β-spectrin in da neurons was increased, for example by using a stronger class IV da neuron driver, such as *ppk-Gal4* driver (5).

In addition, we studied the functional interaction between the N-terminus and the SCA5 ABD-localized mutation, L253P. *In vitro*, we previously showed that the L253P

mutation causes a 1000-fold increase in actin-binding affinity of the β-III-spectrin ABD (6). The L253P mutation localizes to the CH2 sub-domain and is positioned at the CH1-CH2 interface (6). Biophysical analyses indicated that the high-affinity actin binding induced by L253P is due to the effect of the mutation to open the CH1-CH2 interface. This allows CH1 to directly bind actin by unmasking actin-binding residues in CH1, and by repositioning CH2 to avoid steric clash between CH2 and actin (1). We wondered whether the N-terminus was also required for L253P to induce high-affinity actin binding, or for L253P neurotoxicity and dendritic arbor defects in flies. Intriguingly, our *in vitro* co-sedimentation assays showed that truncation of the N-terminus eliminated high-affinity actin binding of the L253P ABD. The N-terminally truncated L253P ABD still bound actin. However, it bound actin with lower affinity (Kd ~ 200 μM) than the wild-type ABD with intact N-terminus (Kd ~75 μM). In *Drosophila*, pan-neuronal expression of the L253P mutant with intact N-terminus caused ~100% lethality (4, 7). In contrast, expression of the N-terminally truncated L253P β-spectrin transgene did not cause lethality. Moreover, in class IV da neurons, the N-terminally truncated L253P β-spectrin did not induce dendritic arbor defects, as were observed for the L253P mutant with intact N-terminus. We further analyzed head extracts to determine the protein level of the SCA5 mutant with and without the N-terminus. The SCA5 mutant with intact N-terminus showed higher protein level compared to the wild-type protein with intact N-terminus. In contrast, the N-terminally truncated SCA5 mutant had a protein level lower than both the SCA5 mutant and wild-type with intact N-terminus. Our CD thermal denaturation studies showed that the L253P mutation causes ~15 °C decrease in thermostability of the β-III-spectrin ABD. This reduced thermal stability likely reflects

the opening of the CH1-CH2 interface and the exposure of hydrophobic surfaces. The N-terminal truncation increases the thermal stability of the L253P ABD by ~1 °C. If N-terminal truncation slightly increases thermal stability, why does the N-terminally truncated L253P mutant have lower protein level than the L253P mutant with intact N-terminus, in *Drosophila*? We suggest that L253P mutant has increased protein level because it can bind actin with high affinity, generating a stable L253P spectrin-actin complex. In contrast, the N-terminally truncated L253P mutant binds actin very weakly. Thus, the N-terminally truncated L253P mutant remains in a highly unstable state, due to the effect of L253P to expose the hydrophobic surfaces and the inability of the truncated mutant to bury these hydrophobic residues by binding actin. The N-terminally truncated L253P mutant is thus likely to have a high protein turnover rate compared to the L253P mutant with intact N-terminus, resulting in low steady state protein level for the truncated mutant. However, we have not determined experimentally the protein turnover rates of the mutant proteins, and thus this proposed mechanism remains to be confirmed.

Why is the N-terminus so important to the binding of β-III-spectrin to actin? Prior structural analyses of filamin A ABD showed that the beginning of CH1 helix A is deformed, repositioned by ~3 angstroms, upon actin binding (8). Iwamoto et al suggested that this structural-induced change, upon the binding of the N-terminal residues to actin, allows CH1 residues to position close and to directly interact with actin. Similarly, we overlayed a homology structure of β-III-spectrin ABD, in the actin unbound state, with the cryo-EM structure of the β-III-spectrin ABD, in bound state. **Figure 4.1**. The homology model predicted that the N-terminus is extended linearly and is continuous with helix A of CH1. In the cryo-EM structure of the actin-bound ABD, a pronounced

bend is present at the junction of the N-terminus and CH1. Further structural analysis shows that residues at the beginning of CH1 (R55, V58, Q59) are predicted to contact CH2 residue, D265 in the actin unbound state. Interestingly, these residues on CH1 are shown to be repositioned by several Angstroms when the ABD is bound to actin. Thus, we suggest a model where the binding of the N-terminus to actin induces a mild conformational change that alters contacts between CH1 and CH2. This conformational change loosens the interface, helping to reposition CH1 residues away from CH2 and exposing the actin-binding sites in CH1. This proposed model may explain why N-terminally truncated wild-type ABD cannot bind actin: the N-terminus is first needed to bind actin, to induce opening of the interface between CH1 and CH2. We observed that the N-terminus is required for L253P-induced high affinity binding. Thus, if our proposed model of the N-terminus is correct, then the L253P mutant must only modestly shift the equilibrium of the ABD from the closed to open state. The N-terminus is needed for L253P to substantially shift the equilibrium to the open, actin binding state. An alternative, but not mutually exclusive, model is that the N-terminus contributes more to direct actin binding than just the N-terminal residues that make up the actin-binding helix (colored magenta in Figure 1). The 6.9 Angstrom cryo-EM structure only resolved this actin-binding helix, which constitutes residue 37-52. Residues 1-36 are predicted to be unstructured in previous homology models of the ABD; however, AlphaFold predicted structure shows that part of the unstructured region (residues 7-24) forms a helix (Figure 1 in chapter one). It is possible that residues 1-36 also make direct contact with actin. This unstructured region would not be detectable, if bound to actin, at 6.9 Angstrom resolution. If residues of the unstructured region bind actin, then their contacts, together

with those of the actin-binding helix, would contribute significantly to the overall actin-binding surface area and affinity. Future studies should truncate only the N-terminal unstructured region to determine its contribution to actin binding and spectrin function *in vivo*.

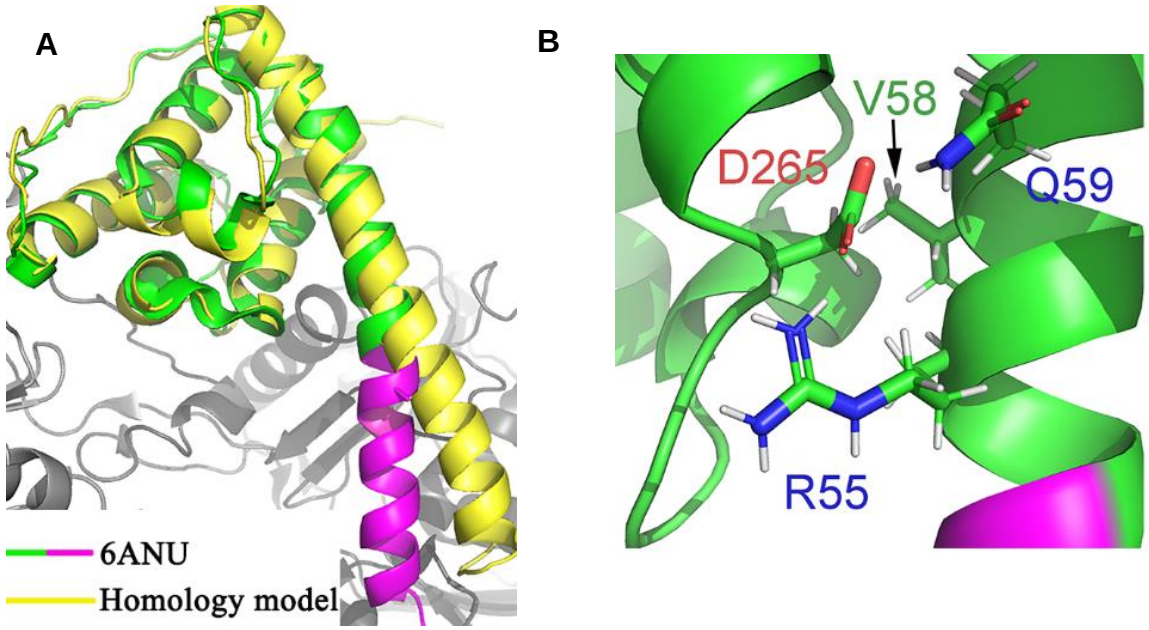

Figure 4.1. Structural analysis of the N-terminus. (A) Imposing β-III-spectrin ABD homology model (yellow) in the actin unbound state on L253P mutant ABD cryo-EM structure (green and magenta) in actin bound state. (B) homology model of β-III-spectrin ABD showing the predicted contacts of CH1 residues with CH2 residue in the actin unbound state.

4.1 Spectrin-Repeat Domain Mutations

Here we summarize key findings, and discuss open questions and future directions pertaining to our studies of the SRD-localized SCA5 mutations. We focused on understanding the molecular consequences of two SCA5 mutations: 1) the SRD2-localized missense mutation, R480W, and 2) the SRD3-localized thirteen amino acid in-frame deletion, E532_M544del. The R480W mutation was reported in several unrelated patients with infantile onset of ataxia and developmental delay (9-12). The

E532_M544del was reported in American kindred descending from the paternal grandparents of the United States President Abraham Lincoln. Affected family members presented with adult onset ataxia that was slowly progressive (13). The difference in age of onset and symptom severity suggested that these mutations disrupt spectrin function by different mechanisms.

The N-terminal SRDs are known to influence spectrin actin-binding activity and to nucleate heterodimer formation with α-II-spectrin. Thus, our experiments focused on testing how these mutations impacted the physical interaction of β-III-spectrin with α-II-spectrin and actin. Using a variety of binding assays, including cell-based FRET, co-immunoprecipitation, native PAGE mobility shift, and co-sedimentation, we did not detect any difference in the binding of the wild-type versus R480W mutant to α-II-spectrin or actin. Our binding data suggested that R480W did not impact these key interactions. However, co-expression of full-length α-II-spectrin and R480W β-III-spectrin proteins in HEK293T cells revealed large cytoplasmic spherical inclusions, which were not observed in control cells expressing the wild-type proteins. These inclusions contained both R480W β-III-spectrin and α-II-spectrin. Moreover, the inclusions are not observed when the R480W mutant is expressed by itself (no α-II-spectrin). This strongly suggests that the inclusions result from a grossly abnormal interaction between the R480W mutant to α-II-spectrin. The molecular mechanism by which R480W causes α-II/β-III-spectrin inclusion formation is unclear, as we did not detect an altered interaction in other binding assays. However, a clue to the molecular mechanism may stem from our circular dichroism denaturation studies on the purified β-III-spectrin fragments (amino acids 1-1066). These studies showed that R480W mutant

protein unfolds at a ~1°C higher temperature than wild-type. This indicates that R480W mutation confers higher thermal stability to β-III-spectrin. Indeed, prior *in silico* analyses have predicted similar stability conferred by both R480W, and another SRD2-localized SCA5 mutation, R437Q (11, 14). We suggest similar to Nuovo et al that this increase in stability might result in a "stiff" protein that adopts a limited pool of conformational states compared to wild-type. Perhaps the R480W mutant locks the α-II/β-III-spectrin complex in a rigid conformation unfavorable for incorporation or retention of the complex in a sub-plasma membrane spectrin-actin cytoskeleton. The formation of α/β-spectrin inclusions has been reported recently in developing axons (15). Boyer et al reported that these inclusions show liquid-liquid phase separation behavior, and that formation of these inclusions was shown to be mediated directly by the SRDs. Interestingly, these spectrin inclusions were suggested to form before incorporation of the spectrin into the sub-plasma membrane cytoskeleton. Potentially, R480W induces inclusion by promoting the formation of a naturally occurring, biologically relevant, biomolecular spectrin condensate. Future studies should determine whether R480W induced inclusions are liquid or solid in physical state, whether these inclusions form in neurons, and whether they form at endogenous protein levels. Moreover, it is important to determine whether other SRD mutations that cause infantile onset of symptoms, such as R437Q, induce formation of similar inclusions.

We found that E532_M544del disrupts β-III-spectrin binding to α-II-spectrin and actin. Our co-immunoprecipitation, native PAGE mobility shift and cell co-localization assays showed that E532_M544del binds α-II-spectrin. However, live-cell FRET, reduced mobility of the E532_M544del β-III/α-II-spectrin complex in native PAGE and

AlphaFold predictions indicated that the C-terminal SRDs of β-III-spectrin do not associate with the complementary SRDs of α-II-spectrin. Collectively, our data supports a model where E532_M544del mutation opens the α-II/β-III-spectrin interface following the dimer nucleation site (β-III-spectrin SRDs 1-2). This reduced coupling of SRDs in the α-II/β-III-spectrin dimer may further reduce assembly of dimers into tetramer. Reduced tetramer formation would impede the actin crosslinking function of spectrin, and interfere with the assembly of a plasma membrane associated spectrin-actin cytoskeleton. The E532_M544del mutation also caused an increase in the presence of cytoplasmic inclusions containing the mutant β-III-spectrin and α-II-spectrin. These inclusions may reflect improperly formed spectrin dimers. The E532_M544del α-II/β-III-spectrin inclusions are small, irregularly shaped, and less frequently observed, compared to the large spherical inclusions formed by the R480W α-II/β-III-spectrin, present in nearly all cells. Thus, both E532_M544del and R480W disrupt the physical association of β-III-spectrin to α-II-spectrin, but by distinct mechanisms.

Actin co-sedimentation assays showed that the E532_M544del mutant additionally binds actin with high affinity. In HEK293T cells, the E532_M544del mutant is abundantly localized to the cell cortex, but shows reduced localization to plasma membrane protrusions such as filopodia and lamellipodia. We observed a similar localization phenotype for the L253P mutant, which binds actin with high affinity (7). Our interpretation is that increased actin binding reduces the mobile pool of spectrin that is available to enter dynamic plasma membrane extensions. This reduced mobility is supported by the reduced localization of the E532_M544del and L253P mutants in the dendrites of transfected primary mouse Purkinje neurons (16). The impact of

E532_M544del on spectrin dimer or tetramer assembly and actin binding is expected to alter localization or remodeling of the spectrin cytoskeleton in dendritic shafts or spines, and is consistent with the reported mislocalization of glutamate receptors in the spines of mouse Purkinje neurons expressing the E532_M544del mutant (17). We predict that an additional SRD3-localized mutation, L629_R634delinsW (18), will similarly alter actin binding and dimerization.

How the SRD3-localized E532_M544del increases actin binding is not clear. Possibly that the mutation allosterically impacts the N-terminal ABD, promoting a shift in ABD conformation to the open, actin binding state. Alternatively, the mutation may expose or generate a *de novo* actin-binding site in the SRDs. We attempted to resolve these two possibilities by truncating the N-terminal ABD and testing if the truncated E532_M544del mutant binds actin. However, difficulties in protein purification precluded performance of these experiments. Our AlphaFold model for the E532_M544del mutant shows that the mutation introduces a disordered region that acts as a flexible hinge. The model shows that the C-terminal SRDs are closely positioned to the N-terminal ABD. Thus, a third possibility is that E532_M544del-induced actin binding results from a novel contact between the N-terminal ABD and C-terminal SRDs. Future FRET experiments using GFP and RFP tags at opposites ends of the spectrin protein may experimentally support a novel contact between the C-terminal SRDs and N-terminal ABD.

Increased actin binding was shown to be a common molecular consequence of many ABD-localized mutations (19), and here we showed that some SRD mutations, such as E532_M544del, can also increase affinity for actin. Our lab has engaged in

translational work to identify small molecule modulators of spectrin actin binding, for SCA5 therapy (20, 21). If increased actin binding is the driver for E532_M544del neurotoxicity, then small molecules may be useful for both the ABD-localized mutations, and a subset of SRD-localized mutations.

References

1. Avery, A. W., Fealey, M. E., Wang, F., Orlova, A., Thompson, A. R., Thomas, D. D. *et al.* (2017) Structural basis for high-affinity actin binding revealed by a β-III-spectrin SCA5 missense mutation Nature Communications **8**, 1350 10.1038/s41467-017-01367-w
2. Jung, M., Kim, D., andMun, J. Y. (2020) Direct Visualization of Actin Filaments and Actin-Binding Proteins in Neuronal Cells Frontiers in Cell and Developmental Biology **8**, 10.3389/fcell.2020.588556
3. Unsain, N., Stefani, F. D., andCáceres, A. (2018) The Actin/Spectrin Membrane-Associated Periodic Skeleton in Neurons Front Synaptic Neurosci **10**, 10 10.3389/fnsyn.2018.00010
4. Denha, S. A., Atang, A. E., Hays, T. S., andAvery, A. W. (2022) β-III-spectrin N-terminus is required for high-affinity actin binding and SCA5 neurotoxicity Scientific Reports **12**, 1726 10.1038/s41598-022-05762-2
5. Grueber, W. B., Ye, B., Moore, A. W., Jan, L. Y., andJan, Y. N. (2003) Dendrites of distinct classes of Drosophila sensory neurons show different capacities for homotypic repulsion Curr Biol **13**, 618-626 10.1016/s0960-9822(03)00207-0

6. Avery, A. W., Crain, J., Thomas, D. D., andHays, T. S. (2016) A human β-III-spectrin spinocerebellar ataxia type 5 mutation causes high-affinity F-actin binding Scientific Reports **6**, 21375 10.1038/srep21375

7. Avery, A. W., Thomas, D. D., andHays, T. S. (2017) β-III-spectrin spinocerebellar ataxia type 5 mutation reveals a dominant cytoskeletal mechanism that underlies dendritic arborization Proceedings of the National Academy of Sciences **114**, E9376-E9385 doi:10.1073/pnas.1707108114

8. Iwamoto, D. V., Huehn, A., Simon, B., Huet-Calderwood, C., Baldassarre, M., Sindelar, C. V. *et al.* (2018) Structural basis of the filamin A actin-binding domain interaction with F-actin Nat Struct Mol Biol **25**, 918-927 10.1038/s41594-018-0128-3

9. Jacob, F.-D., Ho, E. S., Martinez-Ojeda, M., Darras, B. T., andKhwaja, O. S. (2013) Case of infantile onset spinocerebellar ataxia type 5 Journal of Child Neurology **28**, 1292-1295,

10. Parolin Schnekenberg, R., Perkins, E. M., Miller, J. W., Davies, W. I., D'Adamo, M. C., Pessia, M. *et al.* (2015) De novo point mutations in patients diagnosed with ataxic cerebral palsy Brain **138**, 1817-1832,

11. Nuovo, S., Micalizzi, A., D'Arrigo, S., Ginevrino, M., Biagini, T., Mazza, T. *et al.* (2018) Between SCA5 and SCAR14: delineation of the SPTBN2 p. R480W-associated phenotype European Journal of Human Genetics **26**, 928-929,

12. Zonta, A., Brussino, A., Dentelli, P., andBrusco, A. (2020) A novel case of congenital spinocerebellar ataxia 5: further support for a specific phenotype

associated with the p.(Arg480Trp) variant in SPTBN2 BMJ Case Reports CP **13**, e238108,

13. Ranum, L. P., Schut, L. J., Lundgren, J. K., Orr, H. T., andLivingston, D. M. (1994) Spinocerebellar ataxia type 5 in a family descended from the grandparents of President Lincoln maps to chromosome 11 Nature genetics **8**, 280-284,
14. Accogli, A., St-Onge, J., Addour-Boudrahem, N., Lafond-Lapalme, J., Laporte, A. D., Rouleau, G. A. *et al.* (2020) Heterozygous missense pathogenic variants within the second spectrin repeat of SPTBN2 lead to infantile-onset cerebellar ataxia Journal of Child Neurology **35**, 106-110,
15. Boyer, N. P., Sharma, R., Wiesner, T., Delamare, A., Pelletier, F., Leterrier, C. *et al.* (2024) Spectrin condensates provide a nidus for assembling the periodic axonal structure bioRxiv 10.1101/2024.06.05.597638
16. Fujishima, K., Kurisu, J., Yamada, M., andKengaku, M. (2020) βIII spectrin controls the planarity of Purkinje cell dendrites by modulating perpendicular axon-dendrite interactions Development **147**, dev194530,
17. Armbrust, K. R., Wang, X., Hathorn, T. J., Cramer, S. W., Chen, G., Zu, T. *et al.* (2014) Mutant β-III spectrin causes mGluR1α mislocalization and functional deficits in a mouse model of spinocerebellar ataxia type 5 Journal of Neuroscience **34**, 9891-9904,
18. Ikeda, Y., Dick, K. A., Weatherspoon, M. R., Gincel, D., Armbrust, K. R., Dalton, J. C. *et al.* (2006) Spectrin mutations cause spinocerebellar ataxia type 5 Nature genetics **38**, 184-190,

19. Atang, A. E., Keller, A. R., Denha, S. A., andAvery, A. W. (2023) Increased Actin Binding Is a Shared Molecular Consequence of Numerous SCA5 Mutations in β-III-Spectrin Cells **12**, 2100,

20. Guhathakurta, P., Rebbeck, R. T., Denha, S. A., Keller, A. R., Carter, A. L., Atang, A. E. *et al.* (2023) Early-phase drug discovery of β-III-spectrin actin-binding modulators for treatment of spinocerebellar ataxia type 5 Journal of Biological Chemistry **299**, 10.1016/j.jbc.2023.102956

21. Rebbeck, R. T., Andrick, A. K., Denha, S. A., Svensson, B., Guhathakurta, P., Thomas, D. D. *et al.* (2021) Novel drug discovery platform for spinocerebellar ataxia, using fluorescence technology targeting β-III-spectrin Journal of Biological Chemistry **296**, 10.1074/jbc.RA120.015417

APPENDIX

IBC APPROVAL LETTER

OAKLAND UNIVERSITY
Powered by Google

Adam Avery <awavery@oakland.edu>

Committee Action Record - New or De Novo IBC Protocol # IBC-00001103 Approval
1 message

eSirius3GWebServer <no-reply@esirius.cayuse.com> Wed, Sep 21, 2022 at 5:04 PM
To: awavery@oakland.edu

cayuse Hazard Safety

Reference: IBC Protocol # IBC-00001103

Protocol Title: Structural and functional studies of the spectrin superfamily of cytoskeletal proteins

Principal Investigator: Avery, Adam

Approval Period: 09/21/2022 - 09/21/2025

Dear Professor Avery, Adam:

The Institutional Biosafety Committee (IBC), responsible for the review of research involving materials of human origin, recombinant DNA, and biohazardous, infectious or toxic materials, has reviewed the original proposal, noted the revisions provided by you upon committee's request (if applicable), and approved the project referenced above. This is your formal approval notice; please save it for your records.

The proposed activities are approved for a period of three years, starting 09/21/2022 and ending 09/21/2025, and assigned the approval # IBC-00001103. Please be aware that protocols expire at 12:01 AM on the expiration date. The highest BSL level approved for the protocol can be found on the Overview page of the protocol form.

Any unanticipated problems, changes in, or halting of the activities proposed in the project, as described, must be promptly reported to the IBC or the biosafety officer.

In addition, all faculty, staff, and students involved in the project must be trained and qualified to conduct the project in a responsible manner. Please note, in this regard, that you, the Principal Investigator, are fully responsible at all times for limiting or restricting access to laboratories and for assessing, in each circumstance, who may enter or work in a laboratory when biohazardous materials are in use.

Prior to initiating any work on this approved project, please contact me by email (luongo@oakland.edu) to schedule a startup Biosafety Audit. This audit will verify that all biosafety controls described in your application have been implemented.

Please let me know if you have any questions. Thank you.

Sincerely,

Domenic Luongo, CHMM
Director - Laboratory Safety and Compliance

(email ID #400090)

*** THIS IS AN EMAIL NOTIFICATION ONLY. PLEASE DO NOT REPLY ***